PARITY VIOLATION IN Tl^{203} AND RESONANCE TRAPPING OF OPTICAL RADIATION

Melvin Kurt Simmons

(Ph. D. Thesis)

November 17, 1972

Prepared for the U.S. Atomic Energy
Commission under Contract W-7405-ENG-48

LBL-1337
c. 1

DISCLAIMER

Contents

PARITY VIOLATION IN Tl^{203} AND RESONANCE TRAPPING OF OPTICAL RADIATION

Melvin Kurt Simmons

Department of Physics
and
Lawrence Berkeley Laboratory
University of California
Berkeley, California

November 17, 1972

ABSTRACT

This thesis describes an investigation of the feasibility of observing a gamma-ray asymmetry from optically pumped Hg^{203}. Such a parity-violating asymmetry results from the weak interaction between nucleons predicted by the current-current model of the weak interaction. The size of the predicted asymmetry is $\alpha \simeq 1\times10^{-4}$ for a perfectly polarized sample. We have performed optical pumping experiments on Hg^{201} and Hg^{203} to determine if sufficient polarization can be obtained in a high density sample for the predicted asymmetry to be observed. We find that resonance trapping of the optical pumping light causes depolarization in high density samples and prevents observation of the asymmetry.

The phenomemon of resonance trapping was further investigated by observation of a two-photon cascade of calcium in an atomic beam. We observe trapping of the second photon of the cascade. Perturbation of the intermediate atomic state by an external magnetic field was observed by the effect on the angular correlation and linear

polarization correlation of the two photons. These correlations were also affected by resonance trapping.

I. INTRODUCTION

A. Parity Violations in Nuclei

Our understanding of weak interactions can be summarized in a weak interaction Lagrangian which contains only a self-interacting charged current. This Lagrangian succeeds in describing fully leptonic and semi-leptonic processes. It also has had some success in describing non-leptonic strangeness-changing weak decays of hadrons. However the self-interacting current form of the Lagrangian predicts more than that. The diagonal terms in the Lagrangian describe processes not yet observed. Some of these, such as muon-neutrino elastic scattering, are far beyond our technological capabilities and may never be observed. Thus the possible existence of a weak force between nucleons is an important test of our present concept of the nature of the weak interaction.

If the weak interaction between nucleons had no unusual properties, it would be hopeless to try to observe its effects against the background of the nucleon-nucleon strong interaction. The dimensionless coupling constant for the strong nucleon -pion vertex is $g \simeq 10$, whereas the corresponding coupling constant for the weak coupling is $Gm_\pi^2 \simeq 10^{-6}$, so we have a ratio of about 10^7 in the strength of the interaction. Thus the weak nucleon-nucleon coupling can be detected only if it has some effect which could not be caused by the strong interaction. The well-known parity violation of the weak interaction provides such an effect.

A parity-violating nuclear force will express itself in two ways.

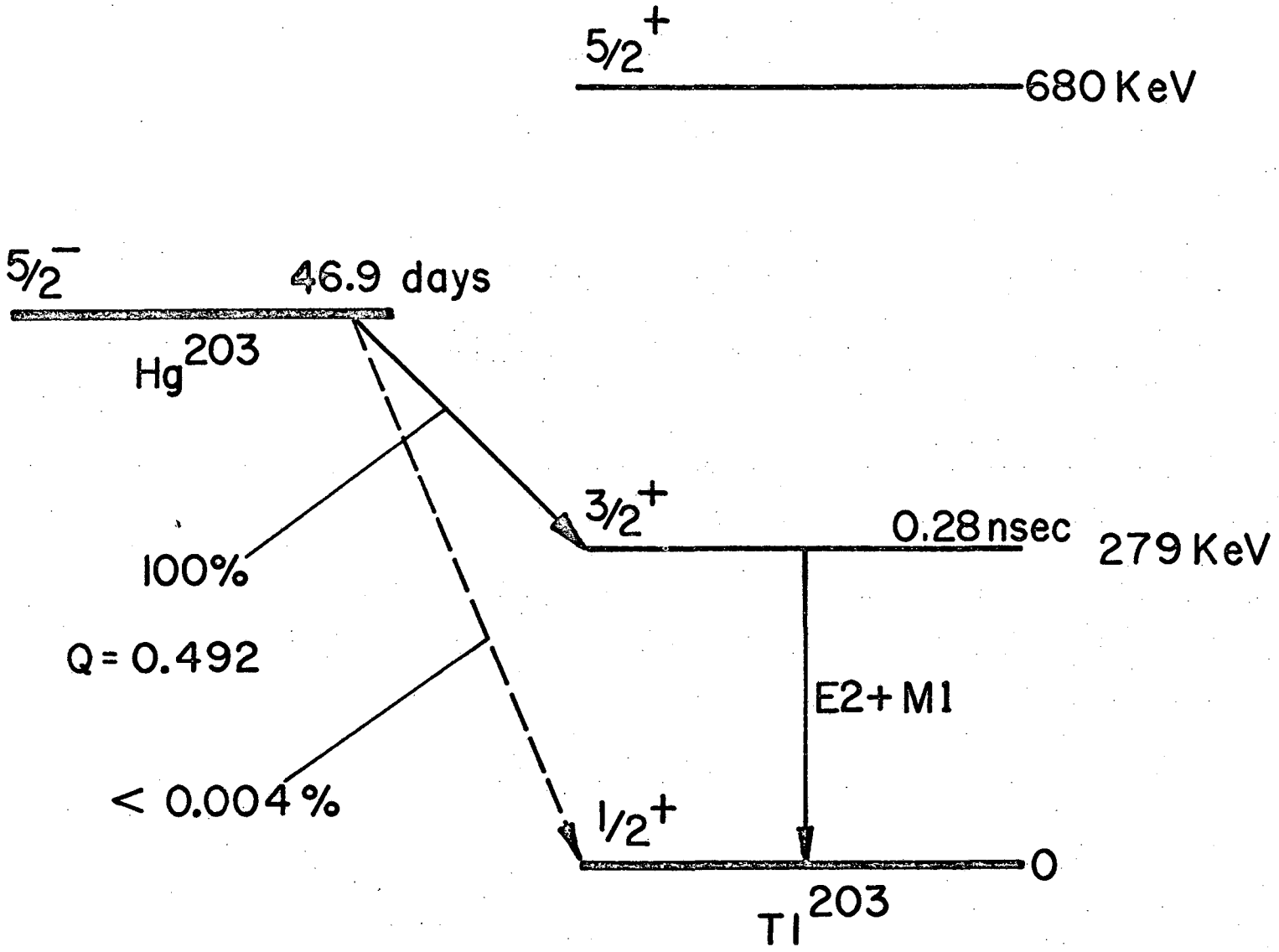

Figure 1. Decay scheme of Hg^{203}.

Transitions which were forbidden by conservation of parity will now proceed with a rate proportional to the square of the weak interaction coupling constant, or about 10^{-14} times the rate of an allowed transition. There will also be non-zero average values of pseudo-scalar quantities because of the interference of the weak and the strong interactions. These quantities will be first order in the weak coupling constant, or about one part in 10^7. These effects are both quite small, but in favorable circumstances the parity-violating amplitudes may be enhanced and become more easily observable.

The effect of the weak potential has been seen in parity-forbidden alpha decay, in the circular polarization (helicity) of nuclear gamma rays, and in the asymmetry of gamma rays emitted subsequent to the capture of polarized neutrons. The evidence in favor of the existence of the weak nucleon-nucleon potential is now rather convincing. However the difficulty in comparing these experiments with theoretical predictions makes it essential that as many experimental cases as possible are investigated.

B. Experimental Approach

We decided to search for an asymmetry of gamma-rays emitted by polarized nuclei. This is analagous to the experiment by Wu et. al. (W57) which observed an asymmetry of beta-rays from polarized Co^{60} nuclei, and first established the existence of parity violation in the weak interaction. We chose this approach because the effect is first order in the weak coupling constant, and because it does not require the measurement of the circular polarization of gamma-rays (for which there exists no efficient technique). The problem one faces in this

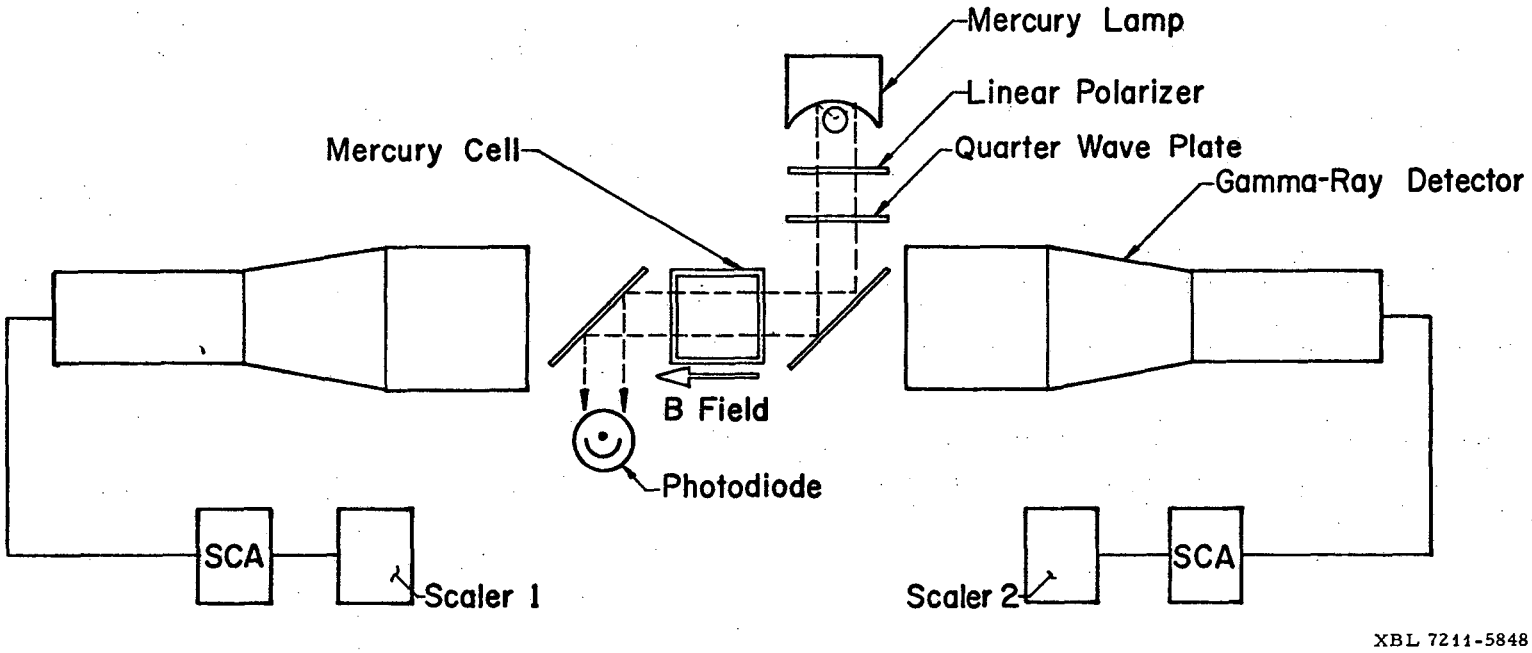

Figure 2. Schematic diagram of the apparatus for observation of a gamma-ray asymmetry from optically pumped Hg^{203}.

approach is to find a way to polarize a large number of radioactive nuclei for the period of time required to measure a very small asymmetry.

We considered many techniques of nuclear polarization, some of them common and some of them bizzare. The most promising technique seemed to be optical pumping of a diamagnetic vapor (only nuclear angular momentum in the atomic ground state). This technique has been widely employed in the measurement of atomic energy level spacings and in the study of atomic collision processes, but had not yet been employed in the study of nuclear processes. The reported experiments on optical pumping had been performed at low atomic densities. To successfully observe a nuclear parity violation, we would have to use a high atomic density to achieve the required high count rate. Thus our first goal was to determine the feasibility of optically pumping a vapor at high atomic densities.

The element most often employed in optical pumping experiments is mercury. It is fortunate that the isotope Hg^{203}, by beta decay to an excited state of Tl^{203} (see figure 1), emits a gamma ray of 279 Kev which can be efficiently detected by NaI(Tl) crystals. Furthermore the normal (parity non-violating) amplitude of this transition is retarded and an enhancement by a factor of about 100 can be expected. This is the case we chose to investigate.

A diagram of the experimental set-up is shown is figure 2. The optical pumping light is supplied by a Hg^{204} resonance lamp, which emits a spectral line which overlaps one of the hyper-fine absorption lines of Hg^{203}. The light is circularly polarized by a linear polarizer

and quarter-wave plate. The Hg^{203} vapor to be polarized is contained in a quartz cell located in a uniform magnetic field. The optical pumping beam is directed through the cell parallel to the magnetic field direction by a mirror. The detector crystals located on the optical pumping axis measure the gamma emission rate parallel and antiparallel to the direction of the induced nuclear polarization. The circular polarization of the optical pumping light is reversed and the count rates of the detectors are examined for an asymmetry correlated with the direction of the nuclear spin. The measurement of this asymmetry is the ultimate goal of this experiment.

II. PARITY VIOLATIONS IN NUCLEI

A. Theory

1. Weak Interactions

Merely the existence of a parity-violating weak interaction between leptons and nucleons suffices to produce a parity-violating coupling between nucleons by exchange of a lepton pair. However this coupling is of second order in the weak interaction, too small to be seen in any conceivable experiment. If the weak interaction Lagrangian is of a self-interacting form, then there should also be a parity-violating nucleon coupling first order in the weak interaction. This was first suggested in the early paper by Feynman and Gell-Mann (FG58) and has been the subject of extensive theoretical investigation. The form usually assumed for the weak Lagrangian is $L = (G/2\sqrt{2}) \cdot (J_\mu J_\mu^\dagger + J_\mu^\dagger J_\mu)$, where the current J_μ includes both leptonic (j_μ) and hadronic (J_μ) currents. The cross-terms in L between various parts of J_μ provide an elegant description of beta-decay, muon decay, and the semi-leptonic decays of hadrons. However the existence of the diagonal terms in L is a crucial test of this form of the weak Lagrangian.

The diagonal terms in L involving the leptonic currents describe $e\text{-}\nu_e$ scattering and $\mu\text{-}\nu_\mu$ scattering. Neither process has been observed experimentally (but $e\text{-}\nu_e$ scattering is believed important in astrophysical processes). Before examining the hadronic diagonal terms in L, we must discuss the properties of the hadronic current J_μ. The current J_μ is an operator on hadronic states. Those states are usually considered to be representations of the SU(3) group, so J_μ will be defined

by its SU(3) properties. The favored SU(3) structure of J_μ is that suggested by Cabbibo (C63), $J_\mu = \cos\theta(V_\mu^0+A_\mu^0) + \sin\theta(V_\mu^1+A_\mu^1)$. The parity non-invariance of L is shown by the simultaneous appearance in J_μ of vector (V_μ) and axial-vector (A_μ) parts. The Cabbibo angle, θ, determines the relative rates of ΔStrangeness=0, $(V_\mu^0+A_\mu^0)$; and $|\Delta\text{Strangeness}|=1$, $(V_\mu^1+A_\mu^1)$, semi-leptonic decays of hadrons. It is assumed that the V_μ and A_μ each transform as an SU(3) octet. In accord with the conserved vector current hypothesis of Feynman and Gell-Mann, V_μ is assumed to be the same octet as that responsible for the electromagnetic interactions of hadrons.

The SU(3) tensor form of the weak Lagrangian is found by substituting the Cabbibo form of the hadronic current into the above equation for L. The non-leptonic part of L is then

$$
\begin{aligned}
L = (G/2\sqrt{2}) \Bigg\{ & \cos^2\theta \left[\frac{2}{(6)^{1/2}} T^{(27)}_{0,2,0} - \frac{1}{(10)^{1/2}} T^{(27)}_{0,0,0} - \left(\frac{12}{5}\right)^{1/2} T^{(8)}_{0,0,0} + \left(\frac{3}{2}\right)^{1/2} T^{(1)}_{0,0,0} \right] \\
& + \sin\theta\cos\theta \left[\left(\frac{2}{3}\right)^{1/2} T^{(27)}_{1,3/2,-1/2} + \left(\frac{2}{3}\right)^{1/2} T^{(27)}_{-1,3/2,1/2} + \left(\frac{2}{15}\right)^{1/2} T^{(27)}_{1,1/2,-1/2} \right. \\
& \left. + \left(\frac{2}{15}\right)^{1/2} T^{(27)}_{-1,1/2,1/2} + \left(\frac{6}{5}\right)^{1/2} T^{(8)}_{1,1/2,-1/2} + \left(\frac{6}{5}\right)^{1/2} T^{(9)}_{-1,1/2,\,1/2} \right] \\
& + \sin^2\theta \left[\left(\frac{2}{5}\right)^{1/2} T^{(27)}_{0,1,0} - \left(\frac{3}{5}\right)^{1/2} T^{(8)}_{0,1,0} + \left(\frac{3}{10}\right)^{1/2} T^{(27)}_{0,0,0} + \frac{1}{(5)^{1/2}} T^{(8)}_{0,0,0} \right. \\
& \left. + \frac{1}{(2)^{1/2}} T^{(1)}_{0,0,0} \right] \Bigg\}
\end{aligned}
$$

where the superscript on T is the dimensionality of the SU(3) representation and the subscripts are Y, I, and I_z. The $\sin\theta\cos\theta$ term in L is responsible for the non-leptonic weak decays of hadrons ($\Delta Y=\pm 1$). The $\cos^2\theta$ and $\sin^2\theta$ terms are reponsible for parity-violation in nuclear forces ($\Delta Y= 0$). The above form for L is not yet completely acceptable because the $|\Delta Y|= 1$ terms include comparable amounts of $|\Delta I|= 1/2$ and $|\Delta I|= 3/2$. Experimentally the selection rule $|\Delta I|= 1/2$ is observed. There are two distinct ways to correct this fault in L. The $|\Delta I|= 3/2$ terms in L appears only in $T^{(27)}$. It has been suggested that the $T^{(8)}$ terms in L are dynamically enhanced relative to $T^{(27)}$, so that the $|\Delta I|= 1/2$ rule is produced (DFS64). The other suggestion is that L includes other current-current terms which cancel the $|\Delta I|= 3/2$ parts found above (DE63). Is has been proposed that the parity-violating nuclear force provides a test which can distinguish these two suggestions (DFG64,T68,FT68). The basic argument is that octet enhancement will increase the amount of $|\Delta I|= 0$ in the $\cos^2\theta$ term, leave the amount of $|\Delta I|= 2$ unchanged, and leave the $\cos^2\theta$ term without any $|\Delta I|= 1$ contribution. However the suggested forms for the extra current-current terms in L would add a $|\Delta I|= 1$ contribution to the $\cos^2\theta$ term without greatly changing the $|\Delta I|= 0$ contribution. Thus a determination of the isotopic spin properties of the parity-violating nuclear force might distinguish between these suggestions.

We now derive a non-relativistic parity-violating internucleon potential from the weak Lagrangian presented above. We follow the procedure of Michel (M64). The $\sin^2\theta$ term from the $|\Delta S|= 1$ current will be ignored for the moment. Since the weak Lagrangian used here

contains only charged currents, there will be a non-zero interaction only between a neutron and a proton. Two related questions arise in the calculation of a neutron-proton scattering amplitude from the weak Lagrangian. What is the momentum transfer dependence of the matrix elements of V_μ and A_μ? What are the wave functions for a neutron and proton in close proximity?

The simplest way to deal with these two questions is to assume that the matrix elements are independent of momentum transfer, q, and equal the $q \simeq 0$ values observed in beta decay; and use plane waves for the neutron and proton wave functions. With these assumptions the weak interaction matrix element for scattering of a neutron and proton of momenta $\vec{p}$ and $-\vec{p}$ to final momenta $-\vec{p}'$ and $\vec{p}'$

$$-iM = \bar{u}_1(\vec{p}')\gamma_\mu(1+\gamma_5)u_1(\vec{p})\,i(G/\sqrt{2})\,\bar{u}_2(-\vec{p}')\gamma_\mu(1+\gamma_5)u_2(-\vec{p})$$

where u and $\bar{u}$ are the usual Dirac plane wave spinors. By replacing the Dirac spinors with their non-relativistic approximations we obtain

$$M = -\sqrt{8}\,G\{M^2 - M^2\vec{\sigma}_1\cdot\vec{\sigma}_2 + M(\vec{\sigma}_2-\vec{\sigma}_1)\cdot(\vec{p}+\vec{p}') + iM(\vec{\sigma}_2\times\vec{\sigma}_1)\cdot(\vec{p}-\vec{p}')\}$$

Now we calculate the non-relativistic potential $V(\vec{r})$ which, in a first Born approximation, produces the scattering matrix element found above. The result is, neglecting the parity-conserving terms,

$$V(\vec{r}) = \sqrt{8}\,G\frac{1}{8M}(\vec{\sigma}_2-\vec{\sigma}_1)\cdot\{\vec{q},\delta(\vec{r})\}_+ - \sqrt{8}\,G\frac{1}{8M}(\vec{\sigma}_2\times\vec{\sigma}_1)\cdot[\vec{q},\delta(\vec{r})]_-$$

where $\{\ ,\ \}_+$ is the anti-commutator and $[\ ,\ ]_-$ is the commutator. This potential has zero range, which results from the assumption that the current matrix elements are independent of q. However the strong interactions between nucleons have a short range repulsive component

which prevents nucleons from approaching closer than about one fermi. Thus the zero-range potential found above would have no effect and we must include the momentum transfer dependence of the matrix elements.

The most general forms for the vector and axial-vector current matrix elements between plane wave states are

$$\langle p'|V_\mu|p\rangle = f_1(q^2)\gamma_\mu + f_2(q^2)i\sigma_{\mu\nu}q_\nu + f_3(q^2)iq_\mu$$

$$\langle p'|A_\mu|p\rangle = [g_1(q^2)\gamma_\mu + g_2(q^2)\sigma_{\mu\nu}q_\nu + g_3(q^2)q_\mu]i\gamma_5$$

The assumption of conserved vector current requires $f_3(q^2) = 0$ and equates f_1 and f_2 with the nucleon electric and magnetic form factors (T63). Invariance under G-Parity requires $g_2 = 0$ and with the conserved vector current form of the vector matrix element, the g_3 term has no effect. It seems reasonable to assume that g_1 has the same q^2 dependence as f_1 and f_2; a range equal to the reciprocal of the rho-meson mass. With these assumptions the changes in $V(\vec{r})$ are that the delta functions of $\vec{r}$ are replaced with distributions of range $1/m_\rho$, and the second term is multiplied by one plus the difference in proton and neutron magnetic moments.

We must now combine the finite range potential with nucleon wave functions which include the effect of the repulsive core. Michel did this by retaining plane wave states for the nucleons and modifying the potential to make it zero for distances less than the hard core distance. This reduced the effect of the potential by about 20%. McKellar instead kept the potential in the form found above and replaced the plane waves for the nucleons with the approximate wave functions used in nuclear physics to estimate the effect of two-particle

correlations (MK68). McKellar found the effect of the potential was reduced by about 60%. The difference between these two results is unimportant in comparison with uncertainties in the nuclear structure part of these calculations.

The $\sin^2\theta$ term in the weak Lagrangian includes a $|\Delta I| = 1$ part. This induces a weak pion-nucleon coupling. Thus, in addition to the rho-meson exchange term considered above, there is a weak potential due to $\pi^{\pm}$ exchange. The contribution from π^0 vanishes (B61) so again the potential only acts between a neutron and a proton. This potential has been calculated by McKellar (MK67) to be

$$V_\pi(\vec{r}) = \frac{gf}{4\pi\sqrt{2}\,M}(\vec{\sigma}_1+\vec{\sigma}_2)\cdot[\vec{q},e^{-m_\pi r}/r]_-$$

where g is the pseudo-scalar pion nucleon coupling constant ($g^2/4\pi = 14.4$) and $f \simeq 5.2\times10^{-8}$ is the weak pion-nucleon coupling constant. This term is decreased relative to the rho-exchange term by $\tan^2\theta \simeq 0.073$, but is enhanced by the longer range of the pion. McKellar finds the effect of this term to be about 25% of the rho-meson term in his calculations using correlated wave functions* (MK68). The relative sign of the two potentials is unknown, but would be positive in a weak interaction theory based on an intermediate boson.

---

*This conclusion is not universal. Olesen and Rao, using a field-current identity, conclude that the rho-exchange term vanishes so the only contribution is from $\pi^{\pm}$ exchange (OR69).

2. Calculations in Nuclei

The two-particle potentials written above are not yet in useful form. We do not possess the many-particle wave functions for the nucleus which would be required for the calculation of the effect of the weak potential acting between each neutron and each proton. Instead, our description of the nucleus is that of a single particle moving in the potential field of a nucleus core composed of the other nucleons. The core may be either the spherical core of the shell model or the deformed core of the Nilsson model (N55). Thus we must replace the two-particle potential by a single-particle potential which represents the effect of the weak interaction on the single proton (neutron) by the neutrons (protons) of the core.

Michel (M64, Appendix A) finds the single-particle weak potential by averaging one of the interacting nucleons in the above potential over the possible states in the core. His calculation assumes that the core is unchanged by the weak potential and that the core has zero total spin. He finds the single-particle potential to be

$$V_{sp} = G'\vec{\sigma}\cdot\vec{p}(1+\tau_z(N-Z)/A) \equiv G''\vec{\sigma}\cdot\vec{p}$$

where $G' = \sqrt{8}G(1+\mu_p-\mu_n)\rho_0/8M$, τ_z is +1(-1) when acting on a proton (neutron), and ρ_0 is the density of nuclear matter. Michel finds $G' \simeq 1\times10^{-8}$ and McKellar finds a value about half of that. Note that the single-particle potential carries the factor $1+\mu_p-\mu_n \simeq 4.7$ which was added by the hypothesis of conserved vector current.

The effect of V_{sp} on a nuclear state I_i of parity π_i will be to admix small amounts of states I_μ of parity π_μ. The new nuclear

state of mixed parity will be

$$|\bar{I}_i\rangle = |I_i\pi_i\rangle + G''\sum_\mu \frac{\langle I_\mu\pi_\mu|\vec{\sigma}\cdot\vec{p}|I_i\pi_i\rangle}{E_i - E_\mu}|I_\mu\pi_\mu\rangle$$

If the nuclear Hamiltonian were spin-independent, then the matrix element in the numerator could be replaced by $-iM\langle I_\mu\pi_\mu|\vec{\sigma}\cdot\vec{r}|I_i\pi_i\rangle(E_i-E_\mu)$ and the energy denominator would cancel. This is the approach taken by Michel. However Wahlborn argues that the significant spin-orbit coupling in nuclei prevents cancellation of the energy denominator (W65). Using the assumption that the radial wave functions for a given orbital angular momentum are independent of the total angular momentum, Wahlborn finds that

$$\langle I_\mu\pi_\mu|\vec{\sigma}\cdot\vec{p}|I_i\pi_i\rangle = -iM\langle I_\mu\pi_\mu|\vec{\sigma}\cdot\vec{r}|I_i\pi_i\rangle\cdot(E_i^0 - E_\mu^0)$$

where E_μ^0 is the energy of the state $|I_\mu\pi_\mu\rangle$ in the absence of spin-orbit coupling. The difference between these two expressions is crucial in the case of the 279 Kev transition of Tl^{203} where Michel's expression predicts a vanishing of the parity violation effect.

3. Parity Mixing in Tl^{203}

The effect of the single-particle weak potential $G''\vec{\sigma}\cdot\vec{p}$ in Tl^{203} has been calculated by Szymanski (S66). The single-particle assignments for the ground state and first excited state in Tl^{203} (figure 1) are proton hole states $|3s_{1/2}\rangle$ and $|2d_{3/2}\rangle$. The single-particle weak potential is a pseudo-scalar so it admixes states of the same total angular momentum and opposite parity. Thus the $|3s_{1/2}\rangle$ ground state will be mixed with the $|2p_{1/2}\rangle$ state and the $|2d_{3/2}\rangle$ excited state will be mixed with the $|2p_{3/2}\rangle$ state. The admixed states will be

$$|g.s.> = |3s_{1/2}> - iG'M<2p_{1/2}|\vec{\sigma}\cdot\vec{r}|3s_{1/2}> \frac{E^0(3s)-E^0(2p)}{E(3s_{1/2})-E(2p_{1/2})} |2p_{1/2}>$$

$$|e.s.> = |2d_{3/2}> - iG'M<2p_{3/2}|\vec{\sigma}\cdot\vec{r}|2d_{3/2}> \frac{E^0(2d)-E^0(2p)}{E(2d_{3/2})-E(2p_{3/2})} |2p_{3/2}>$$

where the assumption of Wahlborn about the spin-orbit coupling is used.

A model of the nuclear states must be selected for evaluation of the matrix elements and energy differences in the above expressions. Szymanski uses the spherical harmonic-oscillator Hamiltonian for the Nilsson model with zero deformation (N55),

$$\mathcal{H} = -(\hbar^2/2M)\nabla^2 + \hbar\omega_0(r/b_0)^2 - \kappa\hbar\omega_0(2\vec{\ell}\cdot\vec{s} - \lambda\vec{\ell}^2)$$

where the parameters κ and λ represent the amount of spin-orbit coupling and are chosen to recreate the proper energy level spacings. The parameters ω_0 and b_0 are chosen to make the extent of the harmonic oscillator wave functions match the observed nuclear radius of $R_0 = 1.2\times10^{-13}\ A^{1/3}$ cm. The matrix elements of $\vec{\sigma}\cdot\vec{r}$ are then easily evaluated (they are proportional to the parameter b_0). The energy differences for the numerator and denominator are found from the eigenvalues of $\mathcal{H}$ with $\lambda = 0.45$ and with $\kappa = 0$ and $\kappa = 0.06$ respectively. The resulting amplitudes of the parity-admixed states are $F \simeq 4\times10^{-7}$.

The validity of the above calculations is hard to estimate. The single-particle model does not even completely describe the electromagnetic properties of the levels of Tl^{203}. There can be no allowed magnetic dipole transition from a d-state to an s-state, so the 279 Kev transition should be electric quadrupole (and higher multipoles). However this transition goes with about equal amounts of magnetic dipole and electric quadrupole. The reason for this discrepancy is

that the single-particle model fails to include the correlations of the motion of the outside nucleon and the core nucleons (B67). The role of these correlations is crucial in calculating the effect of a short-range force such as the weak interaction between nucleons. The calculated parity admixtures in heavy nuclei could easily be incorrect by factors of two or more.

B. Observation of Parity Violation

1. Forbidden Transitions

The addition of the weak interaction to the nuclear Hamiltonian can be seen in two kinds of effects. First, transitions between states which were forbidden by parity invariance will now proceed with rates which are second order in the weak interaction coupling constant. Second, transitions which occured with emission of radiation (alpha, beta, or gamma) in a certain parity eigenstate will now also occur with the radiation in a state of opposite parity. Since the emitted radiation is no longer in an eigenstate of parity, pseudoscalar quantities (such as the helicity, $\vec{\sigma}\cdot\vec{p}$) can have non-zero average values. These pseudoscalar quantities, arising from interference between the two parity states of the radiation, will have values which are first order in the weak interaction coupling constant.

In beta-decay, we already have parity violation in the normal nuclear transitions. Beta decays between states of opposite parity are called forbidden, but still proceed with rates much larger than could be generated by the nuclear parity-violating force. In gamma-ray transitions between two nuclear levels, either EL or ML radiation is allowed, so there are no parity forbidden gamma transitions. In alpha-decay the emitted alpha particle can have high orbital angular momentum and transitions with either even or odd values of L will be allowed. However if either the initial or final states of the alpha-decay have zero angular momentum, then the value of L is already determined by conservation of angular momentum. If the value of L is required to be even (odd) and the initial and final states have

the opposite(same) parity, then the alpha-decay is forbidden.

One example of a parity-forbidden alpha-decay is the transition from the 2^-(8.88 Mev) level of O^{16} to the 0^+ ground state of C^{12}. This transition is especially interesting because both the initial and final states have isospin of zero. Thus only the $|\Delta I| = 0$ part of the weak potential can contribute and the rate of the transition provides information on the isospin properties of the weak interaction. The transition rate has been calculated using the $G''\vec{\sigma}\cdot\vec{p}$ interaction and various nuclear models (HKY69,GK69). The result is expressed as an alpha-decay width of the 2^- level, $\Gamma_\alpha \simeq 1.5\times10^{-10}$ev. As usual, the calculations may be incorrect by a factor of two or more.

In the experimental search for this transition, a N^{15} gas target is bombarded by a deuteron beam. N^{16} is formed, which beta-decays to O^{16} with a branching fraction of 1% for the 2^- level. The energy spectrum of the alpha-particles from the target is observed with solid-state detectors. A large peak in the energy spectrum is seen from the parity-allowed decay of the 2^+ level at 9.84 Mev. The region at the side of this peak is examined for alpha-particles of energy corresponding to decay from the 2^- level. Early experiments could only set an upper limit to the alpha-decay width (SOS61), but a non-zero value of $\Gamma_\alpha = 1.8\pm0.8\times10^{-10}$ ev has now been reported (HHW70). This decay width corresponding to an amplitude for the parity-admixed states of $F \simeq 3\times10^{-7}$, in accord with Michel's estimate of the $|\Delta I| = 0$ parity-violating potential.

2. Circular Polarization

Where a nuclear gamma-ray transition normally proceeds by the multipoles EL,ML+1,EL+2,···(or ML,EL+1,ML+2,···), the parity-admixed states will contribute a component of ML (EL). The interference of the EL and ML components will be seen in two ways, the average helicity of the gamma-rays emitted by unpolarized nuclei will be non-zero, and the angular distribution of gamma-rays from polarized nuclei will be asymmetric with respect to the drection of nuclear spin (BS60b,C67).

Only electric and magnet and magnetic multipoles of the same L can interfere, so the rates of the higher allowed multipole decrease the amount of circular polarization. In general the circular polarization is

$$P_\gamma = 2\frac{\sum_L M(L)^* E(L)}{\sum_L (|M(L)|^2+|E(L)|^2)}$$

In the case most often studied, the allowed transitions occur by M1+E2 and the parity-admixed transition is E1. The, if the ratios of amplitudes are $\delta = E(2)/M(1)$ and $\zeta = E(1)/M(1)$, we have

$$P_\gamma = \frac{2\zeta}{1+\delta^2}$$

The polarization is enhanced if the magnetic dipole rate is retarded, but in those cases the electric quadrupole is usually allowed and the maximum polarization occurs when $\delta = E(2)/M(1) = 1$. The ratio $\zeta = E(1)/M(1)$ is often written as the product of two factors, $\zeta = RF$, where F is the amplitude of the parity admixed state and R is the ratio of the electric dipole amplitude (between that parity-admixed state and the ground state) to the allowed magnetic dipole decay amplitude. We usually have

$F \simeq 3\times10^{-7}$ and in advantagous cases $R \simeq 100$, so $P_\gamma \simeq 6\times10^{-5}$. Where more than one state is admixed to the excited state or where the ground state is also parity admixed, this separation of factors is not meaningful.

Unfortunately, there is no available technique for measuring gamma-ray circular polarization with high efficiency. The best that can be done with Compton polarimeters, which use the polarization-dependent scattering of gamma-rays by the polarized electrons in magnetized iron, is $\varepsilon \simeq 10^{-2}$. With a circular polarization of a few parts in 10^5, this means that a change in gamma counting rate of about one part in 10^7 must be observable. For the statistical error to be this small, one must accumulate about 10^{14} counts. With the fastest counting techniques now available, it is just possible to accumulate that many counts within a year of counting time. However at such high counting rates, the electronics are susceptible to systematic errors (pile-up). No experiment using discrete counting of gamma-rays has yet been able to observe a non-zero circular polarization.

Lobashov and his comrades have devised a system which avoids the problems of discrete counting (L66a). They employ a Compton polarimeter and scintillation crystal, but instead of trying to observe individual pulses from the photodiode viewing the scintillator, they treat this output as an analog signal. The photodiode current is amplified and used to drive a pendulum with a very high Q. The direction of magnetization of the Compton polarimeter is reversed at the resonant frequency of the pendulum. Thus the amplitude and phase of any oscillation produced in the pendulum measures the magnitude and sign of the gamma-ray circular polarization. Extremely high intensity

gamma-ray sources are used. Their Ta^{181} source had an activity of 500 curies! They have observed a circular polarization of the 482 Kev gamma-ray of Ta^{181} of $P_\gamma = -0.6 \pm 0.1 \times 10^{-5}$(167). This is an M1+E2 transition with admixed E1 with R estimated to be about 50, so that F is about 1×10^{-7}. They also find a non-zero circular polarization of the 396 Kev gamma-ray of Lu^{175} of $P_\gamma = 4 \pm 1 \times 10^{-5}$(L66b). The estimated R is 100 so F is about 4×10^{-7}. Both of these observations are consistant with Michel's calculations.

3. Gamma-ray Asymmetry

If by some techique the initial nuclear state of a gamma-ray transition has been polarized, and if the nuclear states are of mixed parity, then a forward-backward gamma-ray asymmetry can exist. The parity-admixed multipole amplitudes will add a small amount of $P_\ell(\cos\theta)$ with ℓ odd to those $P_\ell(\cos\theta)$ with ℓ even which exist in the absence of parity violation. If $W_0(\theta)$ is the sum of the terms with ℓ even, then the angular distribution is $W(\theta) = W_0(\theta) + \alpha A_1 P_1(\cos\theta)$, where $A_1 = \Sigma m b_m / I$ is the initial state nuclear polarization and α is the asymmetry parameter, $\alpha = (W(\theta) - W(\pi))/(W(0) + W(\pi))$ when $A_1 = 1$.

In an M1+E2 transition with parity-admixed E1, and with $\delta = E(2)/M(1)$ and $\zeta = E(1)/M(1)$, we have $\alpha = 2K\zeta/(1+\delta^2)$, where K is a factor of order unity which depends only upon the initial and final values of the nuclear spin (BS60b,C67). The asymmetry from a nucleus 100% polarized is the same order of magnitude as the circular polarization of the gamma-rays from the unpolarized nucleus. In searching for the circular polarization, the observable effect is reduced by the low efficiency of the Compton polarimeters. In searching for the asymmetry, the

observable effect is reduced by the amount of nuclear polarization achievable. If cases can be found where polarizations higher than a few percent are possible, then the asymmetry is the easier effect to observe.

Rose has tabulated 14 different methods of orienting nuclei (R63) and the list continues to grow. However only those methods which produce nuclear polarization (in contrast to alignment) greater than a few percent are useful for observation of a gamma-ray asymmetry. A large subset of these methods involves the coincident observation of a preceding transition which defines an axis along which the nucleus is oriented. If the nuclear state is to be polarized, rather than aligned, then that transition must have violated parity. Thus only beta-decays are useful for the preparation of polarized nuclei by the coincidence technique.

In the brute force technique of nuclear polarization, an intense external magnetic field is combined with extremely low simple temperatures so that the $\vec{\mu}\cdot\vec{B}$ interaction brings about a Boltzman distribution of nuclear polarization of a few percent. The interaction required is about 10^7 gauss/°K, so temperatures of about one millidegree are needed. However the intense radioactive sources required for the large number of counts collected in looking for an asymmetry of one part in 10^5 produce a significant amount of heat. Thus these sources cannot be cooled to sufficiently low temperatures for brute force polarization.

A variation of the brute force technique is to use the coupling to the nuclear spin of the intense hyperfine fields present in some materials. These fields are of the order of magnitude of 500 kG,

so even at temperatures of about 50 millidegrees the nuclear spin is strongly coupled to the electronic moments. The electronic moments can easily be polarized by an external field of a few kilogauss. This technique is also limited by the self-heating of the source, but it has been successfully applied to a case where the asymmetry is anomolously large.

Krane et. al. have observed an asymmetry in the 501 Kev gamma-ray to Hf^{180m} (K71). Natural hafnium was alloyed with zirconium and iron so that the hafnium nuclei were located in an intense hyperfine field. Neutron irradiation produced the 5.5 hour metastable state of Hf^{180}. The sample was cooled to approximately 20 millidegrees and located in an external 2500 G field which aligned the electronic moments. A nuclear polarization of 71% was achieved. The value of the asymmetry parameter observed was -1.49×10^{-2}. This is an extremely large value. The 501 Kev gamma transition is highly retarded (thus the 5.5 hour lifetime) because the transition to the ground state requires a reorientation of the non-spherical nuclear core (K forbiddenness). However it is unclear why the parity-violating amplitude is not similarly retarded. There is no way to relate this experimental result to the strength of the weak potential.

Instead of producing and polarizing the radioactive nuclei as separate processes, it is possible to do both at once if a polarized particle beam is used to irradiate the sample. Polarized beams of neutrons, protons, and deuterons are commonly available. The lifetime of the state produced must be short enough that electronic interactions

or external fields do not depolarize the nuclei before the gamma transition occurs.

The first successful search for a gamma-ray asymmetry was performed with the reaction $Cd^{113}(n,\gamma)Cd^{114}$ (A68). A sample of Cd^{113} was placed in a beam of thermal neutrons which had been polarized by critical-angle reflection from a magnetized cobalt mirror. The thermal neutron capture cross section of Cd^{113} is dominated by a 1^+ resonance. The decay to the 0^+ ground state occurs by an M1 transition with a parity admixture of E1. A large (≃50%) polarization of the 1^+ state was achieved. The value of the asymmetry parameter found was $\alpha = -3.5 \pm 1.2 \times 10^{-4}$. The parity violation effect is greatly enhanced in this case by the existence of many 1^- states close in energy to the 1^+ state (BS60a). The experimental result is at least roughly consistant with Michel's calculations.

There do not seem to have been any attempts to use polarized proton or deuteron beams to produce polarized nuclei. These beams have good polarization, usually 75% or better. However it is not known how well this polarization can be transferred to the target nucleus. Experiments which produce beta-radioactive nuclei where a beta asymmetry displays the nuclear polarization should establish the practicality of this technique.

The daughter nucleus of a beta decay can be highly polarized (≃25%) along the direction of motion of the emitted electron or positron. However to take advantage of this polarization, the beta and the subsequent gamma-ray must be observed in coincidence. To collect the large number of counts required to observe the gamma asymmetry,

fast coincidence techniques must be pushed to their maximum possible rates. Systematic effects can be expected to appear. Attempts have been made to observe the asymmetry of the 279 Kev gamma-ray of Tl^{203} with respect to the direction of the preceeding beta from Hg^{203}. The reported results are $\alpha = (+1.9\pm0.2)\times10^{-4}$ (LB69), $\alpha = (-0.6\pm0.8)\times10^{-4}$ (BH70), and $\alpha=(-2.7\pm0.8)\times10^{-4}$ (D71). At least two of these results are incorrect, possibly all three. It is possible these experiments are being influenced by inner bremstrahlung (see section II.C.4).

It is unnecessary to prepare a system of polarized nuclear spins if the detection system can somehow select gamma-ray transitions from a particular Zeeman level. This is possible with the Mössbauer effect (F62). In transitions with sufficiently long lifetimes (narrow line widths) an externally applied magnetic field can split the Zeeman levels sufficiently for their selection by a constant velocity filter. A search has been made for a gamma asymmetry in the 14.4 Kev transition of Fe^{57} using this technique (GG61). That work was only able to place an upper limit of 10^{-5} on the amplitude of the parity-admixed nuclear states, but improvements should be possible. The difficulty in this technique is finding cases where both the parity violation is enhanced and the conditions for the Mössbauer effect are satisfied.

C. Choice of Nuclear Transition

1. Size of Effect

In choosing which nuclear transition to test for a gamma asymmetry, the first consideration is the size of the effect expected. Thus we look for those cases where special features of the nuclear structure predict significant enhancement of the parity-admixed multipole transition. However this consideration must always be balanced against the practical questions of experimental method. It is also important that the enhancement be calculable with some well-established model of the nucleus in question. The parity-admixed amplitude in the 501 Kev gamma transition of Hf^{180} is experimentally seen to be greatly enhanced, but the usual nuclear models of Hf^{180} do not predict any enhancement—they predict retardation of both the normal and the parity-admixed multipoles. Thus observation of the asymmetry in Hf^{180} does show that a parity violation is occuring, but does not allow comparison of the effect seen with the predictions of the weak nucleon-nucleon potential.

A nuclear multipole transition is retarded when its rate is much less than the Weisskopf value for a fully-allowed single-particle transition of that energy (P62). Usually the single-particle model for that nucleus (shell model or Nilsson model) predicts zero for the transition amplitude of a retarded transition. An example is the 279 Kev transition of Tl^{203}, where the M1 transition amplitude between the single-particle levels $|2d_{3/2}>$ and $|3s_{1/2}>$ vanished identically. The fact that the M1 transition does occur (though with a retarded rate) represents the failure of the single-particle model to exactly describe the nuclear levels in question. However the fact that the M1 transition

is retarded, and other properties of the Tl^{203} nucleus (S66) shows that the single-particle assignments do correctly describe the gross features of the low-lying states of this nucleus.

The states which are parity-admixed to the $|2d_{3/2}>$ and $|3s_{1/2}>$ states Tl^{203} are $|2p_{3/2}>$ and $|2p_{1/2}>$. Now the transitions $|2p_{3/2}> \rightarrow |3s_{1/2}>$ and $|2d_{3/2}> \rightarrow |2p_{1/2}>$ are fully-allowed E1 transitions so we can make reasonable reliable estimates of their amplitudes. The enhancement factor is the ratio of these E1 emplitudes to the normal M1 amplitude for the $|2d_{3/2}> \rightarrow |3s_{1/2}>$ transition. That we cannot calculate the amplitude of the M1 transition in the single-particle model is no problem, because we can measure it. The M1-E2 mixing ratio in this transition has been measured by Coulomb excitation (MS58) and by centrifuge resonance flouresence (DM61). The weighted average of these measurements is $\delta = +1.43 \pm 0.07$. Note that the sign of the retarded M1 transition is known relative to the allowed E2 transition amplitude. The fully-allowed E2 amplitude for the $|2d_{3/2}> \rightarrow |3s_{1/2}>$ transition can be calculated in the same single-particle model used to calculate the E1 amplitude, and thus the relative sign of the E1 and M1 amplitudes can be found. This allows a determination of the sign of the weak potential from the sign of an observed asymmetry.

For the specific model used by Szymanski, we have for the ratio of the amplitudes, with $F = MR_0G''$,

$$\frac{M(E1)}{M(M1)} = \frac{e_1}{e} 2FMR_0 c \frac{1}{<e.s.|g_\ell \vec{\ell} + g_\sigma \vec{\sigma}|g.s.>} \cdot \left\{ <2d_{3/2}|\frac{\vec{r}}{iR_0}|2p_{1/2}><2p_{1/2}|\frac{\vec{\sigma}\cdot\vec{r}}{iR_0}|3s_{1/2}> \cdot \right.$$

$$\left. \cdot \frac{E^0(3s) - E^0(2p)}{E(3s_{1/2}) - E(2p_{1/2})} - <2d_{3/2}|\frac{\vec{\sigma}\cdot\vec{r}}{iR_0}|2p_{3/2}><2p_{3/2}|\frac{\vec{r}}{iR_0}|3s_{1/2}> \frac{E^0(2d) - E^0(2p)}{E(2d_{3/2}) - E(2p_{3/2})} \right\}$$

where e_1 is the effective charge for the E1 transition (P62). If the effect of the spin-orbit coupling had not been included, the two terms in the brackets would cancel. Szymanski finds $M(E1)/M(M1) = +279Fe_1/e$ and the predicted value of the asymmetry coefficient is $\alpha = (1.0\pm0.3)\times10^{-4}$ with Szymanski's estimate of the uncertainty. Errors as large as factors of two may have occured at several stages of the calculations.

In summary, a favorable case of enhancement is one where the normal transition is retarded and the single-particle model predicts that retardation, but also predicts that the parity-admixed transition should be fully allowed (and thus calculable). The retarded amplitude, which cannot be calculated in the single-particle model, should have been measured, including its sign relative to the allowed higher multipole (E2 in this case). These are the conditions for a large and calculable enhancement. Tl^{203} satisfies these as well as any case we know of.

2. Activation and Lifetime

Because the expected asymmetry is small, a large number of counts must be accumulated during the experiment. With an asymmetry coefficent of 10^{-4}, and a nuclear polarization of 30% (which we considered a pessimistic estimate when beginning this work), the expected fractional change in the count rate is 3×10^{-5}. We would like the statistical error to be one part in 10^5 or smaller, so we must accumulate at least 10^{10} counts. With the solid angles and efficiencies of the gamma-ray detectors, we require about 10^{12} decays to occur in the cell for a measurement of the asymmetry. This is an amount of activity not attainable with all isotopes. We require first, a production technique

by irradiation with neutrons, proton or deuterons with a large cross section, and second, a lifetime which is neither too short (so the sample can be brought to the apparatus and polarized before the activity is lost) nor too long (so that most of the radioactive isotope produced will decay in a reasonable amount of counting time). These dual requirements eliminate from consideration many isotopes which would otherwise be favorable cases for investigation.

The requirement of a large production cross section makes the use of charged particle beams for production unlikely. A high incident energy is required to overcome the Coulomb barrier and the production cross sections are usually less than a millibarn, though the elastic scattering cross sections are large. In contrast, the large capture cross sections for thermal neutrons are very attractive. Here the cross sections are on the order of barns and the available flux is high (up to 10^{14} neutrons/cm^2-sec).

There is one potentially important disadvantage to thermal neutron activation of the sample. It may be that the polarization technique employed limits the total amount of all isotopes of the element being studied which can be present in the sample (as is the case in optical pumping). Then the maximum activity attainable (without isotopic separation) is that maximum amount of the chemical element multiplied by the fraction of the sample which can be converted to the radioactive isotope. Even with large capture cross sections and high neutron fluxes, this fraction will not usually exceed 10^{-3}. If, on the other hand, the production technique had employed charged particles, then chemical separation would be sufficient to prepare a sample of high specific activity. We consider using proton irradiation of natural

thallium (30% Tl^{203} and 70% Tl^{205}) to produce Hg^{203} by a (p,n) reaction. However, the small size of the (p,n) cross section and the difficulty of separating a very small amount of Hg^{203} from a massive thallium target made this technique impractical.

The fraction of Hg^{202} which can be converted to Hg^{203} when the irradiation time is short compared to the half-life of Hg^{203} (47 days) is (neutron flux)×(capture cross section)×(duration of exposure). With exposure for one operating cycle (three weeks) of the Idaho MTR (thermal neutron flux of 3×10^{13} n/cm^2-sec) and the Hg^{202} capture cross section of 3.8 barns, a Hg^{203} fraction of $f_{203}\simeq2\times10^{-4}$ is produced. This sample, placed in an optical pumping cell with a volume of 50 cc and a mercury vapor pressure of 25 microns (corresponding to a temperature of 60°C), would have 6×10^{12} Hg^{203} atoms, which is a sufficient number for measuring an asymmetry of about 10^{-4}.

3. Polarization

The literature on optical pumping does not usually report values of the polarizations achieved. However pumping and relaxation times are given, and from these an estimate can be made of the achievable polarization. With a pumping time of 1 second and a relaxation time of 4 seconds (C61), a Hg^{203} nuclear polarization of 50% or better should be possible. It was unclear in the literature on the pumping of mercury vapor which factor limited the maximum density of vapor which could be pumped. Our estimate was that collisions of the excited state mercury atom (lifetime 10^{-7}sec) with other mercury atoms would be the limiting factor. This gave a maximum mercury vapor pressure of 25 microns, the value used in the previous section.

The asymmetry of the gamma-rays depends upon the polarization of the excited state of the Tl^{203} nucleus. This polarization equals the polarization of the Hg^{203} nucleus (T56) if there are no depolarizing effects from the beta-decay process. The electronic rearrangement following beta-decay produces very strong transient hyperfine interactions with the nucleus. In some cases the depolarization of the nucleus during the electronic rearrangement is essentially complete. This depolarization process is quite complex, so we do not try to calculate its effect in the case of $Hg^{203} \rightarrow Tl^{203}$. Rather we refer to the measurement of the 279 Kev gamma-ray circular polarization along the direction of motion of the emitted beta. Foldum has measured the circular polarization coefficient to be $A = -0.37 \pm 0.19$, consistent with the predicted value (neglecting depolarization effects) of -.028 (F63). Thus we conclude that transient hyperfine depolarization does not occur in Tl^{203}.

4. Systematic Effects

In the measurement of a small asymmetry, a multitude of systematic effects can produce spurious results. This has occured repeatedly in the search for parity violations in nuclei. With the proper pattern of data collection and analysis, these systematic effects can be minimized. Two symmetrically-placed gamma detectors are used (figure 2). The sensitivities of these counters should be adjusted so that their gamma counting rates from an unpolarized sample are equal. The count rates are then measured in counters 1 and 2 with the nuclear spins polarized along the +z axis (giving N_1^+ and N_2^+) and along the -z axis (giving N_1^- and N_2^-). Note that the change in spin direction is made by

rotating a linear polarizer in the optical pumping beam, and not by changing a magnetic field or anything else which might be expected to affect the gamma detectors. The value of the asymmetry effect observed is then

$$\Delta = (1/2)[(N_1^+ - N_2^+)/(N_1^+ + N_2^+) - (N_1^- - N_2^-)/(N_1^- + N_2^-)]$$

This method of analyzing the data causes cancellation of spurious changes in count rates.

We now ask if there is any systematic effect causing changes in the gamma rates of the two counters which would reverse direction with the change in nulear spin direction. Such an effect would not cancel out in the calculation of Δ. Since this effect is an asymmetric angular distribution which is correlated with a pseudo-vector (the nuclear spin), it violates parity. Such a parity-violating effect can only be produced by the beta-decay of the Hg^{203}. And indeed the asymmetrically emitted electrons can cause both internal and external bremstrahlung which is correlated with the nuclear spin direction. If the electrons from the beta-decay are stopped in a low Z material, then the inner bremstrahlung dominates over the external bremstrahlung (SG58). This is the case in optical pumping where the electrons stop in the cell walls, so we confine our attention to inner bremstrahlung.

Inner bremstrahlung is a radiative correction to the beta-decay process. The amplitude for the inner bremstrahlung process can be written as the product of two parts*. The first is the amplitude for

---

*This treatment of the inner bremstrahlung process ignores some higher order effects which are important in high Z materials

beta-decay to occur with the emission of an electron of energy W_e and momentum p_e. This amplitude must include the effect of the nuclear Coulomb field on the wave function of the emitted electron. The second term is the amplitude for the electron of energy W_e to give off a photon of energy E_γ and thus have a final energy $W = W_e - E_\gamma$ and a final momentum p. This amplitude can be calculated by a standard application of quantum electrodynamics. The calculation was first performed by Knipp and Uhlenbeck(KU36). The angular distribution is, with θ the angle between the photon and the final direction of the electron,

$$\frac{d\Phi}{d\theta} = \frac{\alpha p \sin\theta d\theta}{2\pi p_e E_\gamma} \left\{ \frac{W_e^2 + W^2}{W_e(W - p\cos\theta)} - \frac{1}{(W - p\cos\theta)^2} - 1 \right\},$$

where all energies are in units of mc^2. Upon integration over θ we obtain the gamma-ray energy spectrum,

$$\Phi = \frac{\alpha p}{\pi p_e E_\gamma} \left\{ \frac{W_e^2 + W^2}{W_e p} \log(W+p) - 2 \right\}$$

From the expression for the angular distribution we find that the asymmetry of the gamma-ray with respect to the final direction of the electron is equal to v/c of the electron.

The above expressions must be summed over the beta energy spectrum and angular distribution to obtain the total inner bremstrahlung spectrum and asymmetry. The beta spectrum is taken from standard tables (NBS52). The resulting energy spectrum of the inner bremstrahlung from the beta-decay of Hg^{203} was calculated by numerical integration and the results are shown in figure 3. The asymmetry of the inner bremstrahlung in this case is 0.41, but this figure is dominated by the low energy

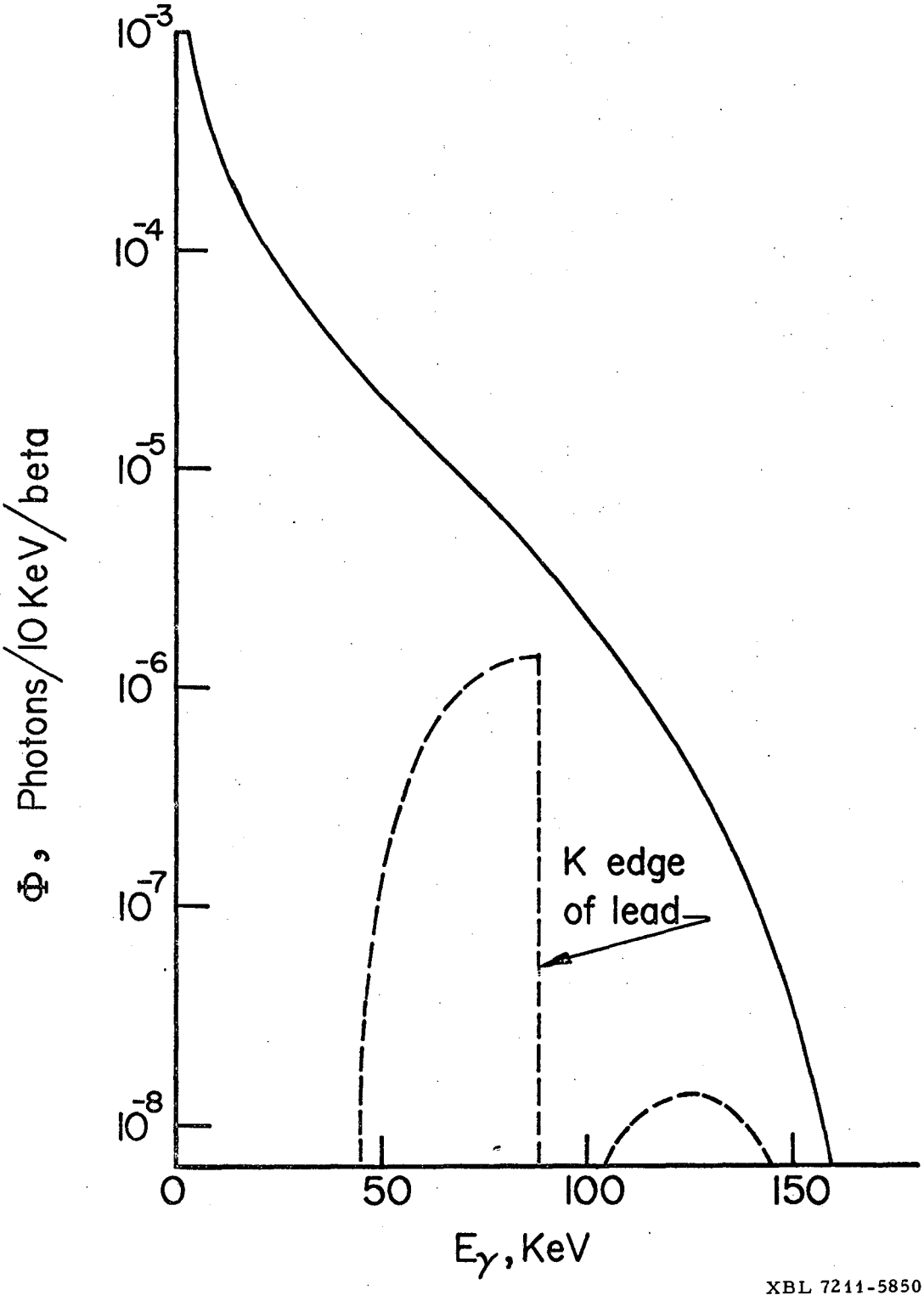

Figure 3. Calculated inner bremsstrahlung energy spectrum from the beta-decay of Hg^{203} before (solid line) and after (broken line) a 1 mm lead filter.

gammas. The infrequent but experimentally important high energy gammas have a slightly lower asymmetry of about 0.38.

The upper energy limit of the inner bremstrahlung spectrum in the case of Hg^{203} is 212 Kev, which is less than the energy of the gamma transition being observed. One would certainly set the gamma counters to accept only gamma-rays of energy close to 279 Kev, so the inner bremstrahlung would not be seen directly. However the copious low energy inner bremstrahlung photons provide a low level background in the counters which will change the number of 279 Kev gamma-ray counted. This sort of systematic effect is very difficult to avoid or correct for.

If an asymmetry is observed, then repeating the experiment with thin lead plates over the gamma-ray detectors will show if the asymmetry is due to bremstrahlung or is genuine. A filter which stops half of the 279 Kev gamma-rays highly attenuates the bremstrahlung (see figure 3). If the asymmetry is due to the 279 Kev gamma-rays, then the value of the asymmetry observed will be unchanged by the filter because both the numerators and denominators in the expression for Δ will be reduced by a factor of two. However if the asymmetry is due to bremstrahlung, then the numerators will be highly attenuated (because the differences in count rates are due to the low energy gamma-rays) while the denominators will only be reduced by a factor of two.

III. OPTICAL PUMPING OF Hg^{203}

A. Theory

1. Introduction

When the angular momenta of a sample located in a magnetic field are in thermal equilibrium with their environment, the Zeeman level populations follow the Boltzman distribution. Because of the smallness of the nuclear magnetic moment, significant equilibrium nuclear orientations can be achieved only at very high magnetic field intensities and very low temperatures. Kastler proposed the technique of optical pumping to achieve a non-equilibrium steady state of angular momentum orientation (K50,H72). In Kastler's scheme an atom is excited from its ground state to a higher energy state by absorption of an optical photon. In returning to the ground state, the atom will not necessarily return to the Zeeman level previously occupied, but will occupy the various Zeeman levels with probabilities determined by the matrix elements of the excitation and decay processes. In this way the ground state populations may be changed from their initial values. Interactions with the environment of the atom will tend to return these populations to thermal equilibrium, but with continuous illumination by optical resonance radiation, a non-equilibrium steady state will be achieved with the Zeeman populations significantly different than their equilibrium values.

When a sufficient hyper-fine interaction couples the electronic and nuclear moments of an atom it becomes possible to achieve nuclear spin orientation by optical pumping. The condition required is that the splitting between hyper-fine levels of the excited state be greater than

the natural line width of that state. Then the excited state is properly described by the total angular momentum of electrons plus nucleus, and the coupling is essentially complete.

Optical pumping was first observed by Brossel, Kastler, and Winter who used the sodium D resonance lines to optically pump an atomic beam of sodium (BKW52). Optical pumping of a diamagnetic atom was first observed by Cagnac who used the $^3P_1 \rightarrow {}^1S_0$ resonance line of mercury to optically pump the nuclear spins of mercury vapor in a cell (C58,C61). The history and present status of optical pumping has recently been reviewed by Happer (H72).

2. Pumping

Optical pumping of mercury has been achieved using the 185 nm transition $^1P_1 \rightarrow {}^1S_0$ (PN64) and using the 254 nm transition $^3P_1 \rightarrow {}^1S_0$ (C58,C61). Because 185 nm radiation is absorbed by atmospheric oxygen and is difficult to polarize, the 254 nm transition is more convenient and was chosen for this work. The lifetime of the $^3P_1$ state is $1.18 \pm 0.02 \times 10^{-7}$ sec (B59) so the natural linewidth is 0.85 MHz. The hyper-fine structure of the $^3P_1$ states of some mercury isotopes is shown is figure 4. The hyper-fine splittings are all greater than 5 GHz so the condition for optical pumping of the nuclear spins is well satisfied.

The doppler width of the 254 nm emission life from a mercury discharge lamp is about 1.7 GHz (MZ34). The doppler width of the 254 nm absorption life of mercury vapor at 400°C is 1.54 GHz. Both of these values are much greater than the natural linewidth so the emission and

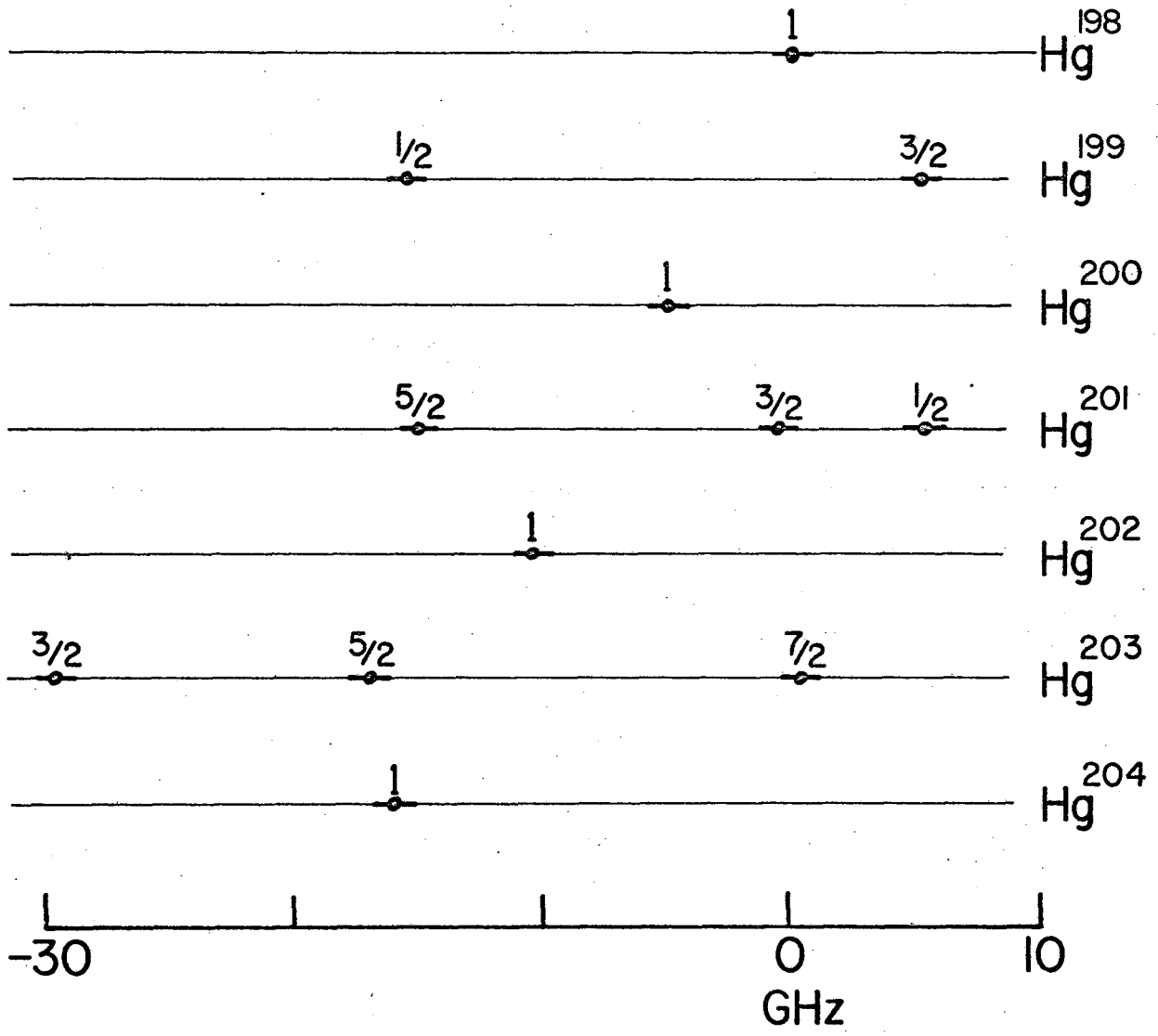

XBL 7211-5851

Figure 4. Hyper-fine structure of the $^3P_1 \rightarrow {}^1S_0$ resonance line of mercury isotopes.

absorption lineshapes are well approximated by gaussian distributions.

A practical requirement for the optical pumping of a radioactive isotope is that some other (stable) isotope have an emission line which overlaps an absorption line of the radioactive isotope. Then one can avoid using large quantities of radioactive material in the optical pumping lamp. There are two stable mercury isotopes which are convenient for optical pumping of Hg^{203}. The emission line of Hg^{198} overlaps the F=7/2 state of Hg^{203} and the emission line of Hg^{204} overlaps the F=5/2 state (TS64,R64). We have also optically pumped Hg^{201} using the overlap of Hg^{198} with the F=3/2 state and the overlap of Hg^{204} with the F=5/2 state.

The excitation rate of an atom exposed to isotropic radiation with a flat spectral distribution is just the Einstein B coefficient of the transition multiplied by the intensity of the radiation. However, when the spectral distribution is not flat and the absorption line is doppler broadened, the average excitation rate of an atom is found by integrating over the spectral distribution

$$p = \frac{2}{\Delta\nu_D}\sqrt{\frac{\ln 2}{\pi}}\,\frac{\lambda_0^2}{8\pi}\,\frac{g_2}{g_1}\int I(\nu)\exp[-2(\nu-\nu_0)^2\ln(2)/\Delta\nu_D^2]d\nu$$

where $\Delta\nu_D$ is the absorption doppler width, λ_0 is the wavelength and ν_0 the frequency of the transition, and g_2/g_1 is the statistical weight of the transition* (MZ34). This is the quantity I shall call the

---

*When the frequency distribution of the incident light overlaps only one of the hyper-fine levels then g_2 is the number of states in that hyper-fine level. Thus when pumping the F=3/2 level of Hg^{201} the statistical weight is 4/4= 1.

pumping rate. For the light intensity used in this work, the pumping rate is of the order of magnitude of 1 sec^{-1}.

When the atom occupies all Zeeman levels of the ground state with equal probabilities, the excitation rate is independent of the directionality or polarization of the incident light and equals the quantity p defined above. However when the Zeeman levels are unequally populated the excitation rate can differ from p. If the direction of the light is along the +z axis, and if the light is right circular polarized (helicity equal +1), then the atom can only make transitions to the excited state with $\Delta m = +1$. The rate of excitation from the $|F_1,m\rangle$ ground state to the $|F_2,m+1\rangle$ excited state will be $p|C(F_1,1,F_2;m,+1)|^2$ where C is a Clebsch-Gordan coefficient (R57), F_1 is the total angular momentum of the ground state, and F_2 is the total angular momentum of the excited state. The excited state will return to the various Zeeman levels of the ground state, $|F_1,m'\rangle$ with relative rates $|C(F_2,F_1,1;m+1,m')|^2$. If the incident light is not perfectly polarized, but instead is an incoherent mixture of right and left circular polarization (such as results from use of an imperfect linear polarizer with a quarter-wave plate), we define p to be the pumping rate due to right circular polarized light and q to be the pumping rate due to left circular polarized light. Then the rate for ground state $|F_1,m\rangle$ to go to ground state $|F_1,m'\rangle$ is

$$T_{m,m'} = p|C(F_1,1,F_2;m,+1)C(F_2,F_1,1;m+1,m')|^2 + q|C(F_1,1,F_2;m,-1)C(F_2,F_1,1;m-1,m')|^2 .$$

These rates, when combined with the corresponding terms for the

relaxation processes, will give the rate equations for the ground state Zeeman polulations.

3. Relaxation

The nucleus of a ground state mercury atom is well shielded from the environment by its spherically symmetric electron shells. Only after many collisions with other mercury atoms or the cell walls will the nuclear spin state change. The nuclear spin relaxation times for mercury isotopes range from seconds to minutes, in contrast to the millisecond relaxation times of paramagnetic atoms (A61). Cagnac has studied the slow nuclear spin relaxation of mercury vapor in quartz cells to determine the causes of that relaxation. First he finds that the presence of impurities (probably oxygen) causes rapid relaxation. Careful cleaning of the cell is essential for sucessful optical pumping (see procedures described in section III.B.). After cleaning the cells, he finds that the relaxation rate is inversely proportional to the size of the cell, i.e. proportional to the rate at which a mercury atom strikes the walls. Cagnac also finds that the relaxation time for Hg^{199} (100 sec in a cell at 300°C) is much longer than the relaxation time for Hg^{201} (1 sec in a cell at 350°C). These isotopes have nearly identical magnetic dipole moments (TS64), but Hg^{201} (nuclear spin 3/2) has an electric quadrupole moment and Hg^{199} (nuclear spin 1/2) does not. From these facts we conclude that the dominant relaxation mechanism for mercury isotopes with nuclear spin greater than one-half is electric quadrupole relaxation on the cell walls.

The hamiltonian for the interaction of an electric quadrupole

moment with an electric field gradient is

$$\mathcal{H}_Q(t) = \frac{eQ}{6I(2I-1)} \sum_{i,j} \frac{\partial^2 V(t)}{\partial x_i \partial x_j} \left(\frac{3}{2}(I_i I_j + I_j I_i) - \delta_{ij} I(I+1)\right)$$

where Q is the quadrupole moment of the nucleus, I is the nuclear spin, V is the electric field potential, and the partial derivitives are to be evaluated at the position of the nucleus (A61). It is convenient to rewrite the hamiltonian in terms of spherical tensors Q_m and V_m,

$$\mathcal{H}_Q(t) = \sum_m Q_m V_{-m}(t)$$

where

$$Q_0 = \frac{eQ}{I(2I-1)} \frac{1}{2} \left(3I_z^2 - I(I+1)\right)$$

$$Q_{\pm 1} = \frac{eQ}{I(2I-1)} \frac{\sqrt{6}}{4} \left(I_z I_\pm + I_\pm I_z\right)$$

$$Q_{\pm 2} = \frac{eQ}{I(2I-1)} \frac{\sqrt{6}}{4} I_\pm^2$$

and

$$V_0 = \frac{1}{2} \frac{\partial^2 V}{\partial z^2}$$

$$V_{\pm 1} = \frac{1}{\sqrt{6}} \left(\frac{\partial^2 V}{\partial x \partial z} \pm i \frac{\partial^2 V}{\partial x \partial z}\right)$$

$$V_{\pm 2} = \frac{1}{2\sqrt{6}} \left(\frac{\partial^2 V}{\partial x^2} - \frac{\partial^2 V}{\partial y^2} \pm 2i \frac{\partial^2 V}{\partial x \partial y}\right)$$

We treat the quadrupole interaction hamiltonian as a stationary random function with a finite correlation time τ_C (BPP48,A61). The average rate at which this interaction causes transitions from Zeeman level m' to Zeeman level m is

$$R_{m,m'} = \int_{-\infty}^{\infty} \overline{\langle m|\mathcal{H}_Q(0)|m'\rangle\langle m'|\mathcal{H}_Q(\tau)|m\rangle} \; e^{-i\omega_{mm'}\tau} \, d\tau$$

where the bar indicates an average over the various electric field gradients experienced by a mercury atom on the cell walls. If the time dependence of the correlation is approximated by an exponential, then the integral yields

$$R_{m,m'} = |\langle m|Q_{m-m'}|m'\rangle|^2 \, \overline{|V_{m-m'}(0)|^2} \, \frac{\tau_C}{1+(\omega_{mm'}\tau_C)^2}$$

In averaging over possible values of the electric field gradient, all orientations are taken to be equally likely. Since the quantities V_m are elements of a spherical tensor, the V_m for one orientation are related to the V'_m of another orientation by the rotation matrix,

$$V_m = \sum_{m'} \mathcal{D}^{(2)}_{m'm}(\Omega) \, V'_{m'} \, .$$

Then, by using the orthogonality of the rotation matrices (R57), we obtain from the average over orientations

$$\overline{|V_2(0)|^2} = \overline{|V_1(0)|^2} = \overline{|V_1(0)|^2} \, .$$

This quantity we shall call ξ^2. The transition rate is then written

$$R_{m,m'} = \left(\frac{eQ}{I(2I-1)}\right)^2 \frac{\xi^2}{4} |\langle m|I_\pm^2|m'\rangle|^2 \frac{\tau_C}{1+(2\mu B\tau_C)^2} \qquad \Delta m = \pm 2$$

$$R_{m,m'} = \left(\frac{eQ}{I(2I-1)}\right)^2 \frac{\xi^2}{4} |\langle m|I_\pm I_z + I_z I_\pm|m'\rangle|^2 \frac{\tau_C}{1+(\mu B\tau_C)^2} \qquad \Delta m = \pm 1$$

Cohen-Tannoudji has examined the relaxation of Hg^{201} and finds no dependence on magnetic field strength below 350 gauss (CT63). He concludes that the coherence time, τ_C, is less than 10^{-7} sec. Thus in this work (performed in fields of less than 10 gauss) the denominator can be replaced by one. The relaxation rate is determined

by $\xi^2\tau_c$. This quantity depends only upon the properties of the cell wall and the electron shell structure of mercury. It is independent of nuclear structure, and thus is the same for all mercury isotopes. We can determine $\xi^2\tau_c$ from the relaxation rate of Hg^{201} and use that value to predict the relaxation rate of Hg^{203}.

We write the transition rates in terms of the average rate, r, of quadrupole-induced transitions for an unoriented nucleus in analogy with the quantities p and q defined earlier.

$$R_{m,m'}(Hg^{201}) = \frac{r_{201}}{24} |\langle m|I_{\pm}^2|m'\rangle|^2 \qquad \Delta m = \pm 2$$

$$= \frac{r_{201}}{24} |\langle m|I_{\pm}I_z + I_zI_{\pm}|m'\rangle|^2 \qquad \Delta m = \pm 1$$

$$R_{m,m'}(Hg^{203}) = \frac{3r_{203}}{448} |\langle m|I_{\pm}^2|m'\rangle|^2 \qquad \Delta m = \pm 2$$

$$= \frac{3r_{203}}{448} |\langle m|I_{\pm}I_z + I_zI_{\pm}|m'\rangle|^2 \qquad \Delta m = \pm 1$$

The quantities r_{201} and r_{203} are related by the quadrupole moments of the nuclei and spin factors. The quadrupole moments have been measured by optical spectroscopy of the hyper-fine structure to be $Q_{203} = 0.40$ barn and $Q_{201} = 0.50$ barn (R64, TS64). Then we have $r_{203}/r_{201} = (56/81)(Q_{203}/Q_{201}) = 0.44$.

4. Rate Equations

We can now write the rate equations for the ground state Zeeman level populations,

$$\frac{da_m}{dt} = -a_m \sum_{m'} W_{m';m} + \sum_{m'} W_{m,m'} a_{m'}$$

Where $W_{m,m'} = T_{m,m'} + R_{m,m'}$ when the pumping light is on and $W_{m,m'} = R_{m,m'}$ when it is off. This set of equations can be solved analytically, but the solutions are too complex to be useful. It is more convenient for our purposes to solve the equations on a computer by Adam-Bashforth numerical integration (H62).

The general behavior of the solutions to the rate equations can easily be described. If the Zeeman populations are initially equal and the pumping light is turned on, the population change toward a steady state distribution with a time dependence which is a sum of exponentials with different time constants. The order of magnitude of the time constants is given by the reciprocal of the sum of the pumping and relaxation rates. The steady state populations will depend upon the relative values of the two pumping rates and the relaxation rate. If the pumping light is turned off, the populations return to a uniform distribution with a time dependence which is a sum of exponentials with time constants whose order of magnitude is given by the reciprocal of the relaxation rate. (however the relative amounts the different exponentials contribute to the total depends also on the previous pumping rates via the steady state populations which had been achieved.) The interesting quantities are not the populations themselves, but those observable quantities dependent upon the populations. Those quantities, discussed below, are calculated as part of the computer program.

5. Measurement of the Polarization

In the optical pumping of a nucleus with spin of one-half, one quantity, the nuclear polarization, suffices to describe the population changes produced and any measurement dependent upon the Zeeman populations acts as a measurement of the polarization. However when the nuclear spin exceeds one-half, 2I+1 different quantities are required to uniquely determine the Zeeman populations. One of these quantities is fixed by the condition $A_0 \equiv \sum_m a_m = 1$. As shown in section II.B. the asymmetry produced by the parity-violating nuclear force is proportional to the nuclear polarization of the I= 3/2 excited state of Tl^{203}. Since this polarization equals the polarization, $A_1 \equiv \sum_m m \cdot a_m / I$, of the Hg^{203} ground state, we must determine that linear combination of the Zeeman level populations. The most direct method would be to measure some other effect which depends upon the same linear combination. We are aware of only one other such effect, the asymmetry of the electrons emitted in the beta decay of the Hg^{203} nucleus. In a coulomb-approximation first-forbidden beta decay such as this, the asymmetry is well approximated by <v/c> multiplied by the nuclear polarization (W61). However the electrons emitted in this decay have small energies and are capable of penetrating only thin foils. The requirements for observing these electrons seem inconsistent with the other requirements for this experiment discussed in section III.B. Thus we must resort to an indirect determination of the Hg^{203} polarization.

The steady state solutions of the rate equations for the Zeeman populations express the populations in terms of just two quantities, the polarization of the pumping light and the ratio of the pumping

and relaxation rates. If we assume that model of the optical pumping process valid for our experiment, then the problem of determining the nuclear polarization is reduced to a measurement of the quadrupole relaxation rate. The strength of the electric quadrupole relaxation can be measured with either Hg^{201} or Hg^{203}.

The only quantity measured in the pumping of Hg^{201} was the attenuation of optical pumping light by the cell. Because of the line shapes of the pumping light and the absorbing medium, the attenuation does not vary exponentially with the path length in the cell. Instead the attenuation is found by an integral over the spectral distribution of the light, $I = \int I_0(\nu)\, \exp[-k(\nu)\ell]d\nu$, where I is the intensity of light transmitted by the cell, $I_0(\nu)$ is the incident spectral distribution, $k(\nu)$ is the absorption coefficient, and ℓ is the length of the cell. For a doppler broadened line the aborption coefficient is usually given by (MZ34)

$$K(\nu) = \frac{2}{\Delta\nu_D}\sqrt{\frac{\ln 2}{\pi}}\,\frac{\lambda_0^2}{\pi}\,\frac{g_2}{g_1}\,\frac{N}{T}\exp[-4\,\ln(2)(\nu-\nu_0)^2/\Delta\nu_D^2]$$

where N is the density of atoms and the other quantities were defined earlier. The quantitiy of interest here is the statistical weight, represented here by g_2/g_1. When the Zeeman levels of the ground state are unequally populated, the statistical weight is not g_2/g_1, but instead depends upon the population distribution and the polarization state of the light (D57,B65). For light circularly polarized parallel to the z axis, the effective statistical weight, S, is given by the sum over the Zeeman populations of the ground state,

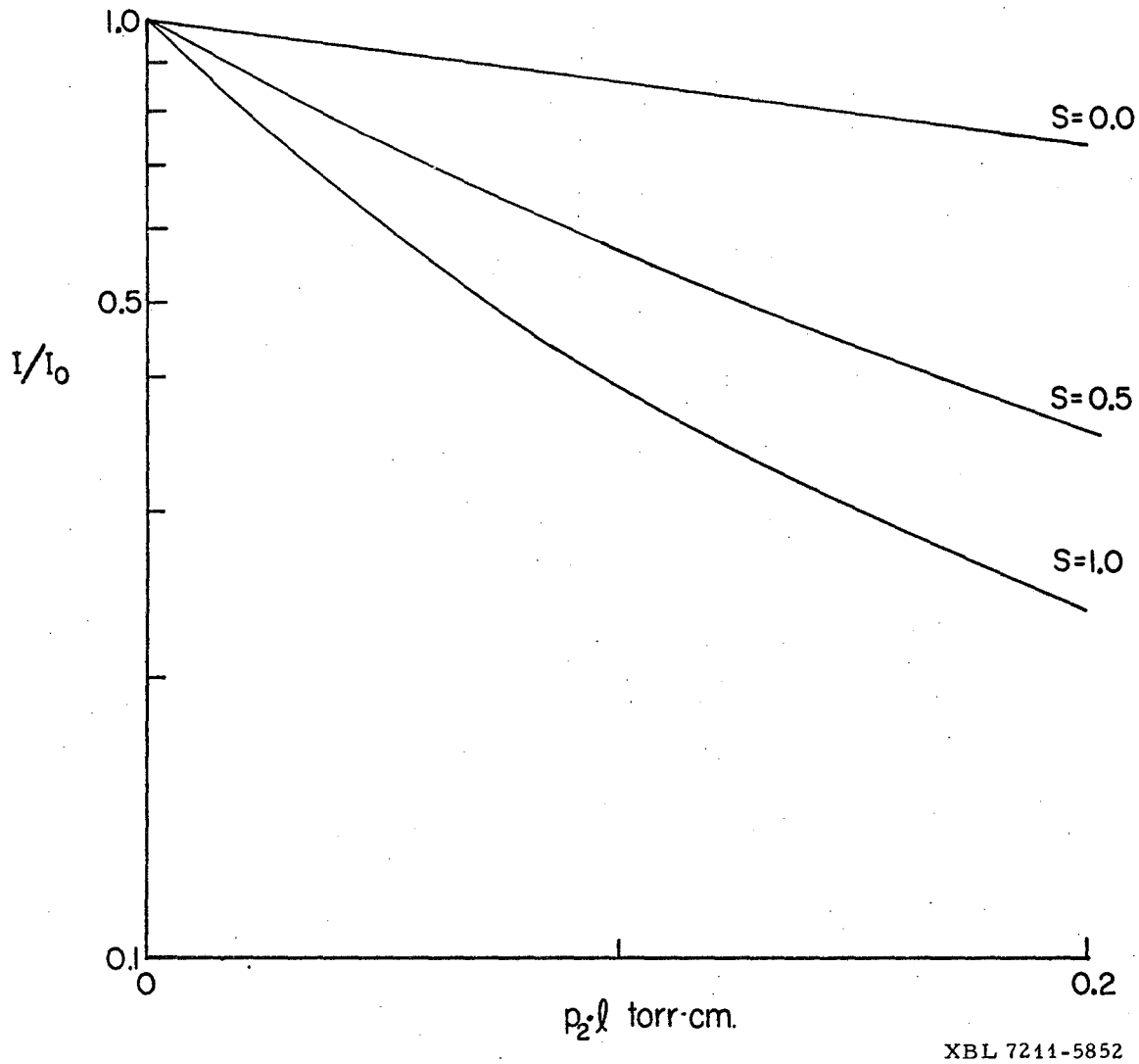

Figure 5. Calculated decay of intensity of Hg^{198} resonance light passing through the optical pumping cell.

$$S = \sum_m a_m |C(F_1,1,F_2;m,+1)|^2 .$$

The fraction of light transmitted by a cell of length ℓ containing mercury vapor at a pressure p_2 was calculated by numerical integration over the doppler lineshape with various values of S. Some results of the calculation for light from an enriched Hg^{198} lamp passing through a cell filled with enriched Hg^{202} at 400°C are shown in figure 5. The absorption with S= 0 is due to the 0.06% of Hg^{198} present in the enriched Hg^{202} sample. The additional absorption with S>0 is due to the 1.38% of Hg^{201}. The value of S can be found from the measured light transmission of the cell by interpolation of the results of the numerical integration.

When the optical pumping light is on, S changes from g_2/g_1 to a value given by the above expression with the steady state populations. By turning the light on suddenly with a faster shutter, we can measure the time, τ_L, for S to change halfway to its steady-state value. By chopping the light off for periods of varied duration, we can observe the dark relaxation of S toward the value g_2/g_1 and thus measure the time, τ_D, for S to relax halfway. The dimensionless quantities $p\tau_L$, $p\tau_D$, and the steady state value of S are calculated by the rate equation computer program as functions of q/p and r/p. Some of the results of the program with the value q/p= 0.1 are shown in figure 6. Because the measurable quantities overdetermine the two parameters, these measurements also serve as a test of the rate equation model.

In the densities of Hg^{203} employed in this work, the Hg^{203} was detectable only by its radioactivity. Because the beta-rays are absorbed by the walls of the optical pumping cell, only the gamma-rays

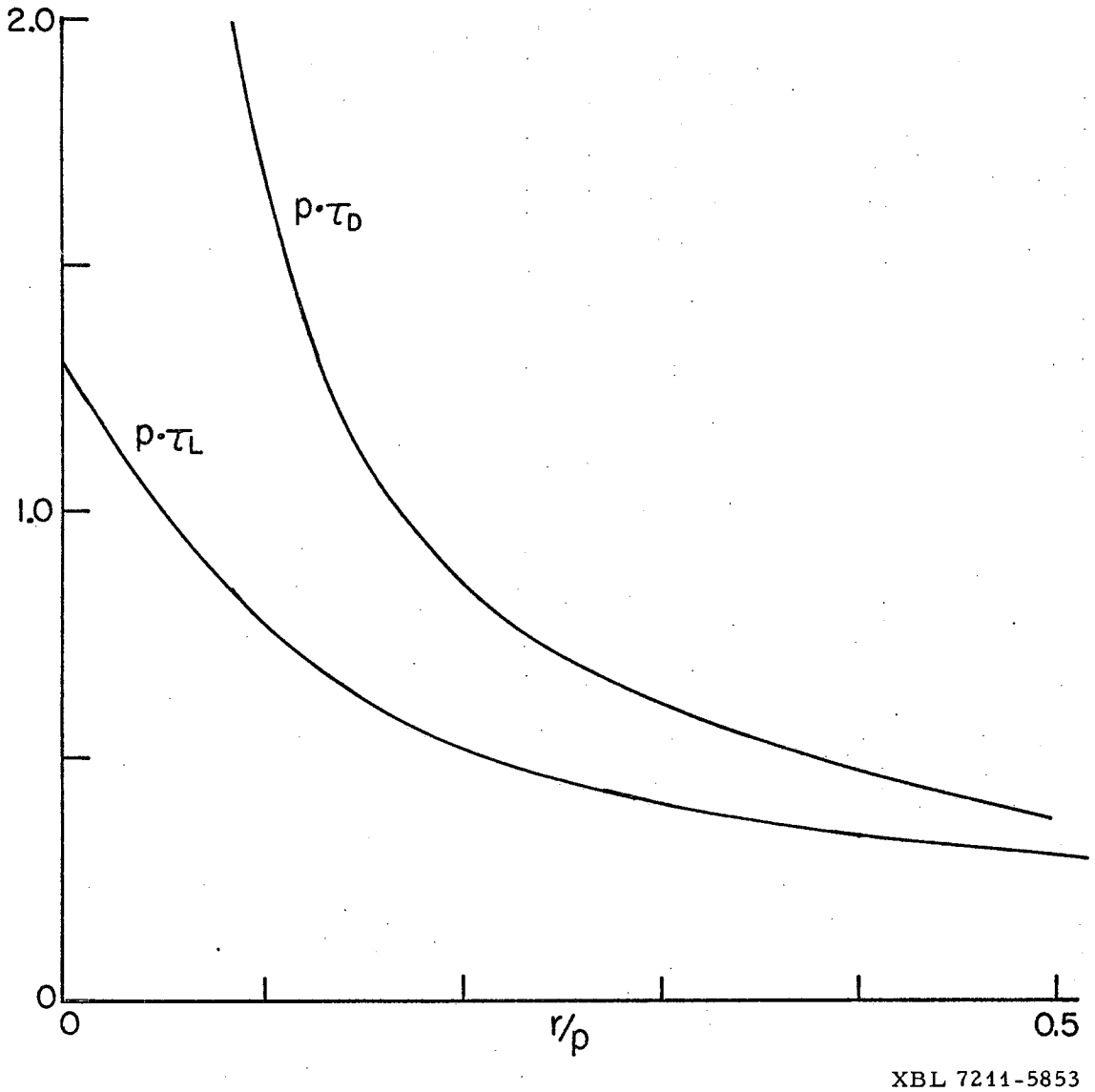

Figure 6a. Quadrupole relaxation model prediction of light and dark transient times as function of relaxation rate.

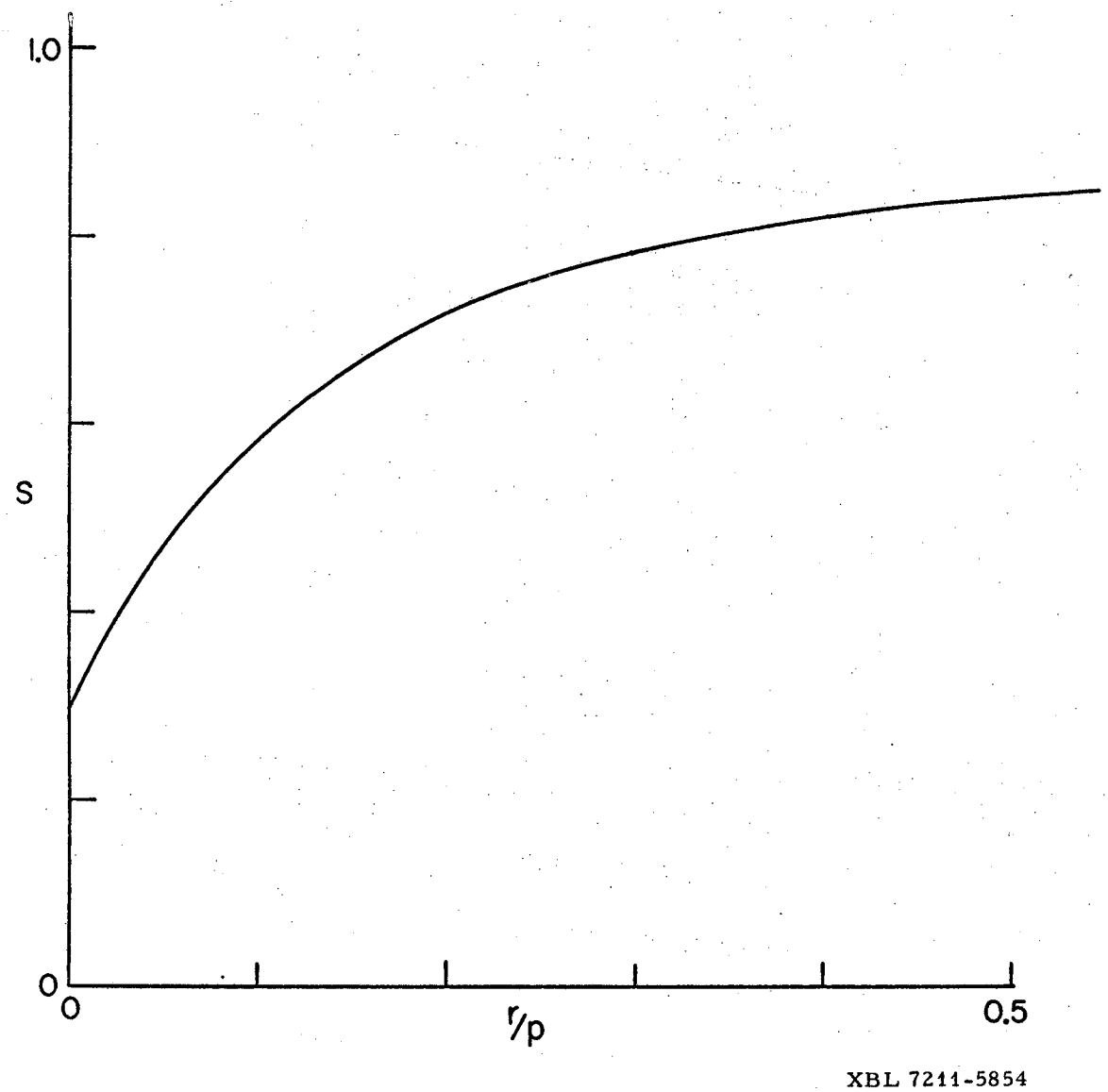

Figure 6b. Quadrupole relaxation model prediction of effective statistical weight as function of relaxation rate.

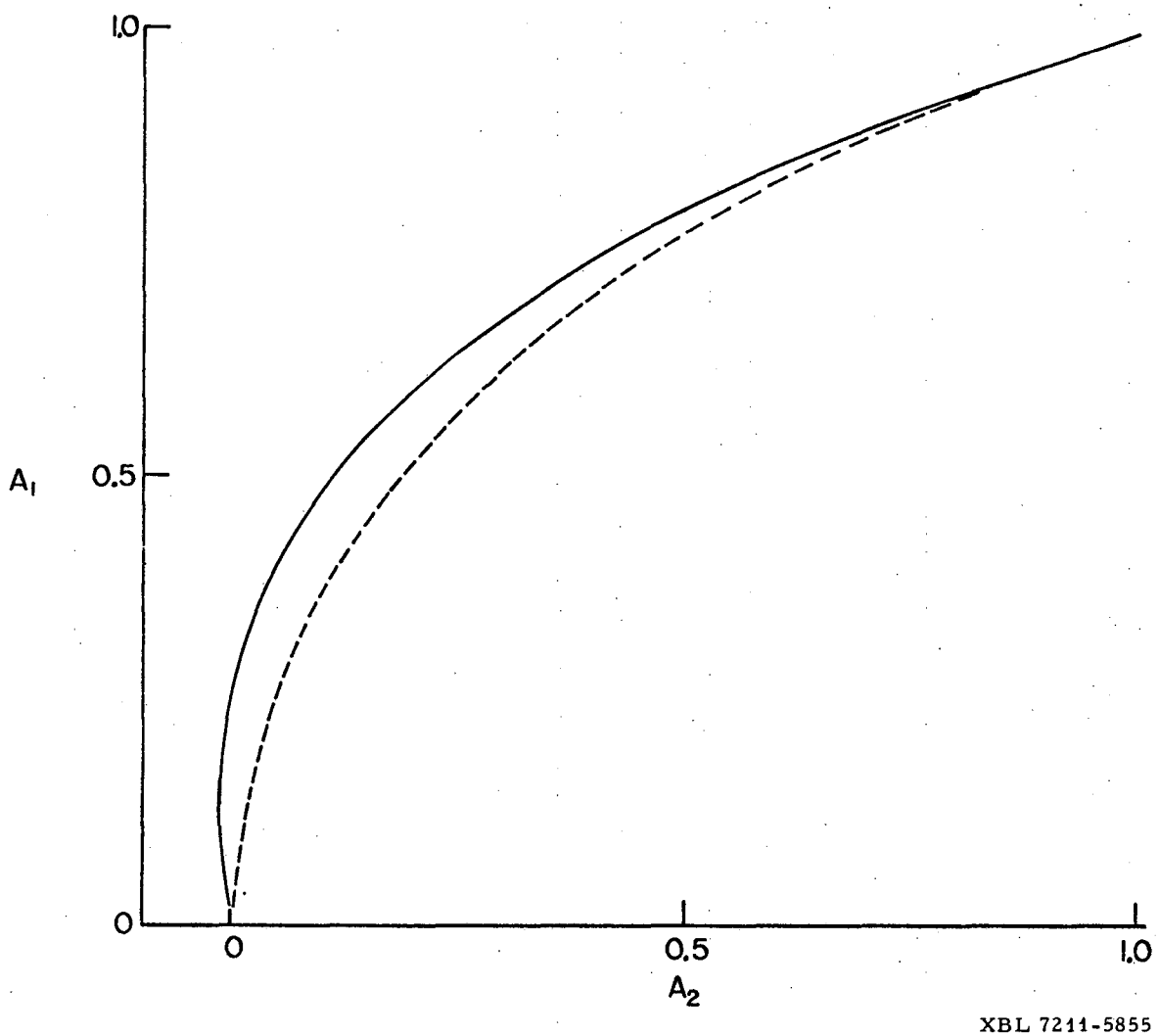

Figure 7. Relationship between A_1 and A_2 in the quadrupole relaxation model (solid line) and in the Boltzman distribution (broken line).

are available for determination of the Zeeman level populations. The gamma-rays are characterized by their angular distribution and their circular polarization measured along the optical pumping axis.* Using the value $\delta = 1.43$ for the M1-E2 mixing ratio, the angular distribution is $\frac{1}{2}W(\theta) = 1.0 - 0.985A_2P_2(\cos\theta)$ and the circular polarization of gamma-rays emitted in the +z direction is (TC53,HTG54) $P_\gamma = 1.21A_1 - 1.19A_3$ where

$$A_1 = \{\Sigma m b_m\}/I$$

$$A_2 = \{3\Sigma m^2 b_m - I(I+1)\}/(2I^2-I)$$

$$A_3 = \{5\Sigma m^3 b_m - (3I^2+3I-1)\Sigma m b_m\}/(2I^3-3I^2+I) \ .$$

The A_k are normalized so that all A_k equal one when $b_{m=I} = 1$ and $b_{m\neq I} = 0$. The b_m are the Zeeman populations of the excited state of Tl^{203}, which are easily expressed in terms of the Zeeman populations of the Hg^{203} ground state.

Measurement of the change in the gamma counting rate seen along the optical pumping axis when the optical pumping light is turned on, measures that linear combination of the populations which appears in A_2. However only within the context of a specific model of the optical pumping process can A_2 be related to the polarization, A_1. The relationship between A_2 and A_1 for the quadrupole relaxation model discussed above is shown in figure 7 (with $q/p = 0$). Also shown is the relation-

---

*This circular polarization observed along a previously defined axis does not represent a violation of parity.

ship between A_2 and A_1 when the Zeeman populations follow a Boltzman type of distribution ($b_m \propto \exp[-\beta m]$). At small polarizations, the ratio of A_2 to A_1 is strongly model dependent.

The gamma-ray polarization depends upon A_1 and A_3 with nearly equal coefficients, but for small polarizations A_3 is much less than A_1. In the quadrupole relaxation model, A_3/A_1 is less than 0.1 for $A_1<0.5$. Thus when the polarization is fairly small, the gamma-ray polarization determines the nuclear polarization to about 10% accuracy.

B. Apparatus

1. Oven

Preliminary optical pumping experiments were performed with commercially supplied Hg^{203} of low specific activity in a quartz cell integral with a glass vacuum pumping stand. This temporary system had several serious faults. Mercury in the sidearm reservoir produced a large background counting rate only partially eliminated by lead bricks stacked around the glass system. Unless the cell was completely valved off from the vacuum system, the mercury slowly migrated to the liquid nitrogen traps. However with the cell valved off, condensed mercury on the walls of the cell caused an undesirable background to the mercury vapor. The heating tape we wrapped around the cell failed to heat the cell above 150°C. No change in the angular distribution of gamma rays (to about 1% accuracy) was observed in these experiments.

These preliminary experiments and the literature on optical pumping of stable mercury isotopes (see section III.A.) suggested criteria for a system to optically pump radioactive mercury. The total amount of mercury in the system should be kept to a minumum and the sidearm reservoir should be well shielded from the gamma detectors. The pressure of mercury vapor in the cell must be kept below the equilibrium mercury vapor pressure corresponding to the temperature of the cell walls. This requires separate temperature control of the cell and the reservoir. The heating system for the cell should be capable of achieving temperatures up to 400°C to minimize depolarization on the cell

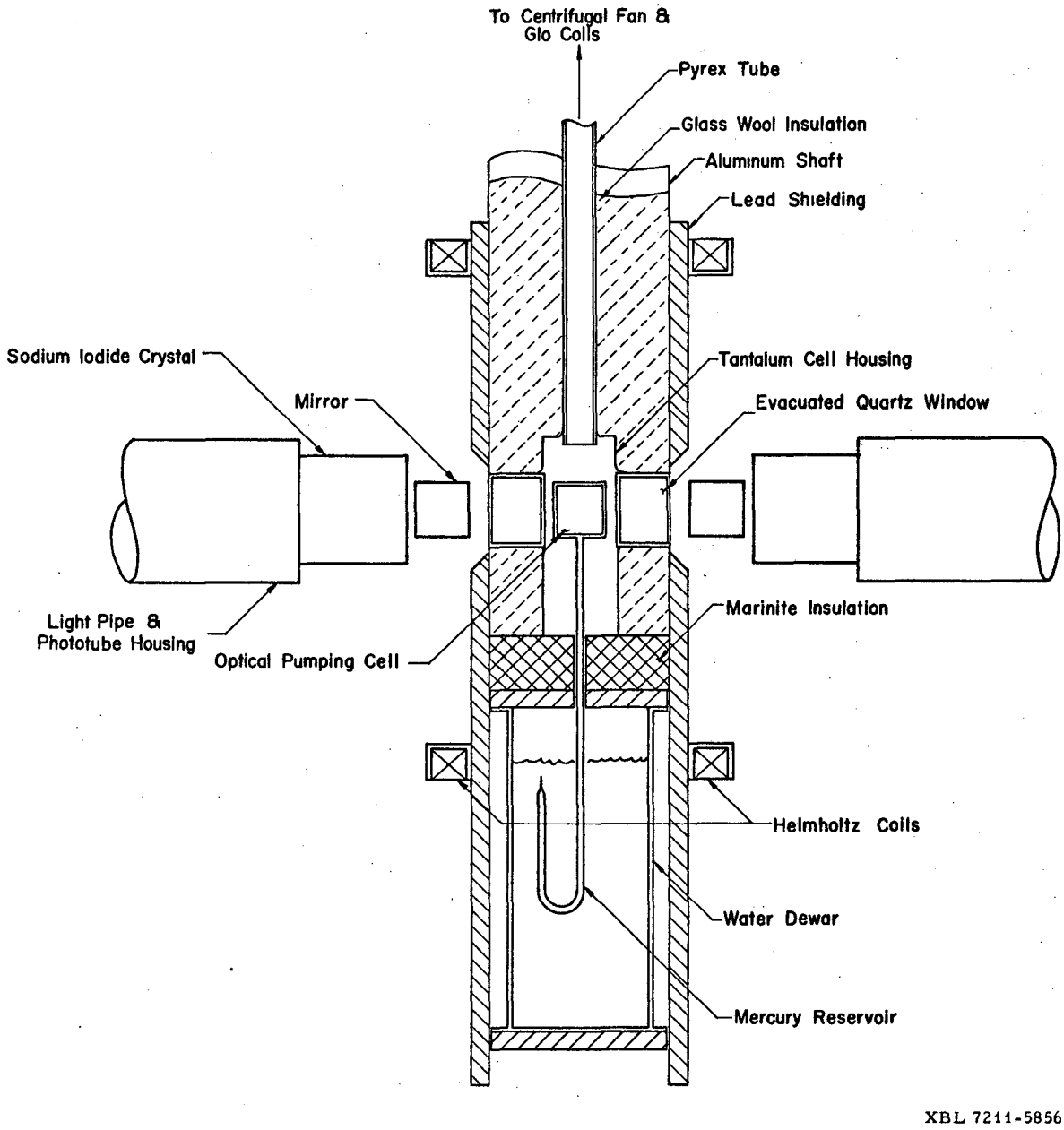

Figure 8. Diagram of the final version of the optical pumping system.

walls (C61). The cell and reservoir should be isolated from any cold traps or vacuum pumps. The gas flow conductance between the cell and reservior should be small enough to make the sitting time of a mercury atom in the bulb longer than the nuclear spin relaxation time. With these criteria in mind we designed and constructed an optical pumping system. (See figure 8.)

The cell could easily be heated to high temperatures by placing electrical heating coils in close proximity to the cell, but we were concerned that the inhomogeneous magnetic field from these coils could cause depolarization. We decided upon a recirculating hot-air system to heat the cell. A centrifugal fan was mounted on a thin-wall stainless tube. The tube was suspended between ball-bearings located outside the oven assembly and was driven at 1670 rpm by an ac motor. The centrifugal fan drew air up a pyrex tube from the cell housing and blew the air into a chamber containing four Glo-coil electrical heaters. The Glo-coils, powered by a Variac, heated the air with up to 2640 watts of power. From this chamber the air moved down another pyrex tube to the cell housing. Thus the air moved around in a closed loop, being heated by the Glo-coils, and in turn heating the optical pumping cell. The centrifugal fan and Glo-coils were mounted in a stainless-steel box which was insulated by 5 cm of glass wool and enclosed in an aluminum outer box. The two pyrex tubes leading to the cell housing were also insulated by glass wool and enclosed in an aluminum shaft. The ac motor and the Glo-coils were 120 cm away from the cell housing and far outside the magnetic field of the Helmholz coils.

The cell housing was contructed from 6 mil tantalum sheet and

insulated with glass wool. Evacuated and sealed-off cylindrical quartz cells made ultraviolet-transmitting windows of low thermal conductivity. There were large windows (diameter 5 cm and height 4 cm) on the front and rear of the housing for the optical pumping beam and small windows (diameter 2.5 cm and height 4 cm) on the sides for observation of the scattered resonance light. A thermocouple, located in the pyrex tube leading from the cell housing up to the centrifugal fan, measured the cell temperature. This system easily and dependably heated the cell to the desired temperature of 400°C.

The gamma-ray counting rate depends critically upon the temperature of the mercury reservoir because of the exponential dependence of equilibrium vapor pressure on temperature.* Fluctuations in reservoir temperature cause statistical variation in the gamma counting rate and must be minimized. We used a recirculating contant-temperature bath (Haake model FJ) to control the reservoir temperature. The manufacturer claims a stability of 0.01°C for this unit. Water was pumped from the constant-temperature bath into a dewer located under the cell housing. The sidearm reservoir of the cell hang down into this dewer. Overflow water from the dewer returned to the constant-temperature bath. This system was capable of controlling the reservoir temperature between room temperature and 100°C.

For our later experiments we wanted to cool the reservoir below

---

*At 40°C a change in temperature of 0.5°C causes a 4% change in vapor pressure (N63).

room temperature. The dewer was lined with styrofoam insulation and filled with a glycerol and water mixture.* The water inlet and outlet pipes were replaced with a coil of copper refrigeration tubing. A standard refrigeration compressor pumped liquid Freon-12 to an expansion valve mounted on the underside of the dewer. The expanding gas, flowing through the copper coil, chilled the glycerol-water mixture. This was capable of cooling the reservoir to -25°C, even with the cell housing at 400°C, but the temperature stability of the reservoir was poor.

The lead shielding was designed to enclose the mercury reservoir as completely as possible. With the dewer in place, the reservoir was surrounded by a 1.3 cm thickness of lead except for openings for the pyrex tube leading up to the cell and for the dewer inlet and outlet. The lead shielding extended upward to 20 cm above the midline of the cell, except for two 5 cm diameter openings facing the gamma-ray detectors.

The magnetic field for optical pumping was produced by a pair of Helmholtz coils. Each of the coils consisted of 36 turns of #12 wire wound on a 36 cm diameter form. The coils, spaced 18 cm apart, produced a field at the cell of 1.8 gauss per ampere of current. They were normally operated at 5 A, producing a field of 9 gauss parallel to the optical pumping beam. The magnetic field (including the Earth's field) varied only a few milligauss over the volume of the cell.

---

*The freezing point of this 70% glycerol and 30% water mixture is -38.9°C (CRC61).

2. Cells

The cylindrical optical pumping cells (diameter 3.8 cm and length 3.8 cm) were constructed of Suprasil-grade fused quartz. The optical pumping light passed parallel to the axis of the cylinder through the 0.03 cm thick end plates. A 3.8 cm length of 0.01 cm inner diameter quartz capillary was sealed onto the side of the cylinder. This constriction reduced the gas flow conductance out of the cell and lengthened the sitting time of a mercury atom in the cell. The molecular flow conductance for a cylindrical tube is $F = 30.48a^3\sqrt{T}/(\ell\sqrt{M})$ liters/sec where a and ℓ are the radius and length of the tube in cm, M is the atomic mass in grams/mole and T is the temperature in °K (D49). With the dimensions of this capillary, the conductance of mercury vapor at 600°K is 1.7 cc/sec. The volume of the cell was 43.4 cc, so the sitting time was 25 sec. This is longer than the depolarization time of mercury nuclei with spin greater than one half (C61).

The quartz capillary was joined by a graded seal to 8 mm ID pyrex tubing. The tubing extended down 30 cm, around a U-bend, and up 5 cm to the point where the cell had been separated from the vacuum system after being filled. The U-bend, during operation the coolest part of the cell system, was the mercury reservoir and its temperature determined the mercury vapor density in the cell.

The density of mercury vapor in the cell differs from the density in the reservoir because the two are at different temperatures. In a steady state the net flow of mercury through the capillary is zero, and it is this criteria we must use to relate the atomic densities in the two regions. If the two regions were connected by an aperture in an

infinitely thin wall, then in a steady state kinetic gas theory gives for the ratio of pressures $p_1/p_2 = \sqrt{T_1/T_2}$ (R79). This result is usually assumed valid for any geometry of connection between regions, but the ratio of pressures for geometries similar to ours actually varies by several per cent from $\sqrt{T_1/T_2}$ (EH65). We use the thin-wall aperture result as an approximation. The ratio of atomic densities is then $N_1/N_2 \simeq \sqrt{T_2/T_1}$.

The vacuum system used for preparing the optical pumping cells was pumped by a liquid nitrogen trap, oil diffusion pump, and mechanical pump. The system included a needle valve for leaking spectroscopic grade helium into the cell and a manometer for reading pressures in the range 0 to 20 torr. In filling a cell with stable mercury, the pyrex sidearm of the cell was joined to a vertical section of pyrex tube which was closed at the bottom and joined to a small pyrex funnel at the top. A pyrex tube from the side of this vertical section was joined to the vacuum system.

In the initial cleaning process, the funnel was sealed with a rubber stopper and the cell was evacuated to about 10^{-5} torr. The cell and pyrex sidearm was heated with a hand-held torch to drive off volatile contaminents. The cell was then let up to atmospheric pressure, the rubber stopper removed, and a small drop of metallic mercury dropped through the funnel to the bottom of the vertical section. The funnel was then pulled off and its connection to the system sealed with a gas-oxygen torch. A dewer of liquid nitrogen was then raised up under the vertical section to prevent migration of the mercury and the system was again evacuated for the second cleaning process.

In the second cleaning process the cell and sidearm were heated with a hand-held torch while being pumped by the vacuum system. Finally the cell was cleaned by running a gaseous discharge of helium in the cell. The cell was valved off from the vacuum system and spectroscopic grade helium admitted until a pressure of 3 torr was reached. Two parallel metal plates, forming a capacitor, were positioned around the cell and connected to the output of a radio frequency oscillator (about 15 watts of power at 5 MHz). A discharge in the cell was started with a tesla coil and allowed to run overnight. The glow of the discharge was examined with a hand-held spectrometer. As the discharge continued, molecular bands appeared and the characteristic helium lines waned. The cell was then evacuated, refilled with fresh helium, and the discharge restarted. This was repeated until the spectrum persistently showed only the helium lines. The cell was then evacuated for the transfer of mercury. The dewer of liquid nitrogen was moved from the vertical section to U-bend below the cell. The drop of mercury in the vertical section was gently warmed with a torch until condensed mercury was seen in the U-bend. The cell and sidearm were then pulled off the vacuum system with a gas-oxygen torch. The cell was then ready for mounting in the optical pumping system.

In filling a cell with radioactive mercury, we tried to avoid putting more than the required amount of mercury into the reservoir. We did this by first sending the Hg^{202} sample to the Berkeley TRIGA Mark III reactor for a short exposure. This produced a small concentration of Hg^{203} in the sample which served as a tracer. This sample was transfered to thin quartz tubes (0.1 cm outer diameter, 2 cm long) in a

manner similar to the filling of a cell described above. The amount of mercury in each tube was determined by measuring the gamma-ray activity with a small sodium iodide detector. The amount of mercury in each tube was adjusted to the desired amount and the tube was pulled off the vacuum system. The tubes were then sent to the reactor for final activation. After activation, one of the quartz tubes and a pyrex-enclosed iron slug were put in the U-bend of an optical pumping cell. The cell was cleaned and pulled from the vacuum system in the manner described above. The iron slug was lifted with a hand-held permanent magnet and dropped on the quartz tube, thus breaking it open and releasing the mercury into the cell.

One of the quartz tubes containing Hg^{203} was sent from the reactor to the high-current mass spectrometer at the Argonne National Laboratory for separation of the Hg^{203} from the stable mercury isotopes. In this spectrometer the ions are collected by impact on a strip of aluminum foil. The mercury ions are buried deep inside the aluminum and cannot escape until the aluminum is melted. The aluminum strip was returned to us. We prepared a cell on a glass system similar to that described above for use with stable mercury isotopes. The aluminum strip was dropped into the glass system, the system was sealed and evacuated, and the cell was cleaned. The mercury was transferred into the cell by heating the section holding the aluminum strip until the aluminum melted and the mercury was released. The mercury was collected in the U-bend of the cell by cooling that part with liquid nitrogen.

3. Optical System

The optical system consisted of a mercury electrodeless-discharge lamp, a linear polarizer and quarter-wave plate to circularly polarize the light, front surface mirrors to direct the light through the pumping cell, and a phototube to monitor the light transmitted by the cell.

The mercury discharge lamp used in our first experiments was a commerical unit produced by General Precision Systems. This was the most intense mercury resonance lamp free of self-reversal that we could find. According to the manufacturer, the 254 nm emission line has a doppler line shape corresponding to a temperature of 800°K. The discharge occured in a 1 cm diameter spherical quartz bulb containing a small drop of mercury and filled with argon buffer gas to several torr of pressure. The quartz bulb was held in the coil of a 5 MHz oscillator. The oscillator employed one 2N3553 RF power transistor in a class C mode of operation. The discharge was started with a tesla coil and the DC supply voltage adjusted to give the desired intensity of discharge. A stream of air cooled the quartz bulb.

The output of the discharge lamp was measured by an Eppley thermopile. The 254 nm line was separated by an interference filter (20 nm bandwidth, 12% transmission at 254 nm) supplied by Baird-Atomic. The General Precision lamp had no reflector (the bulb was suspended just above the printed circuit board by the oscillator coil) so the light intensity decreased approximately with the square of the distance from the lamp. The measured intensity of the 254 nm line at a distance of 8 cm from the lamp was 0.12 mW/cm^2. This corresponds to a total

output by the bulb of 90 mW in the 254 nm line.

After several preliminary attempts at optical pumping, we desired a more intense pumping light. We tried using a spherical quartz condenser lens (7.5 cm diameter, f:1) to direct the light into the cell, but this gave no great improvement. We then tried putting a metal reflector around the bulb to focus the light, but all the metal reflectors tried changed the coupling of the oscillator coil sufficiently to prevent oscillation. Finally a new lamp was designed and built. A parabolic reflector was machined out of lucite and polished. A film of aluminum several hundred nm thick and a protective coating of magnesium oxide were evaporated onto the lucite surface to make an ultra-violet mirror. The skin depth of aluminum for 5MHz radiation is approximately 40 microns, so the thin film did not affect the operation of the oscillator. Cooling air blew over the quartz bulb from the holes in the reflector for the coil leads. The circuit was adapted from that of the General Precision lamp and the same bulbs were used. The new lamp gave an intensity at 23 cm distance of 0.56 mW/cm^2. This was about 30 times the intensity of the General Precision lamp at the same distance. Total output of the bulb was the same. The flux of 254 nm photons at the cell (without polarizers in place) was about 0.7×10^{15} photons/cm^2-sec.

The General Precision lamp was supplied with several bulbs containing the natural mixture of mercury isotopes. We obtained

enriched samples* of Hg^{198} and Hg^{204} from the Oak Ridge National Laboratory and had General Precision prepare several bulbs containing these enriched mercury isotopes. Attempts at making our own bulbs were unsuccessful.

The linear polarizer was a 5 cm diameter disc of type PL-40 polarizer (produced by Polacoat Corp.). The typical transmission for 254 nm light was 37% for light polarized parallel to the pass axis and 2.3% for light polarized perpendicular to the pass axis (MN61). This polarizer, when combined with a perfect quarter-wave plate, would produce a beam of 88% circular polarization. The polarizers slowly deteriorated in the intense ultra-violet light and were replaced occasionally.

Commerical quarter-wave plates for ultra-violet are available, but only with small apertures. For large apertures (5 cm) other techniques must be used. We chose to use the photoelastic effect of fused silica (K57,M68). Fused (non-crystaline) silica is normally optically inactive, but when put under stress it displays optical activity. A vise was machined from a brass plate to hold a 5cm×5cm×0.6cm fused silica plate. A screw pressed upon a brass bar which distributed the pressure across one end of the silica plate. Teflon pads were placed around the silica plate to assure the stress was uniform. The vise was adjusted by putting it between crossed polarizers in a beam of

---

*The Hg^{198} sample contained 94.4% 198, 3.9% 199, 0.9% 200, 0.3% 201, 0.4% 202, and 0.1% 204. The Hg^{204} sample contained 3.0% 198, 4.9% 199, 6.7% 200, 3.9% 201, 11.0% 202 and 70.6% 204.

254 nm light and adjusting the screw until the transmission of light through the system no longer varied as the second polarizer was rotated about the axis of the light beam. The transmission of the quarter-wave plate for 254 nm light was 85%. The loss was due mostly to surface reflections.

One must know the helicity of the optical pumping light to deduce the sign of any observed asymmetry of gamma-rays. Thus one must identify the fast and slow axes of the quarter-wave plate. The axes can be identified by comparision with a previously labeled quarter-wave plate, but several commercially supplied and labeled quarter-wave plates borrowed from other researchers were not unanimous in their identification of the fast and slow axes. We decided that the most unambiguous procedure was to compare the quarter-wave plate with circularly polarized light whose handedness can be deduced from simple physical principles. Such light results from linear polarized light obliquely reflected from a metal surface. Because of the finite skin depth of the metal, light beams polarized parallel and perpendicular to the surface experience different phase lags during reflection (see Appendix I). When the linear polarization vector is tilted to the right (as seen when looking toward the source) and the angle of incidence has the correct value (dependent upon the skin depth of the metal and the wavelength of the light) then the reflected light is left circularly polarized. By performing this experiment we concluded that the direction of application of pressure on the silica plate becomes the slow axis of the quarter-wave plate.

The mirrors which direct the light throught the pumping cell were made by evaporating aluminum on the front surface of thin (0.8 mm) pyrex plates. The mirrors were made thin to minimize the scattering of gamma-rays. No protective coating could be used because thin dielectric layers alter the polarization state of light in oblique reflection.

The light transmitted by the cell was monitored by a 1P28 phototube wired as a photodiode (all dynodes shorted to the anode). The window of the phototube was blocked down to a square centimeter opening and covered with an interference filter (20 nm bandwidth, 6% transmission at 254 nm). The phototube sensitivity was calibrated against an Eppley thermopile.

4. Gamma Detectors

Sodium iodide (thallium doped) crystals (Harshaw type 12A12) were chosen as the gamma detectors for their high detection efficiency. The efficiency of the cylindrical crystal (diameter 7.6 cm and length 7.6 cm) for the 279 Kev gamma-ray of Tl^{203} is 85% in the compton peak (B64). Each detector crystal was joined by optical coupling grease to a 60 cm long lucite light pipe which was joined to an RCA 8575 photomultiplier tube. The light pipe was wrapped in aluminum foil, a magnetic shield was placed over the photomultiplier, and the assembly was enclosed in a light-tight housing. The long light pipe was used to keep the photomultiplier and its magnetic shield far outside the magnetic field of the Helmholz coils. A standard design was used for the photomultiplier high-voltage circuit (RCA70).

The anode pulses of the photomultiplier were shaped and amplified

by a model 198 amplifier (produced by the LBL shops). The output of the amplifier went either via a Hamner NC-14 single channel analyzer, or sometimes directly, to an Ortec 430 scaler. The scalers were gated on for runs of preset duration by an Ortec 431 timer-scaler. The contents of the scaler were printed out by an ASR-33 teletype under control of an Ortec 432 printout control.

5. Compton Polarimeters

The circular polarization of gamma-rays can be measured by the gamma-ray polarization dependence of their Compton scattering by polarized electrons (S65,F38,T56). The polarized electrons employed are those d-state electrons responsible for the magnetism of ferromagnetic materials. The polarization dependence of the cross section can be observed by measuring the intensity of either the unscattered gamma-rays (transmission method) or the gamma-rays scattered at some finite angle (scattering method). The geometry of the optical pumping system precluded the use of the complex assembly of magnets and shields required for the scattering method, so we employed the less efficient transmission method.

The fraction of gamma-rays transmitted by a length L of magnetized iron is $T= \exp[-(\tau_c+\delta\tau_c+\tau_{ph}+\tau_{pair})L]$ where τ_c, τ_{ph}, and τ_{pair} are the ordinary gamma-ray attenuation coefficients for Compton scattering, photo-effect, and pair production as tabulated by Davisson and Evans (DE52). The quantity $\delta\tau_c$ is the polarization dependent part of the Compton attenuation coefficient, which is always small compared to the ordinary term. When the intensity of transmitted gamma-rays is measured with the electron spins parallel (N_+) and anti-parallel (N_-)

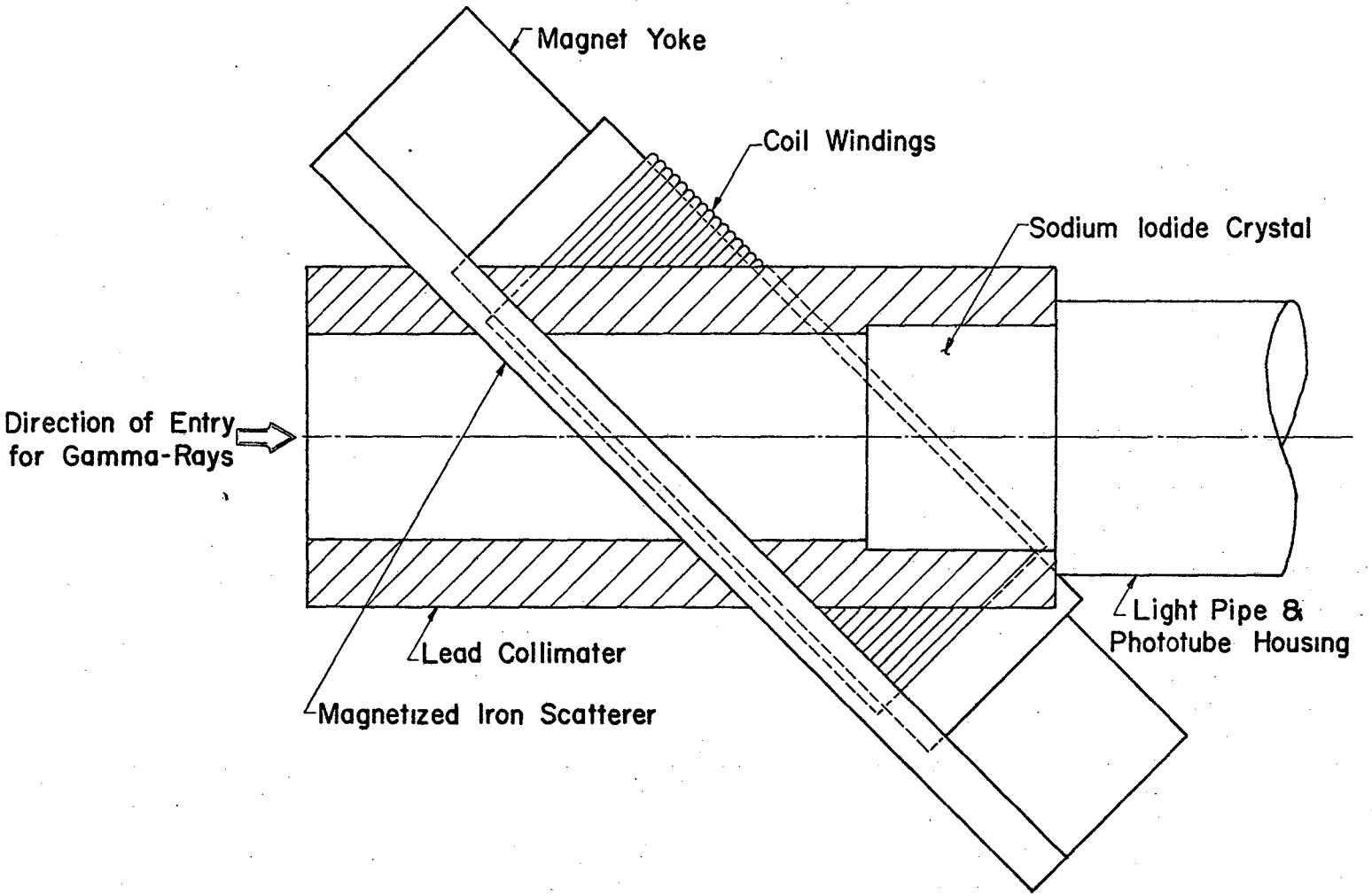

Figure 9. Cross-section view of one of the Compton polarimeters.

to the direction of the gamma-rays we have $(N_+-N_-)/(N_++N_-)\simeq \delta\tau_c \cdot L \equiv \epsilon P_\gamma$, so the efficiency of the polarimeter is proportional to its thickness. However the counting rate decreases exponentially with thickness and the maximum signal to noise ratio is obtained with $(\tau_c+\tau_{ph}+\tau_{pair})L = 2$.

If the polarimeter is designed to bring the magnetization of the iron parallel to the direction of the gamma-rays, then the curved magnetic flux lines at the front and rear of the polarimeter make calculation of the effeciency difficult. By compromising on efficiency and tilting the magnetization direction to 45° from the gamma-rays, we simplified the geometry of the field (see figure 9). By integrating the polarization-dependent Compton differntial-cross section (F57) over angles we obtain

$$\delta\tau_c = n_e P_e \cos(45°) P_\gamma 2\pi \frac{e^4}{m^2c^4} \left[\frac{1+4k_0+5k_0^2}{k_0(1+2k_0)} - \frac{1+k_0}{2k_0} \ln(1+2k_0)\right]$$

where n_e is the density of electrons, P_e is the electron polarization, and k_0 is the gamma-ray energy in units of mc^2. For the 279 Kev gamma-ray of Tl^{203} we have $\delta\tau_c/n_e P_e P_\gamma = 0.015$ barn.

The magnetization of the iron was measured by winding 10 turns of wire around the scattering section and connecting this coil to a Hewlett-Packard 2212 voltage-to-frequency converter. An Ortec scaler counted the output pulses of the converter as the magnetization direction was reversed. The instantaneous voltage across the coil is proportional to the rate of change of flux through the coil, so the accumulated counts in the scaler measures the integrated change in flux from the reversal. With 20 amps of current in the magnet coil, the magnetization of the iron was 1070 ergs/gauss-cm^3. This corresponds

to 1.1×10^{23} polarized electrons/cm^3 (or 1.3 polarized electrons per iron atom). Thus we have $\delta\tau_c/P_\gamma = 1.7\times10^{-3}$ and the efficiency of the 2.7 cm thick polarimeter is $\varepsilon = 3.9\times10^{-3}$.

C. Observations

Our intended procedure was to first carry out a series of measurements on Hg^{201} and Hg^{203} to verify the rate equation model discussed in section III.A and to determine the relevant parameters of the model. This would allow the calculation of the nuclear polarization of Hg^{203} we could achieve. We would then have set up the experiment for the automatic sequencing and data collection required for the observation of the expected small parity-violation effect.

In the course of filling and experimenting with the first few optical pumping cells, we developed the cell cleaning and filling techniques described in section III.B. We also discovered that the entrance and exit windows of these cells were optically active. When placed between crossed linear polarizers, the cells showed the dark cross characteristic of a radial stress pattern. The pattern did not change when an evacuated cell was let up to atmospheric pressure, so we concluded that the optical activity was due to residual strains left in the quartz from assembly. Annealing the cells in an oven for several hours after assembly produced cells free of any observable optical activity.

Optical pumping of Hg^{201} with a Hg^{198} lamp was performed in several different cells. A motor-driven chopping wheel was used to observe the transient optical transmission of the mercury vapor. Typical results were $\tau_L = 1.0 \pm 0.2$ sec and $\tau_D = 3.5 \pm 0.4$ sec with the reservoir at 60°C and the cell at 400°C. The values of τ_D varied somewhat from cell to cell, but most of the cells which were carefully cleaned and filled had values in the range indicated. The efficiency of the linear

polarizer gave a value of $q/p \simeq 0.1$ for the optical pumping light, so the values of τ_L and τ_D can be interpretated with the computer calculations shown in figure 6.

The observed ratio of τ_D to τ_L corresponds to a value $r/p = 0.04^{+0.06}_{-0.01}$. From the value of τ_L and this value for r/p we conclude that p is about 0.2 sec^{-1} and r is between 0.04 sec^{-1} and 0.12 sec^{-1}. The value of r agrees with that found by Cagnac under similar conditions (C61). The relaxation rate increased rapidly as the cell was cooled below 300°C. The relaxation rate was approximately constant for cell temperatures between 300 and 400°C.

The transmission of the optical pumping light through the cell was measured with the magnetic field turned off so that the Zeeman populations remained equal. The transmission was measured as a function of the reservior temperature and compared with the transmission calculations with the effective statistical weight, S, set equal to one. The observations agreed with the calculations to within 10% accuracy. The magnetic field was then turned on to 9 gauss and the change in transmission measured. This change in transmission was compared with the numerical calculations to determine the value of the effective statistical weight. Under the same conditions that gave $\tau_L \simeq 1$ sec and $\tau_D \simeq 3.5$ sec, we found $S = 0.80 \pm 0.03$. From figure 6 we see that this value of S corresponds to $r/p = 0.35 \pm 0.07$. This is in complete disagreement with the value $0.04^{+0.06}_{-0.01}$ found from the measurements of τ_L and τ_D. These experiments were repeated with several cells. The values of τ_D and S varied somewhat from cell to cell, but in every cell the two

methods of determining r/p disagreed.

Optical pumping of Hg^{203} was performed with the enriched Hg^{202} sample (which contained 1.38% Hg^{201}) after neutron irradiation in the TRIGA Mark III reactor. Thus the optical pumping cell contained both Hg^{201} and Hg^{203}. This allowed measurements to be performed on the two isotopes under indentical conditions. The values reported above for Hg^{201} actually came from one of these samples. The Hg^{203} measurements were made with one gamma-ray detector located on the optical pumping axis 12 cm away from the optical pumping cell. The gamma-ray counting rate was measured with the optical pumping light on (N_1) and off (N_2). From the equation for the angular distribution of gamma-rays in section III.A we have $A_2 = 1.02(N_2-N_1)/N_2$. A series of runs with the sample discussed above gave $A_2 = 0.061 \pm 0.015$. Measurements with other samples consistently gave similar values. Comparison with the results of the rate equation calculations for Hg^{203} with quadrupole relaxation yields $r/p \simeq 0.5$. The dependence of A_2 on r/p in this range is such that an accurate value of r/p cannot be deduced. However this result is definitely in disagreement with the value $r/p \simeq 0.04$ found from measuring τ_L and τ_D for Hg^{201} in the same cell at the same temperature. The value of r measured for Hg^{203} should actually be smaller than the value of r for Hg^{201}.

These measurements with Hg^{201} and Hg^{203} show that the rate equation model with quadrupole relaxation did not correctly describe the processes occuring in the optical pumping cell. Yet the relaxation time observed was in agreement with Cagnac's work where the dominant

relaxation mechanism was shown to be electric quadrupole. While still trying to understand these results, we started construction of the Compton polarimeters. Our experiments so far had not ruled out the existence of a sizable (≃50%) nuclear polarization of the Hg^{203}. We expected measurement of the gamma-ray circular polarization to show if the amount of nuclear polarization was sufficient for us to proceed with the search for a gamma-ray asymmetry.

By the time the Compton polarimeters were ready for use we had realized that resonant trapping of the optical pumping light was responsible for the failure of the quadrupole relaxation model, and that the mercury reservoir temperature must be lowered below room temperature. The freon refrigerator and water-glycerol dewer were installed. The sample used with the Compton polarimeters was the isotopically separated Hg^{203} from the Argonne mass spectrometer. The expected Hg^{203} fraction in this sample was $f_{203} \simeq 5\times10^{-3}$.

With the Compton polarimeter in place the distance from the cell to the gamma-ray detector was increased to 75 cm. Combined with the e^{-2} attenuation of the iron scatterer, this change reduced the gamma-ray counting rate by a factor of 350. The amount of mercury in the cell had also been reduced by lowering the reservoir temperature. We hoped that a high concentration of Hg^{203} in the Argonne sample would compensate for these losses in count rate so that we could measure A_1 and A_2 in a reasonable amount of counting time.

The gamma-ray counting rate was measured as a function of the density of mercury vapor in the cell. The extrapolation to zero density showed a background rate of 10 cps. At a reservoir temperature

of -10°C (the temperature we hoped to use for optical pumping) the total count rate was only 14 cps. This counting rate corresponds to a Hg^{203} fraction in the sample of $f_{203} \simeq 1 \times 10^{-4}$, much smaller than expected. Measurement of the attenuation of the optical pumping light in the cell as a function of mercury vapor density indicated the presence of a mercury isotope (either Hg^{198} or Hg^{201}) with an absorption line conincident with the Hg^{198} lamp. This meant the reservoir temperature could not be raised to increase the gamma-ray counting rate without causing resonance trapping. We were able to measure A_2 with this low count rate, but because of the low efficiency of the Comptons polarimeters ($\varepsilon = 3.9 \times 10^{-3}$) measurement of the gamma-ray circular polarization was not feasible. The value of A_2 found was 0.05 ± 0.02, consistent with the values found at higher reservoir temperatures.

D. Conclusions

From the results of our optical pumping experiments on Hg^{201} and Hg^{203} we see that the quadrupole relaxation model failed to describe the processes occuring in the optical pumping cells. The various samples and cells used all gave results in drastic disagreement with the predictions of that model. This constancy in the results from different cells suggests that the cause for this was not relaxation due to the impurities in the cells. The fact that the dark relaxation rate we observed was consistent with the values reported in the literature is further evidence against relaxation due to impurities and also suggests that the pumping process may be responsible. The results described above are consistent with a relaxation caused by the pumping light. This could cause the poor values of steady state polarization observed and yet not affect the dark relaxation rate.

We believe that the reabsorption in the mercury vapor of the pumping light (also called resonance trapping or diffusion of resonance radiation) was responsible for the failure to achieve significant optical pumping of the mercury vapor. This limitation on optical pumping has been discussed in the recent review by Happer (H72). The phenomena of resonance trapping will be discussed in detail in the next section of this work. Here we only indicate how this effect limits the optical pumping of Hg^{203}.

The first absorption and emission of a photon after entering the optical pumping cell occurs as d scribed in section III.A. However after that process, the photon may be moving in any direction in the

cell and is no longer circularly polarized. As a result, if the photon is absorbed by a second atom, it may induce a $\Delta m = -1$ transition, rather than the $\Delta m = +1$ transition desired. Thus, in continued scatterings in the cell, the photon may depolarize atoms which were already polarized. This has the same effect as if the cell were illuminated with isotropic, unpolarized, resonance radiation. As a depolarization process it is quite effective.

In the experiments performed with a reservoir temperature of 60°C, the mercury vapor pressure was 25 microns. At this density about half of the light from the Hg^{198} lamp was scattered by the cell. However those photons with frequencies in one wing of the doppler spectrum of the optical pumping beam were located at the center of the absorption curve of the Hg^{201}. For those photons the mean free path* in the cell was about one tenth of the cell dimensions. Thus those photons most likely to first be absorbed by the Hg^{201} atoms had a very small chance of escaping the cell without reabsorption.

For those photons with frequencies at the center of the Hg^{201} absorption curve to see an optically thin cell, the mercury vapor pressure must be less than 0.1 micron (reservoir temperature below 0°C, H72). This means that the number of Hg^{203} atoms which may be pumped is reduced by a factor of 250 from the estimate made in section II.C. Thus the smallest statistical error which can be achieved by this technique is larger than the size of the expected effect.

---

*The definition of mean free path must be modified in a doppler broadened absorbing medium (H47).

IV. RESONANCE TRAPPING

A. Introduction

The remainder of this thesis describes a series of experiments intended to test the feasability of measuring resonance trapping effects by observation of cascade photons from an atomic beam. This work was motivated by the existence of an apparatus built to observe coincident photons from an atomic cascade of calcium, and by our interest in trapping stemming from the work described in the previous part of this thesis.

The apparatus had been built by S. Freedman, J. Clauser, and D. Rehder to perform an experimental test of hidden-variable theories (CHSH69,FC72,F72). That experiment required measurement of the correlation of linear polarization of the two photons emitted in a $J= 0 \rightarrow J= 1 \rightarrow J= 0$ atomic cascade. The atom chosen for study was calcium and the transitions employed were the $4p^2\ ^1S_0 \rightarrow 4s4p\ ^1P_1$ transition of 551 nm and the subsequent $4s4p\ ^1P_1 \rightarrow 4s^2\ ^1S_0$ transition of 423 nm to the calcium ground state (see figure 10). This choice of transition was motivated by the previous work by Kocher (K67). A schematic diagram of the apparatus used by Freedman is shown in figure 11, which is reproduced from his thesis. Ground state calcium atoms are excited to the high $^1P_1$ levels by ultraviolet excitation. Some of the excited atoms decay to the $4p^2\ ^1S_0$ state, and then cascade to the ground state via the 4.7 nsec $^1P_1$ state. The two photons are observed in coincidence by the two photomultipliers in polarization states selected by the two linear polarizers. The correlation of the linear polarization results

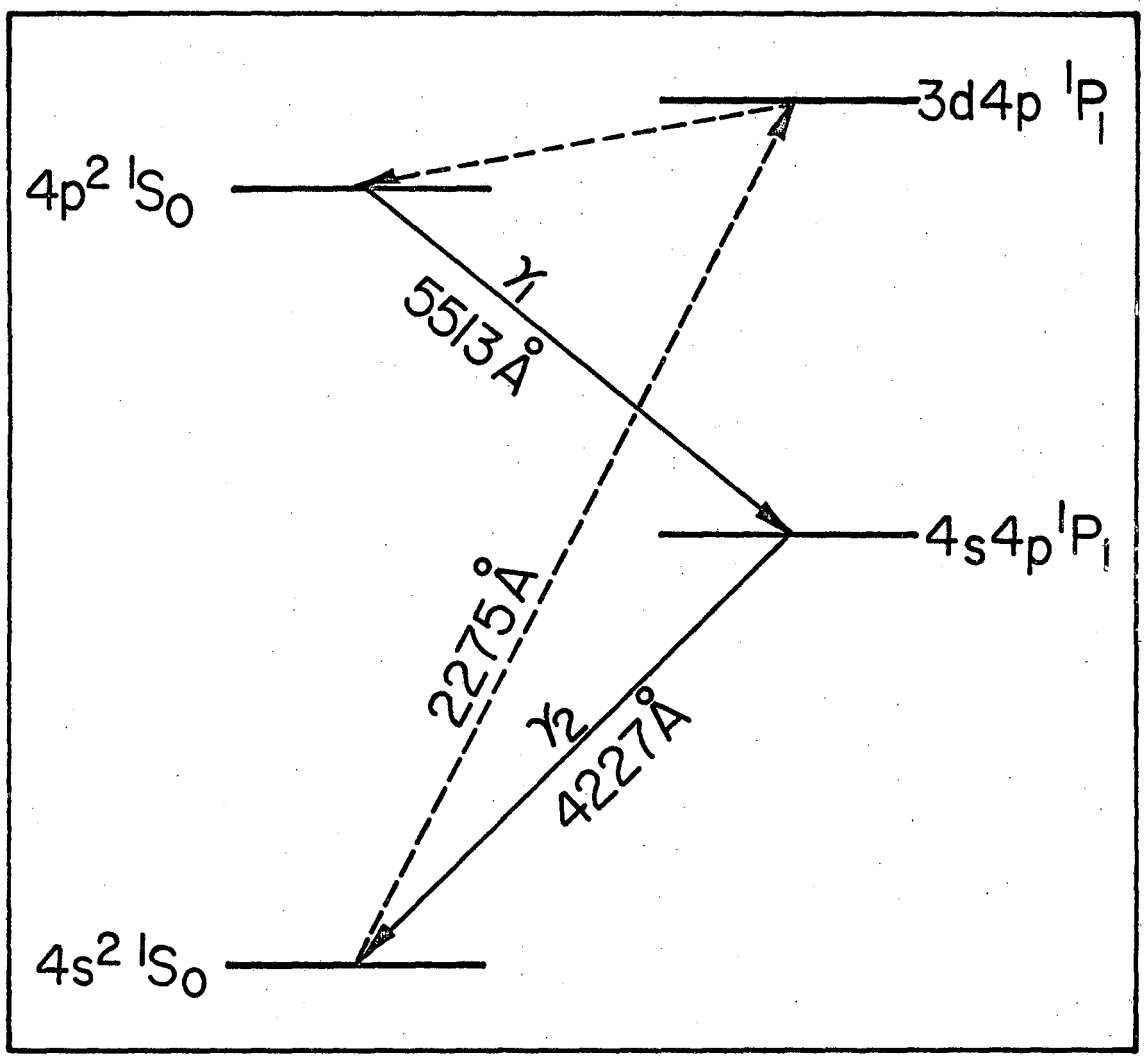

XBL 7211-5858

Figure 10. Atomic cascade of calcium (from F72).

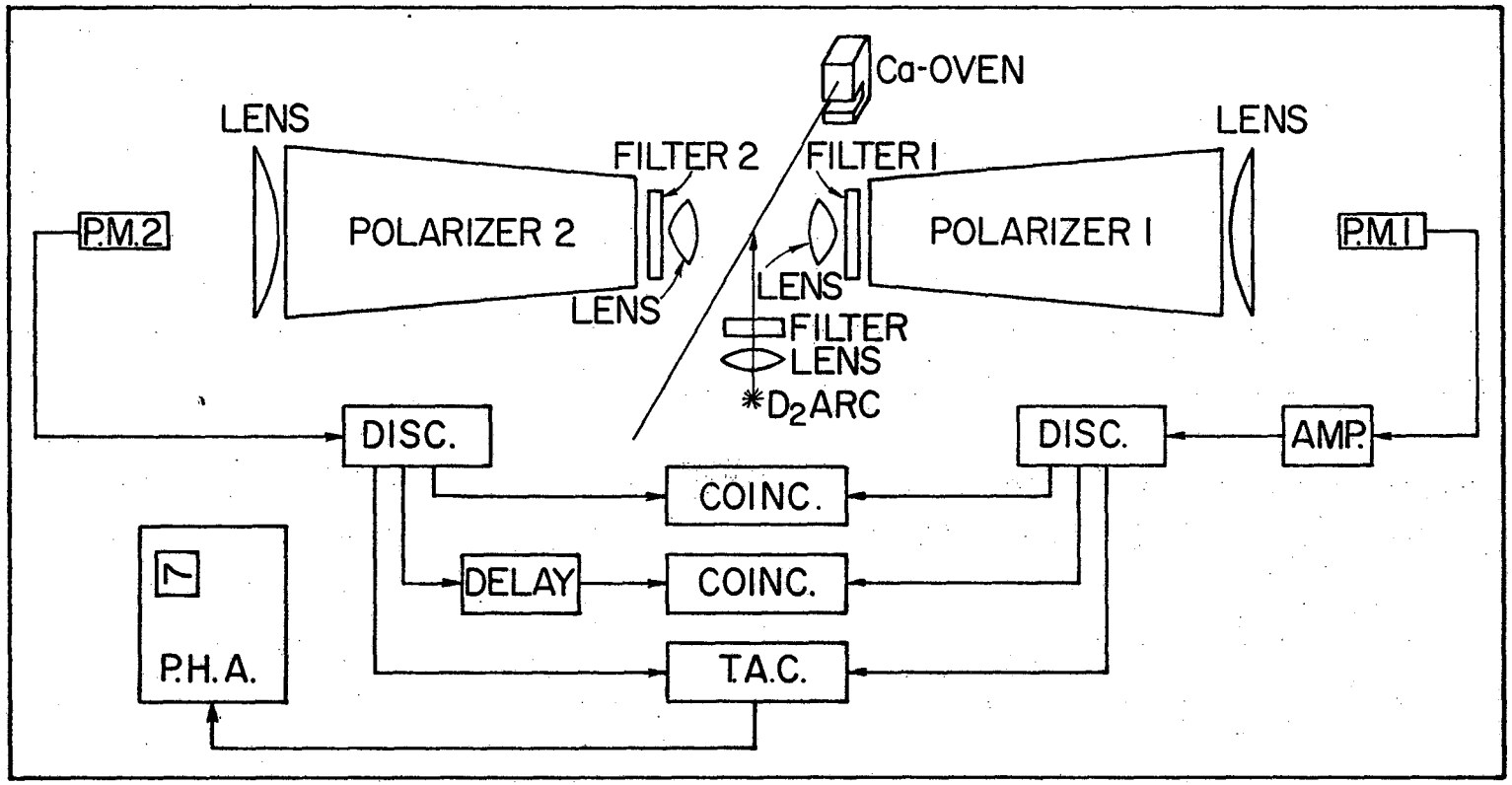

XBL 7211-5859

Figure 11. Apparatus for studing the calcium cascade (from F72).

from the requirement that the total angular momentum of the two photons be zero.

We intended to extend the work described in Freedman's thesis in two ways: to perturb the correlation of the two photons by application of a magnetic field to the intermediate state of the cascade, and to extend measurements of the intermediate state lifetime and of photon correlations to high atomic beam densities where resonance trapping becomes important. The first of these was attempted by Kocher (K67), but without success. Freedman had observed some trapping, but was not able to produce beams of high density with the existing atomic beam oven.

B. Theory

1. Classical Theories

Observation of resonance trapping began with the classic investigation of R. W. Wood into the nature of resonance fluorescence. Wood employed the transition used in nearly all the work on resonance trapping to be discussed here: the 254 nm $^3P_1 \rightarrow {}^1S_0$ transition of mercury. Wood observed that the resonance fluorescence excited in one region of a cell of mercury vapor spread to the other regions. Installation of a quartz plate which divided the cell into halves did not affect the spread of the fluorescence from one half of the cell to the other half. Wood deduced that the spread of fluorescence was due to diffusion through the cell of the resonance light, and not diffusion of excited state mercury atoms (W12). K. T. Compton extended this idea to discuss the behavior of helium arcs (C23).

The early efforts to construct a quantitative description of resonance trapping depended upon an analogy with classical diffusion processes (C23,M26). The time and space dependence of the excitation of the vapor was assumed to be governed by a diffusion equation of the form $\partial n/\partial t = D \cdot \nabla^2 n$. The diffusion constant, D, in analogy with the diffusion of atoms, was written as $(1/3)\bar{\lambda}\,\bar{v}$, with $\bar{\lambda}$ the mean free path of the resonance radiation in the vapor, and $\bar{v}$ the average speed. The interpretation given $\bar{v}$ was the ratio of the mean free path, $\bar{\lambda}$, to the natural (untrapped) lifetime, τ, of the excited atomic state. Compton and Milne (who used a modified version of the above equation) found that the dependence on the atomic density, N, of the duration of the

excitation of the vapor was of the form $\tau'/\tau = 1+\text{constant}\cdot N^2$.

Measurements of the density dependence of the trapped lifetime of resonance radiation in mercury vapor were performed by Zemansky (Z27) and later by Holstein (H49). A thin flat cell containing mercury vapor was illuminated on one face by 254 nm resonance radiation which could be chopped off suddenly. The decay time of the 254 nm light emitted from the opposite face was measured as a function of mercury vapor density. A log-log plot of the decay time and the atomic density showed a slope of approximately one in the region of densities 10^{14} to 10^{15}/cc (where the decay times are 1 to 10 μsec), rather than the slope of two predicted by Milne from the diffusion equation.

The problem was reexamined by Holstein (H47) in an analysis which was the culmination of the classical (non-quantum mechanical) theory of resonance trapping. Holstein pointed out that in a medium with either a Doppler or a Lorentzian resonance lineshape, the mean free path of resonance radiation is infinite because the light in the wings of the distribution has a vanishingly small absorption coefficient. This divergence of the mean free path explains the failure of the diffusion equation approach to a theory of resonance trapping. The assumption that one makes in writing the equation $\partial n(\vec{r},t)/\partial t = D\cdot\nabla^2 n(\vec{r},t)$ is that the rate of change of excitation at the point $\vec{r}$ depends only upon the excitation distribution in the immediate neighborhood of $\vec{r}$. But if the mean free path of the resonance radiation is infinite, then the excitation at points $\vec{r}'$, far from the point $\vec{r}$, clearly has an effect on the rate of change of the excitation at the point $\vec{r}$.

Holstein expressed the rate of change of the excitation at the point $\vec{r}$ in terms of an intergral over the volume occupied by the vapor,

$$\frac{\partial n(\vec{r},t)}{\partial t} = -\gamma n(\vec{r},t) + \gamma \int G(\vec{r}',\vec{r}) n(\vec{r}',t) d^3r'$$

where

$$G(\vec{r}',\vec{r}) = \frac{1}{|\vec{r}-\vec{r}'|^2} \int_0^\infty P(\nu) \exp[-k(\nu)|\vec{r}-\vec{r}'|] \, k(\nu) d\nu$$

and γ is the natural (untrapped) decay constant of the transition. $G(\vec{r}',\vec{r})$ represents the probability (averaged over photon frequencies) of a photon emitted by an atom at $\vec{r}'$ being absorbed by an atom at $\vec{r}$. $P(\nu)$ is the spectral distribution of the emitted resonance light and $k(\nu)$ is the spectral distribution of the absorption coefficient. $P(\nu)$ is usually, but not always, proportional to $k(\nu)$ (H47, Appendix I).

This formulation by Holstein provides a complete description of the time and space variation of the intensity of trapped resonance radiation*, but it does note include polarization phenomena. The influence of trapping on the polarization of resonance radiation was ignored for another decade.

The second term in the differential equation for $n(\vec{r},t)$ becomes significant when the product of the absorption coefficient at the center of the spectral line and the linear dimensions of the cell approaches one. The cells employed the experimental work on trapping are of the order of magnitude of 1 cm in extent, so we can say that

---

*Actually, Holstein has ignored the possibility of a velocity dependent distribution of excitation among the atoms, but this approximation is almost universally accepted.

trapping becomes significant when $k(\nu_0) \simeq 1\ cm^{-1}$. For a vapor with a natural linewidth, visible light, and a lifetime of 10 nsec, $k(\nu_0)$ reaches $1\ cm^{-1}$ at $N \simeq 1\times10^{11}$/cc. For a Doppler line shape corresponding to atomic velocities $v_{RMS} \simeq 10^5$ cm/sec, $k(\nu_0)$ reaches $1\ cm^{-1}$ at $N \simeq 1\times10^{11}$/cc.

The solution of the integral equation for $n(\vec{r},t)$ is extremely difficult. It is crucial that the correct line shapes for $k(\nu)$ and $P(\nu)$ are used. The geometry of the cell must also be treated in a realistic manner. By rewriting the integral equation for $n(\vec{r},t)$ as a variational equation, Holstein showed that there exists a complete and denumerable set of solutions of the form $n_n(\vec{r},t) = \psi_n(\vec{r})\exp[-\beta_n t]$. Thus the general solution can be written as $n(\vec{r},t) = \sum_n c_n\psi_n(\vec{r})\exp[-\beta_n t]$. At sufficiently long times, the smallest eigenvalue, β_1, dominates the behavior of $n(\vec{r},t)$. Holstein calculated an approximate expression for β_1 for the experimental geometry described above, and found the duration of excitation to be $\tau'/\tau \simeq \text{constant} \cdot N\sqrt{\ln(N)}$, which is in reasonable agreement with the experimental results for atomic densities below 10^{15}/cc (above 10^{15}/cc collisional broadening becomes important).

At high densities and for durations only a few times the natural lifetime, there may be many terms in the eigenfunction expansion for $n(\vec{r},t)$ which are of comparable size. If this is the case, the decay of excitation may be strongly non-exponential. However the experimental data on the decay of excitation* is always fitted to an exponential and the theoretical calculations are directed toward providing an

---

*When polarization effects are included, several decay constants appear in the development. However it is still assumed that the sum of the populations of all Zeeman levels decays with a single time constant, γ_0.

approximate value for this decay constant.

The problem of resonance trapping in an atomic beam, rather than in a cell, has an additional complication. The velocity vectors of the atoms are all parallel but the atoms have a (approximately) Maxwellian distribution of speeds. Thus there is a Doppler shift which is dependent on the direction of a photon relative to the direction of the atomic beam. The absorption coefficient, k, depends on the direction of the photon momentum as well as photon frequency. If the velocity distribution of atoms in the beam is n(v), then the absorption coefficient is $k(\omega,\theta)= \int n(v)K(v,\omega,\theta)dv$, where $K(v,\omega,\theta)$ is the absorption coefficient for an atom with a velocity along the photon direction of $v\cdot\cos\theta$. K has a Lorentzian lineshape,

$$K(v,\omega,\theta) = \frac{\lambda_0^2}{2\pi}\frac{g_2}{g_1}\frac{\gamma^2/4}{\gamma^2/4+(\omega-\omega_0(1+v/c\ \cos\theta))^2}$$

With the usual approximation for the velocity distribution of an atomic beam, we have

$$K(\omega,\theta) = \frac{\lambda_0^2\gamma^2 N}{2\pi v_0^3\sqrt{\pi}}\frac{g_2}{g_1}\left\{\int_0^\infty \frac{v^2\exp[-v^2/v_0^2]dv}{\gamma^2/4+(\omega-\omega_0(1+v/c\ \cos\theta))^2}\right\}$$

where $v_0= \sqrt{2kT/M}$ is the most probable atomic velocity in a volume of gas (R56). Evaluation of the integral appearing in the definition of $k(\omega,\theta)$ is an essential step in the calculation of resonance trapping in an atomic beam. By defining $x= v/v_0$, $\alpha=2\omega_0 v_0\cos(\theta)/\gamma c$, and $\beta=2(\omega-\omega_0)/\gamma$, we can write the integral inside the brackets as $4G_2(\alpha,\beta)/\gamma^2 v_0^2$, where

$$G_2(\alpha,\beta) = \int_0^\infty \frac{x^2\exp[-x^2]dx}{1+(\alpha x-\beta)^2}$$

The regions where $G_2(\alpha,\beta)$ must be evaluated include α close to zero (photon moving perpendicular to the atomic beam) and β close to zero (ω close to ω_0). G_2 can be expressed in terms of the error function of complex argument, but the cases $\alpha=0$ and $\beta=0$ correspond to singularities in the argument of the error function. Of course these singularities cancel in the calculation of $k(\omega,\theta)$ for physical frequencies and angles, but the appearance of the singularities in the intermediate expressions makes this approach impractical for solving the resonance trapping problem. The evaluation of $G_2(\alpha,\beta)$ is further discussed in Appendix II.

The full equation to be solved for the trapping of resonance radiation in an atomic beam is more complicated than that used by Holstein because the velocity distribution of the excited atoms must be included. Even if the excitation process is such that the probability of excitation is independent of atomic velocity, the decay of those atoms with velocities in the wings of the distribution will probably occur without reabsorption because of the extreme Doppler shift of those photons relative to most of the beam. Thus, after several lifetimes, the atoms still excited will be dominantly those in the peak of the velocity distribution.

We have calculated the trapped lifetime of resonance radiation in an atomic beam by Monte Carlo simulation. In this simulation, case histories of individual excitations are generated from sets of random numbers. The program generates an initial position and velocity of an excited atom. It then generates a decay time and the frequency

and direction of the emitted photon. It generates reabsorption by another atom or escape from the beam with probabilities given by the absorption coefficient, $k(\omega,\theta)$, for a photon of that frequency traveling in that direction relative to the beam, and the distance it must travel to the boundry of the beam. If reabsorption occurs, then it generates another decay time, photon frequency, and photon direction. This continues until escape occurs. The times of escape are recorded on a histogram. Usually 500 case histories were generated to determine the trapped lifetime for a given atomic density (which required about 3 seconds of time on a CDC 6600 computer). The lifetimes were derived from the histograms by the integration technique of Bennett (BKM64). The Monte Carlo program is described in more detail in Appendix III.

2. Polarization and Trapping

Since the first experiments by Hanle on zero-field level-crossing, the polarization of resonance radiation has been employed to measure the lifetime of excited states of atoms. Measurement of the polarization as a function of applied magnetic field produces a Lorentzian curve, whose width is interpreted as the coherence time of the polarization in the vapor. While it was known that high atomic densities decreased the amount of polarization observed (MZ34), the possible effect of atomic density on the coherence time (coherent trapping) was ignored for many years. Thus measurements of the lifetime of the $^3P_1$ state of mercury by the Hanle effect yielded a variety of conflicting results.

The classic experiment on optical double resonance by Brossel and Bitter (BB52) continued this error. That experiment was performed

with a mercury vapor density corresponding to a mercury reservoir held at 0°C. They reported the lifetime of the $^3P_1$ state to be $(1.55\pm0.03)\times10^{-7}$ sec and the g factor to be 1.4838 ± 0.0004. They did not realize that both of these values were in error because of trapping. After a number of other experiments had found the lifetime of the $^3P_1$ state to be about 1.1×10^{-7} sec, Blamont repeated the experiment of Brossel and Bitter for different densities of mercury vapor. He found that the coherence time of the polarization increased with atomic density, and concluded that the transfer of excitation in resonance trapping was a coherent process (GBB56,B57). That is, if the first atom was in a coherent superposition of Zeeman levels, then some of that coherence survives the transfer of excitation to the second atom. Thus the measured coherence time (by Hanle effect or by double resonance) is longer than the natural lifetime of the state.

The theory of resonance trapping was extended to include coherence effects by Barrat (B59). Barrat developed an equation similar to Holstein's, but which describes the change in the amplitude for the n^{th} atom to be in the m Zeeman level,

$$i\frac{da_m(n,t)}{dt} = (\omega_0 - i\gamma/2)a_m(n,t) + i\sum_{n'm'} C_{mm'}(n',n,t)a_{m'}(n',t)$$

where

$$C_{mm'} = \frac{3}{4}i\gamma\frac{\exp[ik_0R_{nn'}]}{k_0R_{nn'}}\exp[i\Delta\omega t]\sum_{\lambda}\langle m|\hat{\varepsilon}_\lambda\cdot\vec{D}|gs\rangle\langle gs|\hat{\varepsilon}_\lambda\cdot\vec{D}|m'\rangle\cdot$$

$$\cdot\exp[-kR_{nn'}/2]$$

This equation can be seen to be just the quantum-mechanical extension

of Holstein's equation to include the existence of the Zeeman levels and the coherence of their amplitudes. The $\hat{\varepsilon}_\lambda$ is the unit polarization vector of the transferred photon and $\vec{D}$ is the electric dipole operator. This equation does not yet include the shape of the resonance line; the attenuation due to the vapor between atoms n and n' is written simply as $\exp[-kR_{nn'}/2]$. Actually Barrat had not been the first to calculate the coherent transfer between atoms. In one of the first applications of the quantum theory of radiation, Weisskopf performed this calculation in 1931 (W31), but the implications of his work for resonance trapping were ignored.

The expression written above does not include any loss of coherence during trapping. To correct that, we must write an equation for the rate of change of the density matrix, and then perform an average over the possible positions of the atoms engaged in the transfer of excitation. Barrat, working from the above expression, has done this and derived approximate expressions for the coherence time of the polarization. However Barrat had not included the Doppler shape of the resonance line.

D'yakonov and Perel (DP65) extended Barrat's work to include the Doppler shape of the resonance line. They also expressed the density matrix of the excited state Zeeman levels, $\rho_{mm'} = a^*_{m'} a_m$, in a spherical basis. The elements of the density matrix in this basis are $\rho^{(0)}$, $\rho^{(1)}_m$, and $\rho^{(2)}_m$. $\rho^{(0)}$ is the sum of the populations of the Zeeman levels, $\rho^{(1)}_m$ measures the polarization of the excited state, and $\rho^{(2)}_m$ measured the alignment. In a cell with spherical symmetry, each of $\rho^{(L)}$ decays with its own time dependence, usually approximated by

the decay constants γ_0, γ_1, and γ_2. Resonance trapping in an atomic beam does not satisfy this assumption of spherical symmetry because of the angle-dependent absorption coefficient, so the spherical tensor are coupled and do not decay independently. However, with the approximation of cylindrical symmetry of the atomic beam, the spherical tensor elements of a given m are not coupled to the elements of a different m. Thus a theoretical treatment of trapping in an atomic beam might be directed toward calculating the five decay constants for m= +2 to m= -2.

Except for an analysis of trapping during diffuse reflection (D071), there have not been calculations of resonance trapping performed which include realistic tratments of experimental geometries. The Monto Carlo technique which we have employed to calculate the decay time of the excitation did explicitly include the actual experimental geometry. This technique could be extended to include polarization effects, but only at a considerable cost in program complexity and execution time. Of course a Monte Carlo simulation does not increase our understanding of a physical process, it is only a synthetic experiment. However a study of the effect of various approximations on the Monte Carlo simulation might provide guidance in the development of an analytical theory of trapping.

C. Atomic Cascades

With the development of photomultiplier tubes and fast counting electronics, it has become possible to observe in coincidence the two photons emitted by an atom during a cascade. This allows a direct determination of the lifetime of the state intermediate between emission of the two photons. Freedman has tabulated the reported observations of atomic cascades (F72).

A particularly interesting case of an atomic cascade occurs when both the initial and final states of the atom have zero total angular momentum (the intermediate state will then have total angular momentum of one). The two photons are then required to have zero total angular momentum. The state vector of the two photon system can then be written in terms of the angular momentum states, $|J,J_z>$, of the individual photons, $|\Psi>=|1,1>_1|1,-1>_2-|1,0_1|1,0_2+|1,-1>_1|1,1>_2$. When one of the two photons is observed in a certain polarization state, the wave function collapses to a state of definite polarization of the second photon. It is this quantum-mechanical correlation of spatially separated systems which makes this case an example of the Einstein-Podolsky-Rosen paradox (EPR35) and led to its use as a test of local hidden-variable theories (FC72).

If the photons from the cascade are observed with imperfect polarizers, or polarization-independent detectors, then the photons are not in pure quantum-mechanical states. A description in terms of a density matrix is then useful. The density matrix of the two photon system is $\rho= |\Psi><\Psi|$, with $|\Psi>$ as written above. The two detector

systems (including the polarizers) are represented by the operators $\varepsilon^{(1)}$ and $\varepsilon^{(2)}$. These operators include the solid angle of acceptance and any polarization dependence of the detectors. The coincidence counting rate is then written $R= Tr\{\varepsilon^{(1)}\varepsilon^{(2)}\rho\}$ where the trace operation involves both a sum over polarization states and an integral over photon directions.

The application of a static magnetic field splits the Zeeman levels of the intermediate state. If the B field defines the z axis, then the state of the two photon system becomes $|\Psi>=|1,1>_1|1,-1>_2 e^{i\omega t}$ $-|1,1>_1|1,0>_2+|1,-1>_1|1,1>_2 e^{-i\omega t}$, where ω is the Lamour frequency and t is the time the atom spent in the intermediate state. With polarization-independent point detectors located on the plus and minus y axis, the counting rate is found by projecting $|\Psi>$ onto eigenstates of photon direction and helicity, $|\hat{n},\lambda>$, with $\hat{n}_1= +\hat{y}$ and $\hat{n}_2= -\hat{y}$, and then summing over photon helicities. The projection of angular momentum states on the states of definite direction and helicity is given by the rotation matrix, $<1,m|\hat{n},\lambda>= \lambda D^{(1)}_{m,\lambda}(\hat{n})$ (JW59). We then find the correlation with no polarizers, $R(t)= (1/2)\exp[-t/\tau](1+\cos^2\omega t)$. The calculations of the count rate with polarizers in place and oriented parallel is carried out in the same manner, but with the photon states projected onto states of linear polarization. The polarizer-in correlation is then $R(t)= \exp[-t/\tau]\cdot\cos^2\omega t$. This magnetic field perturbation of the polarization correlation has previously been observed by Dumont et. al. (D70) and by Popp et. al. (P70).

With detectors which subtend a finite solid angle, a geometry

correction must be added to the expressions for the count rates. The geometry factor is most easily found from the density matrix description of the photon states. The no-polarizer correlation is given by

$$R(t) = Tr\{\varepsilon^{(1)}\varepsilon^{(2)}\rho(t)\}$$

$$= \int_{\Omega_1} d\Omega_1 \int_{\Omega_2} d\Omega_2 \sum_{\lambda_1,\lambda_2} \langle \hat{n}_1,\lambda_1|_1\langle \hat{n}_2,\lambda_2|_2\ \rho(t)|\hat{n}_1,\lambda_1\rangle_1|\hat{n}_2,\lambda_2\rangle_2$$

where $\Omega_1(\Omega_2)$ is the solid angle subtended by detector 1 (detector 2) and $\rho(t) = |\Psi(t)\rangle\langle\Psi(t)|$. We define $f^{(i)}_{mm'} = \int_{\Omega_i} d\Omega \sum_\lambda D^*_{m\lambda}(\hat{n})D_{m'\lambda}(\hat{n})$. For symmetric detector systems on the plus and minus y axes we have $f^{(2)}_{mm'} = (-1)^{m-m'}f^{(1)}_{mm'}$. Then the correlation is

$$R(t) = \frac{1}{3}e^{-2i\omega t}f_{1-1}f_{-11} + \frac{1}{3}e^{-i\omega t}\{f_{10}f_{-10} + f_{0-1}f_{01}\}$$

$$+ \frac{1}{3}\{f_{11}f_{-1-1} + f_{00}f_{00} + f_{-1-1}f_{11}\}$$

$$+ \frac{1}{3}e^{i\omega t}\{f_{01}f_{0-1} + f_{-10}f_{10}\} + \frac{1}{3}e^{2i\omega t}\ f_{-11}f_{1-1}$$

For detectors with a half-angle of acceptance of θ, we have

$$f_{11} = \frac{3\pi}{2}(1-\cos\theta) - \frac{\pi}{6}(1-\cos^3\theta)$$

$$f_{00} = \pi(1-\cos\theta) + \frac{\pi}{3}(1-\cos^3\theta)$$

$$f_{1-1} = \frac{\pi}{2}(1-\cos\theta) - \frac{\pi}{2}(1-\cos^3\theta)$$

and $f_{10} = 0.$

Then we find

$$R(t) = \frac{2}{3}|f_{11}|^2 + \frac{1}{3}|f_{00}|^2 - \frac{2}{3}|f_{00}|^2 + \frac{4}{3}|f_{1-1}|^2 \cos^2\omega t$$

$$= C\,(1+A_2 \cos^2\omega t)$$

where $A_2 = 4|f_{1-1}|^2/(2|f_{11}|^2+|f_{00}|^2-2|f_{1-1}|^2)$. With the 30° half-angle detector systems employed in this work, $A_2 = 0.59$.

The density matrix description of the cascade process can be extended to include resonance trapping. Only the second photon can be trapped, of course. Observation of the first photon in detector system 1 defines the initial value of the density matrix of the intermediate state. The time development of this density matrix is then described by the differential equations developed by Barrat (or D'yakonov and Perel). The observation of the second photon then provides a measurement of the density matrix after a time interval t. Unfortunately we have only approximate solutions for trapping in a cell, and no solutions which have been derived for the special conditions existent in an atomic beam.

D. Apparatus

1. Pre-existing Apparatus

The apparatus used for this part of the present work has been described in detail by Freedman (F72), so only a brief description will be given here. The basic elements of the apparatus are a vacuum system and an oven to provide the beam of calcium atoms; an ultraviolet excitation lamp, filter, and monitor; two optical systems for observation of the cascade photons, each composed of lenses, a filter, a linear polarizer, and a phototube; and the electronics for observing coincidences and time interval distributions (figure 11). The changes made in the apparatus for the present work were the construction of a new atomic beam oven and the addition of a pair of coils to provide a magnetic field in the interaction region.

The vacuum system maintained a pressure $\lesssim 10^{-5}$ torr during runs so the mean free path of calcium atoms was long compared to the distance from the oven to the interaction region. The large capacity atomic beam oven was heated to about 700°C to produce the calcium beam. The density of the calcium beam was monitored by the photon singles rates observed for a given intensity of excitation light. Measurement of the thickness of the calcium deposited on the bulkhead facing the oven provided an absolute calibration of the calcium beam density. The beam baffles defined a beam rectangular in cross section with a size at the interaction region of 0.38 cm wide by 0.57 cm high.

The data collection runs in the present work used the Oriel C-42-72-12 deuterium arc lamp to provide the excitation light. These

lamps provide a continuous ultraviolet spectrum. Light of the desired wavelength (≃227 nm) was selected by an interference filter. The intensity of light at the interaction region was about 2×10^{13} photons/cm^2-sec-nm. An RCA 1P28 phototube monitored the intensity of the excitation light during the runs.

The two detector systems were symmetrically placed on opposite sides of the interaction region. The cone of rays collected by the 423 nm system is centered on a line making an angle of 60° with the forward direction of the atomic beam. An aspheric lens located one focal length from the interaction region brought the collected photons into a (approximately) parallel beam. Each beam then passed through the interference filter for that detector system (selecting either 423 nm or 551 nm) and entered the linear polarizer. The linear polarizers each consisted of ten parallel plates of thin glass tilted at nearly Brewster's angle to the beam. The plates could be moved in or out of the beam and the entire polarizer could be rotated about the axis of the light beam. The photons passed by each polarizer were collected by a second lens and directed onto the face of a photo-tube (RCA 8850 for the 423 nm side and RCA C31000E for the 551 nm side). The overall efficiencies (including solid angle) of the two detector systems (with polarizer plates out) were measured by Freedman to be $\eta_1\simeq1.7\times10^{-3}$ for the 513 nm system and $\eta_2\simeq1.5\times10^{-3}$ for the 423 nm system.

The anode pulses from the phototubes went to fast timing discrim-inators. The singles rates from the two discriminators were counted. The logic pulses from the discriminators also went to a fast coincidence

module to measure the total coincidence rate, and to the start and stop inputs of a time-to-amplitude converter (TAC). The output of the TAC was recorded by a pulse-height analyzer (PHA). The contents of the PHA memory were later recorded by a typewriter and on punch cards.

2. Atomic Beam Oven

The oven used in the previous work on this apparatus (F72) was machined from a block of tantalum. The orifice of that oven was heated by a circuit separate from that which heated the body. The beam effused from a 3.5 cm long by 0.25 cm diameter cylindrical channel. However during operation, the mean free path of calcium atoms in the oven is only about 0.3 cm, so the conditions for channeled flow were not satisfied. Furthermore the high impedence of this long channel restricted the flow of calcium when attempts were made to run at high beam densities (to check for the effects of trapping).

A new oven was designed for the present work with several criteria in mind: the oven orifice should approximate the ideal of an aperature in a thin wall so that high beam densities can be achieved, the oven should hold a large charge of calcium, and the oven should provide a stable beam density during runs of long duration. The requirement of a large oven suggests that a material less expensive than tantalum be used. A stainless steel oven of classical design which was sealed with a tapered plug of stainless steel had been tried before, but calcium had leaked out around the edges of the plug.

The new oven was contructed from 304 stainless steel. The opening for loading the charge was sealed with a 304 stainless steel flange which was fastened to the oven body by eight 1/4-20 stainless

steel bolts. A disc of 10 mil tantalum sheet was used as a gasket between the flange and the oven body. The flange and bolts were painted with Aqua-dag collodial graphite before assembly to prevent the parts from seizing during operation at high temperatures. There was no sign of leakage from the flange during operation and disassembly after a run was easier than had been the case with the previous tantalum oven.

The heating elements in this oven were connected into one circuit. The tapped bolt holes for mounting the flange prevented heaters from being placed close to the top of the oven. One data collection run was interrupted by a noisy phototube, so the oven was removed and opened before the charge had been exhausted. It was found that the calcium had all migrated to the top of the oven chamber, nearly blocking the oven orifice. This may be the reason that the oven showed poor beam stability, even when operated from a constant current power supply.

3. Magnetic Field Coils

The criteria for the magnetic field coils were that they should provide a magnetic field of up to 350 gauss at the interaction region, the field should be constant in time to a few percent accuracy, and the fields should not vary over the volume of the interaction region by more than a few percent. The apparatus had been designed without provision for adding magnetic coils. The position of the vacuum chambers and the large linear polarizers prevented placing the coils outside the vacuum chamber. The coils were designed to fit inside the vacuum in the space left around the light baffles. A Helmholtz

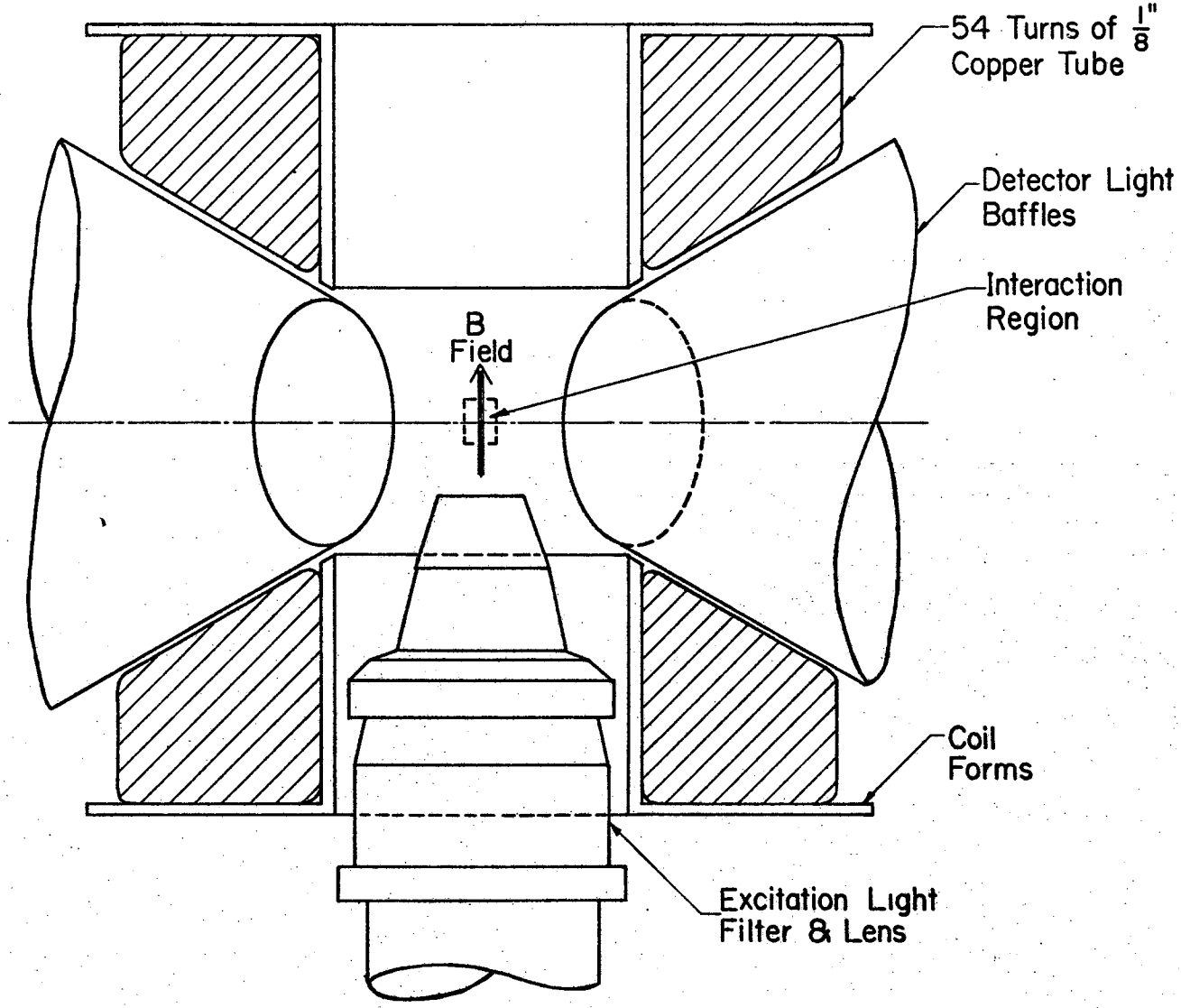

XBL 7211-5860

Figure 12. The magnetic field coils added to the calcium apparatus.

configuration would have been preferred for magnetic field uniformity, but that would have necessitated drastic alterations of the two detector optical systems. Instead the two coils were placed as close to the Helmholtz spacing as the pre-existing optical systems would allow (figure 12).

The first version of the coils were wound with solid copper wire on brass water-cooled forms. These coils over-heated when used to produce fields of about 100 gauss. The final coils were wound with copper refrigeration tubing which was insulated with woven glass tubing and held in place with vacuum-grade epoxy (Torr-Seal). The coils were hooked in series electrically and connected in parallel to the cooling water. The coils produced a field of 4.5 gauss per ampere of current. With a field of 300 gauss at the center of the interaction region, the field (which increased away from the center because the coil spacing was greater than the Helmholtz spacing) varied by 4.3 gauss (or 1.4%) over the interation region.

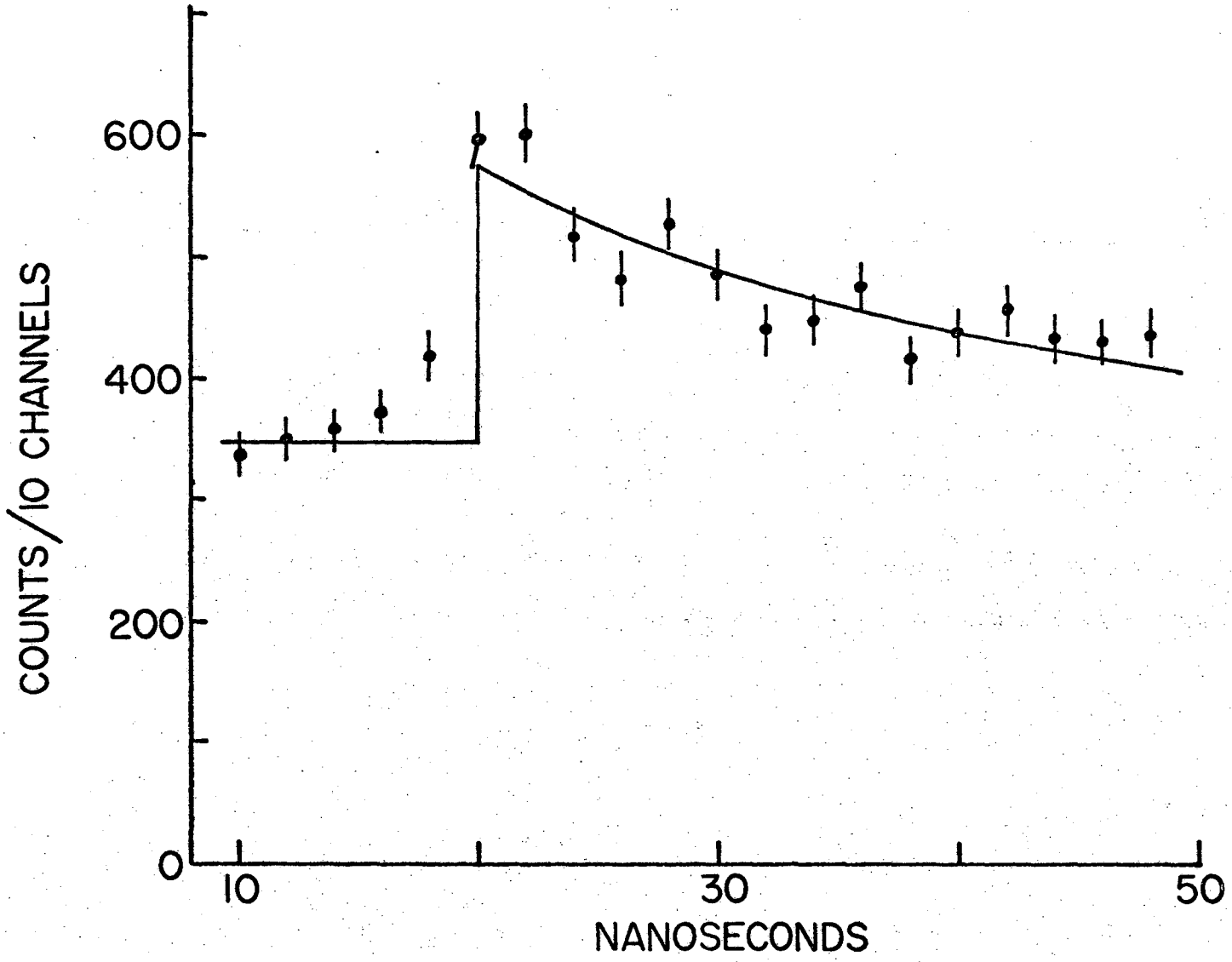

XBL 7211-5861

Figure 13. Decay curve of calcium obtained in a high-density run (no magnetic field).

E. Observations

1. Lifetime

With the new atomic beam oven, we had hoped to produce stable, reproducible high atomic densities of calcium. However the new oven, while indeed capable of producing beams of very high density, was unstable in its operation. The calcium deposited on the bulkhead facing the oven was not uniform in thickness. At the highest beam densities this nonuniformity was drastic, projections of calcium deposits 1 cm thick appearing at spots. The continuous monitoring of the calcium beam density by observation of the photon singles rates indicated that the beam density also fluctuated in time. It was not possible to assign a definite value of atomic density to any of the high density runs. Even the ordering of the runs by atomic density is uncertain. At low densities (less than 5×10^{10}/cc) the calcium deposited was uniform and the singles rates indicated a stable beam density. The result from the low density runs were consistent with those recorded earlier by Freedman (F72), and with other measurements of the lifetime of the $^1P_1$ state (WSM69).

The time interval distribution obtained in one of the high density runs is shown in figure 13. The least-squares fit gives a lifetime of 21.6±2.4 nsec, or 4.6 times the natural lifetime. Thus a high degree of trapping had been established. From the thickness of the calcium deposited during this run, the beam density is estimated to be 5×10^{11}/cc, however considerable uncertainty must be attached to this number. The signal-to-noise ratio for this run is much worse

than for the low density runs. With a constant intensity of excitation light, the effect of increasing the beam density is to collect the same number of true coincidences from an oven charge, but in a shorter time. Because both of the photons singles rates increases linearly with beam density, the accidental coincidence rate increases with the square of the beam density. Thus the ratio of accidental to true coincidences is proportional to the beam density.

The Monte Carlo program CREON gives a trapped lifetime of 5.18 times the natural lifetime (or 23.5 nsec) for an atomic density of 5×10^{11}/cc in the interaction region. Interpolation of the results of CREON with various densities indicates that a density of 4.2×10^{11}/cc would produce the observed trapped lifetime of 4.6 times the natural lifetime. This close agreement with the estimated density of 5×10^{11}/cc must be considered fortuitous.

Shortly after this work began, we became aware of the measurements of Kluge, Otten, and Zimmerman, who had studied the resonance trapping of the same atomic transition of calcium by a level crossing technique (KOZ69). They succeeded in constructing a cell for calcium vapor cleaved crystals of MgO. A cell had several advantages over an atomic beam: the atomic density in a cell can be accurately controlled by adjusting the cell temperature, the cell does not require refilling as does as atomic beam oven, and the calculation of trapping in a cell is easier because of the isotropy of atomic motion. Kluge, et. al. have obtained good measurements of trapped lifetime as a function of atomic density. The atomic beam method does not seem capable of yielding data of similar quality.

2. Angular Correlation

The time delay distribution was measured with a magnetic field of about 90 gauss at the interaction region and with both polarizers removed from the system. The atomic density in the interaction region was maintained at about 5×10^{10}/cc. The time distribution in an ideal system (no trapping, no geometry correction, no background) would be $(1/2)\exp[-t/\tau](1+\cos^2\omega t)$. The observed time delay spectrum from one of these runs is shown in figure 14. Also shown is a least-squares fit of the form $A\cdot\exp[-t/\tau](1-R+R\cdot\cos^2\omega t)+B$, where the free parameters were A, τ, ω, and R. The values of the parameters found for this run were A= 925 counts, τ= 5.0 nsec, ω= 9.0×10^8 radians/sec, and R= 0.21. This value of τ is close to the untrapped lifetime of 4.7 nsec. Using the value of 90 gauss for the strength of the magnetic field, the value of ω corresponds to a g factor of 1.13. This is in acceptable agreement with the expected g factor of one, since the magnetic field calibration was only 10% accurate.

The value of R expected in the absence of trapping is 0.5 multiplied by the geometry factor of 0.75, or 0.37. At densities higher than that used in the run shown in figure 14, the correlation disappeared completely. Thus the angular correlation seems to be very strongly affected by trapping, even at densities such that the lifetime is nearly equal to its natural value. The analysis of D'yakonov and Perel (DP65) suggests that the angular correlation (which depends upon the $\rho^{(2)}$ tensor) should be more strongly affected by trapping than the duration of excitation (which depends upon the $\rho^{(0)}$ tensor). That is,

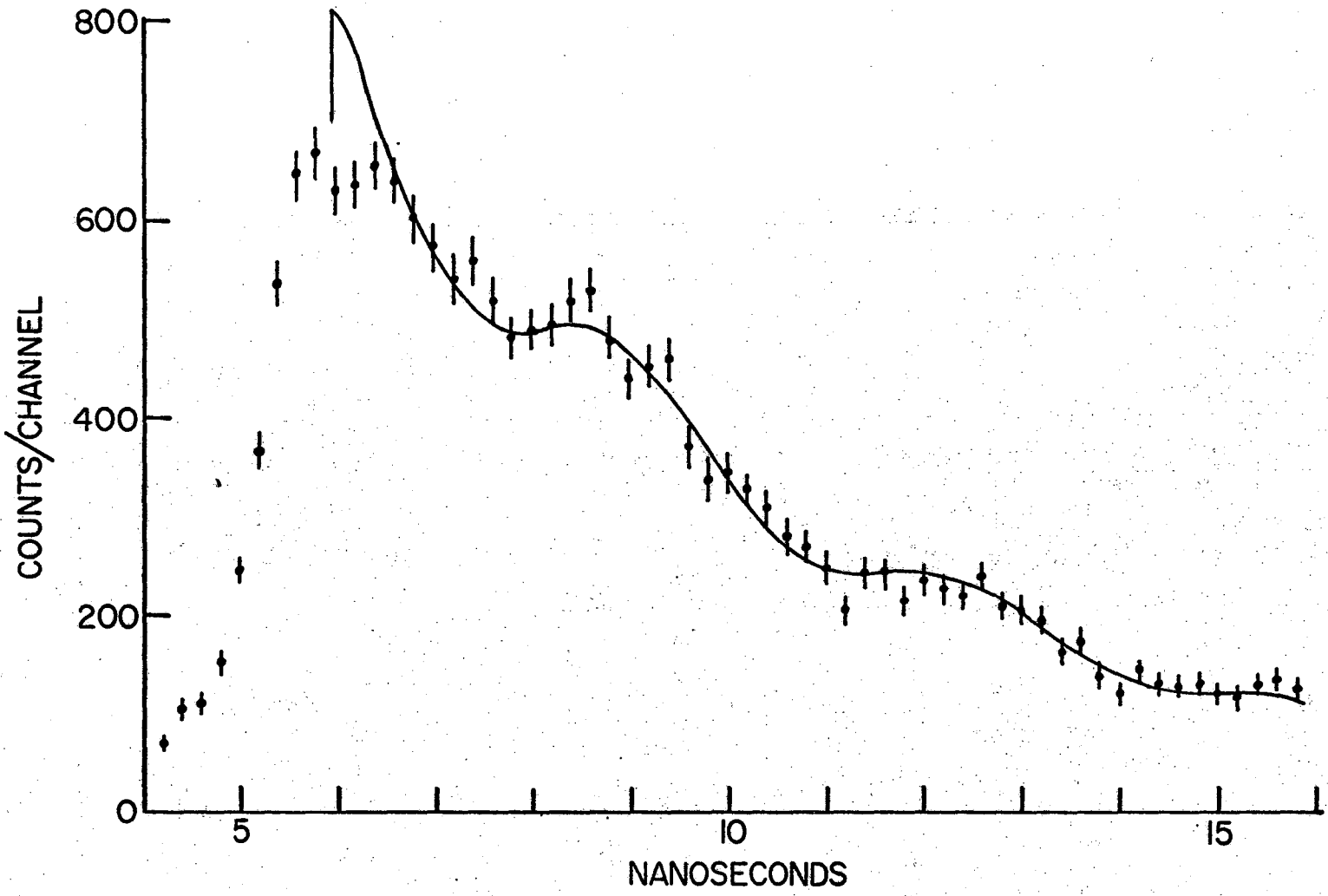

XBL 7211-5862

Figure 14. No-polarizers correlation observed with a magnetic field of 90 gauss.

γ_2 is larger than γ_0 at the same atomic density. However the apparent ratio of γ_2 to γ_0 in the case studied here is larger than can be justified by the results of D'yakonov and Perel. This may be due to the peculiar nature of the angle-dependent coefficient for an atomic beam, but without a quantitative theoretical analysis of this problem, we can only speculate.

3. Polarization Correlation

The time delay spectrum of the linear polarization correlation was measured with a field of about 90 gauss at the interaction region and with the two linear polarizers oriented parallel to each other. The distribution observed in one of these runs is shown in figure 15. Also shown is a least-squares fit of the same form as used for the angular correlation. For this run the fitted values of the parameters were A= 145 counts, τ= 7.7 nsec, ω= 9.3×10^8 radians/sec, and R= 0.42. The value of τ indicates the presence of some trapping (the atomic density was close to 1×10^{11} during this run). Using 90 gauss for the strength of the magnetic field, the value of ω corresponds to a g factor of 1.17.

The value of R expected in the absence of trapping is the ideal value of one multiplied by the geometry factor of 0.75. The equations developed by Barrat define a relationship between the trapped lifetime and the polarization of the escaping resonance radiation. While the situation of trapping in an atomic beam clearly does not satisfy the assumptions made in Barrat's analysis, his results do provide a convenient approximation to our observations. In his parameterization

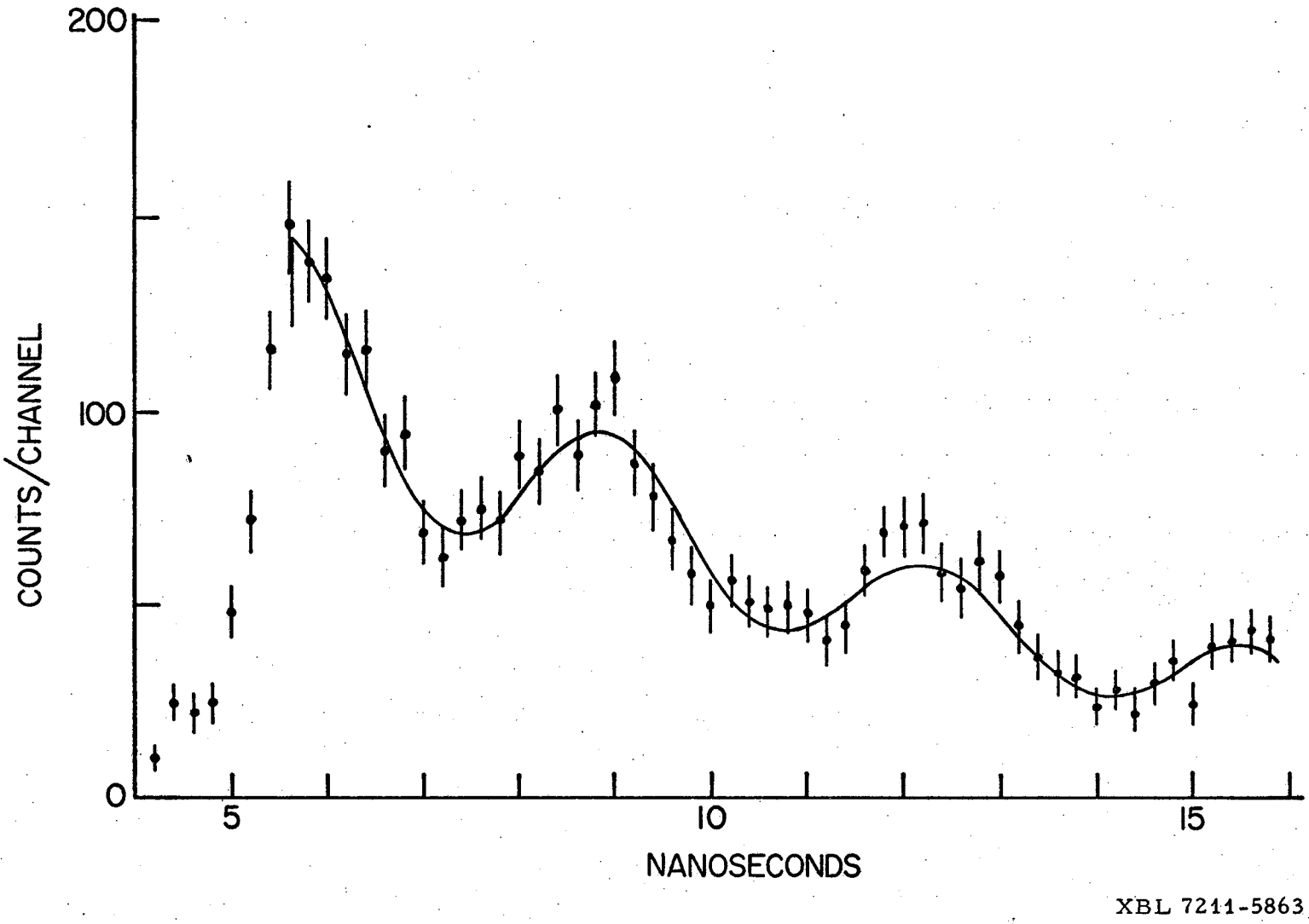

Figure 15. Polarizers-in correlation observed with a magnetic field of 90 gauss.

of trapping, the lifetime observed in this run suggests that the average probability of photon escape, x, was 0.4. For an atom with a J= 1 to J= 0 transition, Barrat gives the polarization of escaping radiation as (1-x)/(1-3x/5), which yields 0.79 for x= 0.4. Combining this with the geometry factor of 0.75, we predict a value of R of 0.59, larger than the observed value of 0.42. This discrepency might be interpreted as resulting from the unusual properties of the absorption coefficient of an atomic beam, but Barrat also found that the polarization of resonance light from a cell failed to follow the predicted dependence on atomic density.

V. CONCLUDING REMARKS

Our experiments with the optical pumping of Hg^{203} have shown the limitations of this technique for the measurement of parity violation effects. The dual requirements for the observation of the small gamma-ray asymmetry induced by the weak nuclear potential are the achievement of a high degree of polarization, but with a sample of high activity. We have found that the resonance trapping of the optical pumping light prevents the simultaneous satisfaction of these two requirements. While optical pumping of radioactive isotopes may be a useful technique for the measurement of larger effects (such as the electron asymmetry in beta decay), it does not appear to be applicable to the measurement of the very small effects associated with parity violating nuclear forces.

ACKNOWLEDGEMENTS

I wish first to thank my research advisor, Professor Eugene Commins, for his guidance, constant encouragement, and friendship.

I wish to thank my friend and colleague Stuart Freedman for his assistance and advice on the second part of this work, which draws heavily upon his experience.

I am grateful to Professor Howard Shugart, Professor Richard Marrus, and other members of the Atomic Beam Group for much valuable assistance.

I wish to thank Mio Nishi for typing the final draft of this thesis.

This work was supported by the U.S. Atomic Energy Commission.

Appendix I.

Polarization of Light Reflected from a Surface of Finite Conductivity

We consider the problem of a parallel beam of polarized light incident from a vacuum onto a flat surface of a metal of conductivity σ. We choose a coordinate system with the z-axis normal to the metallic surface and the direction of the incident light beam (given by the unit vector $\hat{k}$) is assumed to be in the x-z plane. The electric field of the incident light beam is written

$$\vec{E}_i = E_0(\epsilon_1\hat{y} + \epsilon_2\cos\theta\hat{x} + \epsilon_2\sin\theta\hat{z})\ \exp[i\vec{k}\cdot\vec{x}]$$

where θ is the angle between $\hat{k}$ and the z-axis so that $\hat{k} = \sin\theta\hat{x} - \cos\theta\hat{z}$. The electric field of the reflected beam is

$$\vec{E}_r = E_0(\epsilon_1'\hat{y} - \epsilon_2'\cos\theta\hat{x} + \epsilon_2'\sin\theta\hat{z})\ \exp[i\vec{k}'\cdot\vec{x}]$$

where $\hat{k}' = \sin\theta\hat{x} + \cos\theta\hat{z}$ is the direction of the reflected light beam. Using the relation $\vec{H} = \hat{k}\,\vec{E}$, which is valid in a vacuum, we have

$$\vec{H}_i = E_0(\epsilon_1\cos\theta\hat{x} + \epsilon_1\sin\theta\hat{z} - \epsilon_2\hat{y})\ \exp[i\vec{k}\cdot\vec{x}]$$

$$\vec{H}_r = E_0(-\epsilon_1'\cos\theta\hat{x} + \epsilon_1'\sin\theta\hat{z} - \epsilon_2'\hat{y})\ \exp[i\vec{k}'\cdot\vec{x}]$$

By matching the boundry conditions at the metal surface, we obtain equations relating ϵ_1' and ϵ_2' to the incident polarization coefficients ϵ_1 and ϵ_2.

With a metal of infinite conductivity, the tangential component of the electric field vanishes at the boundry. However with a metal of finite conductivity, the tangential components of $\vec{E}$ and $\vec{H}$ are related

by the equation (J62)

$$\vec{E}_t = \sqrt{\frac{\omega}{8\pi\sigma}}\,(1-i)(\hat{z}\cdot\vec{H}_t).$$

In terms of the quantities defined above, we have for the tangential components of the fields, evaluated at the origin,

$$\vec{E}_t = E_0[(\varepsilon_1+\varepsilon_1')\hat{y} + (\varepsilon_2-\varepsilon_2')\hat{x}\cos\theta]$$

$$\vec{H}_t = E_0[(\varepsilon_1-\varepsilon_1')\cos\theta\hat{x} - (\varepsilon_2+\varepsilon_2')\hat{y}]$$

Substituting these expressions into the boundary condition, we obtain,

$$\varepsilon_1' = \frac{-1 + \sqrt{\frac{\omega}{8\pi\sigma}}\,(1-i)\cos\theta}{1 + \sqrt{\frac{\omega}{8\pi\sigma}}\,(1-i)\cos\theta}\,\varepsilon_1$$

$$\varepsilon_2' = \frac{\cos\theta - \sqrt{\frac{\omega}{8\pi\sigma}}\,(1-i)}{\cos\theta + \sqrt{\frac{\omega}{8\pi\sigma}}\,(1-i)}\,\varepsilon_2$$

The reflectance for normal incidence is $R\simeq 1-4\sqrt{\omega/8\pi\sigma}$, and the measured reflectance of aluminum for 254 nm light is 0.90, so we have $\sqrt{\omega/8\pi\sigma}\simeq 0.025$. With $\beta = \cos\theta\sqrt{\omega/8\pi\sigma}$ and $\gamma = \sqrt{\omega/8\pi\sigma}/\cos\theta$, we have

$$\varepsilon_1'/\varepsilon_1 = (1-\beta+i\beta)/(1+\beta-i\beta)$$

$$\varepsilon_2'/\varepsilon_2 = (1-\gamma+i\gamma)/(1+\gamma-i\gamma)$$

Thus the phase change for light polarized parallel to the surface is $\phi_1\simeq \arcsin 2\beta$ and the phase change for light polarized perpendicular to the surface is $\phi_2\simeq \arcsin 2\gamma$. As the direction of the incident light changes toward glancing incidence, γ becomes large and the phase retardation of the perpendicular component becomes larger than the retardation of the parallel component. Thus left hand circular

polarization is produced from an incident light beam with $\varepsilon_1 = -\varepsilon_2$ when the incident angle is such that $\gamma \simeq 0.5$.

Appendix II.

The Integral $G_2(\alpha,\beta)= \int_0^\infty \frac{x^2\exp[-x^2]\,dx}{1+(\alpha x-\beta)^2}$

Any scheme to solve the resonance trapping problem in an atomic beam by numerical methods (either by integration of the differential equation or Monte Carlo simulation) must evaluate $G_2(\alpha,\beta)$ many times with a wide range of values of α and β. The usual numerical integration techniques, while capable of high accuracy, are not fast enough when the integral must be evaluated many times during a calculation. Thus we have looked for techniques by which this integral might be rapidly evaluated to rough accuracy.

We consider the related complex integral $f_2(z)= \int_0^\infty x^2\exp[-x^2]\cdot(x-z)^{-1}dx$. The real and imaginary parts of $f_2(z)$ are, with $z= a+ib$,

$$\mathrm{Re}\{f_2(z)\} = \int_0^\infty (x-a)x^2\exp[-x^2]((x-a)^2+b^2)^{-1}\,dx$$

$$\mathrm{Im}\{f_2(z)\} = b\int_0^\infty x^2\exp[-x^2]((x-a)^2+b^2)^{-1}\,dx$$

So that $G_2(\alpha,\beta)= (1/\alpha)\,\mathrm{Im}\{f_2(\beta/\alpha+i/\alpha)\}$. By defining the complex integral $f_0(a+ib)= \int_0^\infty \exp[-x^2](x-a-ib)^{-1}dx$, we have

$$\frac{1}{b}\,\mathrm{Im}\{f_2(a+ib)\} = \frac{\sqrt{\pi}}{2} + 2a\mathrm{Re}\{f_0(a+ib)\} + (a^2/b - b)\mathrm{Im}\{f_0(a+ib)\}$$

so that the evaluation of G_2 is reduced to the evaluation of $f_0(a+ib)$. By defining a new variable, $t= x^2$, f_0 can be written as a Fourier transform and looked up in a table (CF42).

$$f_0(a+ib) = \frac{\pi}{2}(-a-ib)^{-\frac{1}{2}}\exp[-a-ib]\mathrm{Erfc}(\sqrt{-a-ib})$$

Thus G_2 has been expressed in terms of a well known function, the error function of complex argument. However $f_0(\beta/\alpha+i/\alpha)$ has singularities at important values of α and β. These singularities cancel to give finite values of $G_2(\alpha,\beta)$, but numerical approximations for $\mathrm{Erfc}(\sqrt{-z})$ cannot be employed in the region of these singularities.

We note that $G_2(\alpha,\beta)$ can be explicitly evaluated for $\alpha=\beta=0$, $G_2(0,0) = \int_0^\infty x^2\exp[-x^2]dx = \sqrt{\pi}/4 = 0.443$. We ask if it is possible to generate values for G_2 for non-zero values of α and β from this value at the origin. It is possible to make a power series expansion of G_2 about the origin, $G_2(\alpha,\beta)= \sqrt{\pi}/4-\beta^2\sqrt{\pi}/4-3\alpha^2\sqrt{\pi}/8+\alpha\beta+\cdots$. However the region of α, β for which G_2 must be evaluated extends out to $\alpha\simeq\beta\simeq 90$, far beyond the region of convergence of the power series.

Is there a differential equation satisfied by G_2 such that $G_2(\alpha,\beta)$ can be found from the initial condition $G_2(0,0)= \sqrt{\pi}/4$? We define $G_n= \int_0^\infty x^n\exp[-x^2](1+(\alpha x-\beta)^2)^{-1}dx$ and note that

$$G_2(\alpha,\beta) = \sqrt{\pi}/(2\alpha^2) - (1+\beta^2)G_0/\alpha^2 + 2\beta G_1/\alpha$$

The G_n can be explicitly evaluated for $\alpha=0$; $G_2(0,\beta)= \sqrt{\pi}/(4+4\beta^2)$, $G_1(0,\beta)= 1/(2+2\beta^2)$, $G_0(0,\beta)= \sqrt{\pi}/(2+2\beta^2)$. Furthermore the functions G_1 and G_0 are solutions of a set of coupled first order differential equations,

$$\frac{\partial G_0}{\partial\alpha} = \sqrt{\pi}/(4\alpha^3) - (1/\alpha+(2+2\beta^2)/\alpha^3)G_0 + 4\beta G_1/\alpha^2$$

$$\frac{\partial G_1}{\partial\alpha} = -1/\alpha^3 + \sqrt{\pi}\beta/\alpha^4 - 4\beta(1-\beta^2)G_0/\alpha^4+(-2/\alpha-(2+10\beta^2)/\alpha^3)G_1$$

A computer program was written which evaluated $G_2(\alpha,\beta)$ by calculating

$G_1(0,\beta)$ and $G_0(0,\beta)$, integrating the coupled differential equations from the point $(0,\beta)$ to the point (α,β), and calculating G_2 from the values of G_1 and G_0 found there. However this program was no faster than a straight-forward numerical integration of the original expression for G_2.

The evaluation technique finally employed in the Monte Carlo simulation of trapping depended upon the fact that while the denominator of the integrand was a rapidly varying function of x for some α and β, the numerator was always a smooth function (the numerator only expresses the velocity distribution of the atoms). Thus the function $x^2\exp[-x^2]$ was replaced by a sequence of constant values, f_i, over 30 intervals from x= 0 to x= 3.0. Within each interval the integral can be explicitly evaluated,

$$\int_{x_{i-1}}^{x_i} f_i(1+(\alpha x-\beta)^2)^{-1}dx = (f_i/\alpha)[\arctan(\alpha x_i-\beta) - \arctan(\alpha x_{i-1}-\beta)]$$

Thus we have the approximation

$$G_2(\alpha,\beta) \simeq (1/\alpha) \sum(f_i-f_{i-1}) \arctan(\alpha x_i-\beta)$$

which only requires the use of a library routine for the arctan function.

Appendix III.

The Monte Carlo Program CREON

CREON performs a Monte Carlo simulation of the trapping of unpolarized resonance radiation in an atomic beam. CREON generates random starting positions in the beam for excitation of an atom at time t= 0. The transfer of excitation from atom to atom by a resonance photon is followed until the photon escapes from the beam. The time of escape is recorded on a histogram, and the process is repeated. Thus CREON simulates the count rate distribution of photons escaping from the beam as a function of time elapsed since the initial excitation process (emission of the preceeding photon in the case of a cascade).

The sequence of events in a CREON simulation is as follows. Wherever the word generated is used, it means the quantity referred to is calculated from a (set of) random numbers(s).

1. Start. Contents of the histogram are set to zero.
2. Initial position of excitation is generated, time is set to zero.
3. Velocity of the initial atom is generated.
4. Duration of excitation of that atom is generated. Time is incremented by that amount.
5. Direction of emitted photon is generated.
6. Frequency of emitted photon is generated.
7. Propagation distance of photon is generated.
8. New position of the excitation is calculated.

9. If the new position is outside the defined boundries of the beam, the photon has escaped and the program goes to step 11. If the new position is inside the beam, the program goes to step 10.

10. Velocity of the new excited atom is generated. Program goes to step 4.

11. One count is added to correct channel of the histogram. Program goes to step 2.

The program cycles through step 2 for the number of simulated events desired. As usual in Monte Carlo simulations, the accuracy of the results improves with the number of events generated, but at a cost of computer time.

The random generating library routines, when called, return a number, R, uniformly distributed in the interval $0 \leq R < 1.0$. From this uniformly distributed quantity the random variables to be generated in each step are derived in the manner described below.

Step 2. The coordinates x, y, and z are uniformly generated in a rectangular solid by formulas such as x= (R-0.5)*(width of atomic beam).

Step 3. In the excitation process employed in this work, all atoms in the interaction region have equal probability of being excited. Thus the probability of the initial excited atom having a velocity v is proportional to the number of atoms with that velocity, $v^2 \cdot \exp[-v^2/v_0^2]$. This function has already been approximated (for the calculation of $G_2(\alpha,\beta)$) by a

series of constant values on 30 intervals from $v/v_0 = 0$ to $v/v_0 = 3.0$. The total area under these rectangles is $\sqrt{\pi}/4 = 0.443$. If any random quantity, x, has a probability distribution P(x) on the interval (a,b), then the quantity

$$S = \frac{\int_a^x P(t)dt}{\int_a^b P(t)dt}$$

is uniformly distributed on the interval (0,1.0). This suggests how any probability distribution can be generated from a uniform distribution. A quantity called SET is generated by SET= R*0.443. The value of v, such that the area under the rectangles from v= 0 to that value of v equals SET, is then found. This value of v has the desired probability distribution.

Step 4. The decay of the excitation of the atom follows an exponential distribution with a lifetime of τ. The duration of excitation is generated by $\Delta t = -\tau * \ln(R)$.

Step 5. A uniform spherical distribution of polar angles θ, ϕ is generated by $\cos\theta = 2.*R-1.$ and by $\phi = 2\pi*R$.

Step 6. The frequency of the emitted photon follows a Lorentzian distribution of width γ, centered at ω_0 plus a Doppler shift corresponding to the velocity of the atom and the direction of the photon relative to that velocity. The frequency is generated by $\omega = \omega_0(1+(v/c)\cos\theta)+(\gamma/2)\tan(\pi R-\pi/2)$.

Step 7. First the attenuation coefficient $k(\omega,\theta)$ is calculated

from $G_2(\alpha,\beta)$ in the manner described in Appendix II. The propagation distance follows an exponential distribution with mean distance $1/k(\omega,\theta)$. The distance is generated by $\ell = -\ln(R)/k(\omega,\theta)$.

Step 10. The procedure here is similar to Step 3, except that the probability of the photon being absorbed by an atom of velocity v is proportional to the number of atoms of that velocity multiplied by a Lorentzian absorption curve. This function is the one which was integrated from v= 0 to v= 3.0 to calculate $G_2(\alpha,\beta)$. A quantity SET is generated by SET= $R*G_2(\alpha,\beta)$, and the value of v such that the area under the function from zero to that value of v equals SET is found.

REFERENCES

A61 A. Abragam, The Principles of Nuclear Magnetism (Clarendon Press, Oxford, 1961).

A68 Y. G. Abov, et. at. Physics Lett. 27B, 16 (1968).

AKO65 Y. G. Abov, P. A. Krupchitskii, and Y. A. Oratovskii, J. Nucl. Phys. (U.S.S.R.) 1, 479 (1965).

B57 J. E. Blamont, Ann. de Physique 2, 551 (1957).

B59 J. P. Barrat, J. Phys. Radium 20, 541, 633, and 657 (1959).

B61 G. Barton, Nuovo Cimento 19, 512 (1961).

B64 J. B. Birks, Theory and Practice of Scintillation Counting (Pergamon Press, Oxford, 1964).

B65 M. A. Bouchait, J. Physique 26, 415 (1965).

B67 G. E. Brown, Unified Theory of Nuclear Models and Forces (North Holland, Amsterdam, 1967).

BB52 J. Brossel and F. Bitter, Phys. Rev. 86, 308 (1952).

BH70 K. D. Baker and W. D. Hamilton, Phys. Lett. 31B, 557 (1970).

BS60a R. J. Blin-Stoyle, Phys. Rev. 118, 1605 (1960).

BS60b R. J. Blin-Stoyle, Phys. Rev. 120, 181 (1960).

BKM64 W. R. Bennett, P. J. Kindlemann, and G. N. Mercer, Applied Optics Suppl. 1, 34 (1964).

BKW52 J. Bossel, A. Kastler, and J. Winter, J. Phys. Radium 13, 668 (1952).

BPP48 N. Bloembergen, E. M. Purcell, and R. V. Pound, Phys. Rev. 73, 679 (1948).

C23 K. T. Compton, Phil. Mag. 45, 750 (1923).

C58 B. Cagnac, J. Phys. Radium 19, 863 (1958).

C61 B. Cagnac, Ann. de Physique 6, 467 (1961).

C63 N. Cabbibo, Phys.Rev. Lett. 10, 531 (1963).

C67 R. A. Carhart, Phys. Rev. 153, 1077 (1967).

CF42 G. Campbell and R. Foster, Fourier Integrals for Practical Applications, (Bell Telephone Laboratory, New York, 1942).

CT63 C. Cohen-Tannoudji, J. Physique 24, 653 (1963).

CRC61 Handbook of Chemistry and Physics, (Chemical Rubber Co., Cleveland, 1961).

CHSH69 J. F. Clauser, M. A. Horne, A. Shimony and R. A. Holt, Phys. Rev. Lett. 23, 880 (1969).

D49 S. Dushman, Scientific Foundations of Vacuum Technique (Wiley and Sons, New York, 1949).

D57 H. G. Dehmelt, Phys. Rev. 105, 1487 (1957).

D70 A. M. Dumont, C. Camhy-Val, M. Dreux, and R. Vitry, Compt. Rend. 271, B1021 (1970).

D71 F. Dydak, et. al., Phys. Lett. 37B, 375 (1971).

DE52 C. M. Davisson and R. D. Evans, Rev. Mod. Phys. 24, 79 (1952).

DE63 B. D'Espagnat, Phys. Lett. 7, 209 (1963).

DM61 B. I. Deutch and F. R. Metzger, Phys. Rev. 122, 848 (1961).

DO71 B. Dodsworth and A. Omont, Phys. Rev. A3, 1901 and 1912 (1971).

DP65 M. I. D'Yakonov and V. I. Perel, Sov. Phys. -JETP 20, 997 (1965).

DFS64 R. F. Dashen, S. C. Frautschi, and D. H. Sharp, Phys. Rev. Lett. 13, 777 (1964).

DFGH64 R. F. Dashen, S. C. Frautschi, M. Gell-mann, and Y. Hara, Octet Enhancement, Cal Tech Report (1964). Reprinted in M. Gell-mann and Y. Ne'eman, The Eightfold Way, (W. A. Benjamin, New York, 1964).

EH65 T. Edmonds and J. P. Hobson, J. Vac. Sci. and Tech. 2, 182 (1965).

EPR35 A. Einstein, B. Podolsky, and N. Rosen, Phys. Rev. 47, 777 (1935).

F38 W. Franz, Ann. Physik 33, 698 (1938).

F57 U. Fano, Rev. Mod. Phys. 29, 74 (1957).

F62 H. Frauenfelder, The Mössbauer Effect, (Benjamin, New York, 1963).

F63 B. Foldum, Z. der Physik 176, 159 (1963).

F72 S. J. Freedman, Experimental Test of Local Hidden-Variable Theories (Ph.D. Thesis), Lawrence Berkeley Laboratory Report LBL-391, May 1972 (unpublished).

FC72 S. J. Freedman and J. F. Clauser, Phys. Rev. Lett. 28, 938 (1972).

FE57 W. Franzen and A. G. Emslie, Phys. Rev. 108, 1453 (1957).

FG58 R. P. Feynman and M. Gell-mann, Phys. Rev. 109, 193 (1958).

FT68 E. Fischbach and K. Trabert, Phys. Rev. 174, 1843 (1968).

G70 M. Gari, Physics Lett. 31B, 627 (1970).

GG61 L. Grodzins and F. Genovese, Phys.Rev. 121, 228 (1961).

GK69 M. Gari and H. Kummel, Phys. Rev. Lett. 23, 26 (1969).

GBB56 M. A. Guiochon, J. E. Blamont, J. Brossel, Compt. Rend. 243, 1859 (1956).

H47 T. Holstein, Phys. Rev. 72, 1212 (1947).

H49 T. Holstein, Phys. Rev. 76, 1257 (1949).

H62 R. W. Hamming, Numerical Methods for Scientists and Engineers (McGraw-Hill, New York, 1962).

H72 W. Happer, Rev. Mod. Phys. 44, 169 (1972).

HHW70 H. Hättig, K. Hünchen, and H. Wäffler, Phys. Rev. Lett. 25. 941 (1970).

HKY69 E. M. Henley, T. E. Keliher, and D.U.L. Yu, Phys. Rev. Lett 23, 941 (1969).

HTG54 C. D. Hartogh, H. A. Tolhoek, and S. R. deGroot, Physica 20, 1310 (1954).

J62 J. D. Jackson, Classical Electrodynamics (Wiley, New York, 1962).

JW59 M. Jacob and G. C. Wick, Annals of Physics 7, 404 (1959).

K50 A. Kastler, J. Phys. Radium 11, 255 (1950).

K57 R. S. Krishnan, et. al., Nature 179, 540 (1957).

K67 C. A. Kocher, Polarization Correlation of Photons Emitted in an Atomic Cascade (Ph.D. Thesis), Lawrence Berkeley Laboratory Report UCRL-17587, May 1967 (unpublished).

K71 K. S. Krane, et. al., Phys. Rev. Lett. 26, 1579 (1971).

KU36 J. K. Knipp and G. E. Uhlenbeck, Physica 3, 425 (1936).

KOZ69 H. J. Kluge, E. W. Otten, and G. Zimmermann, Journal de Physique C1, 15 (1969).

L66a V. M. Lobashov, et. al.,J.E.T.P. Letters 3, 76 (1966) transl. p. 47.

L66b V. M. Lobashov, et. al.,J.E.T.P. Letters 3, 268 (1966) transl. p. 173.

L67 V. M. Lobashov, et. al., Phys. Lett. 25B, 104 (1967).

LB69 H. Leuschner and P. Bock, Externer Bericht 3 (1969) 1 des KFZ Karlsruhe, Germany (unpublished).

M26 E. A. Milne, J. London Math. Soc. 1, 1 (1926).

M64 F. C. Michel, Phys. Rev. 133, B329 (1964).

M68 A. J. Michael, J. Opt. Soc. Am. 58, 889 (1968).

MK67 B. H. J. McKellar, Phys. Lett. 26B, 107 (1967).

MN61 M. N. McDermott and R. Novick, J. Opt. Soc. Am. 51, 1008 (1961).

MK68 B. H. J. McKellar, Phys. Rev. Lett. 20, 1542 (1968).

MS58 F. K. McGowan and P. H. Stelson, Phys. Rev. 109, 901 (1958).

MZ34 A. C. G. Mitchell and M. W. Zemansky, Resonance Radiation and Excited Atoms (Cambridge Press, London, 1934).

N55 S. G. Nilsson, Klg. Danske Videnskab. Selskab, Mat. Fys. Medd. 29, No. 16 (1955).

N63 A. N. Nesmeyanov, Vapor Pressure of the Chemical Elements, ed. Robert Gary (Elsevier Publ. Co., New York, 1963).

NBS52 National Bureau of Standards, Tables for the Analysis of Beta Spectra (U.S. Printing Office, Washington, 1952).

OR69 P. Olesen and J. S. Rao, Physics Lett. 29B, 233 (1969).

P62 M. A. Preston, Physics of the Nucleus (Addison-Wesley, Reading, Mass., 1962).

P70 M. Popp, G. Schäfer, and E. Bodenstedt, Z. Physik 240, 71 (1970).

PN64 I. M. Popescu and L. N. Novikov, Compt. Rend. 259, 1321 (1964).

R56 N. F. Ramsey, Molecular Beams (Clarendon Press, Oxford, 1956).

R57 M. E. Rose, Elementary Theory of Angular Momentum (Wiley & Sons, New York, 1957).

R63 M. E. Rose, Nulcear Orientation (Gordon and Breach, New York, 1963).

R64 O. Redi, Quarterly Prog. Report No. 74, Research Lab of Electronics, MIT, (July 1964), (unpublished).

R79 O.Reynolds, Phil. Trans. Roy. Soc. London 170, 727 (1879).

RCA70 RCA Photomultiplier Manual, RCA Technical Series PT-61 (1970).

S65 K. Siegbahn, Alpha-, Beta-, and Gamma-Ray Spectroscopy (North Holland, Amsterdam, 1965).

S66 Z. Szymanski, Nuclear Physics 76, 539 (1966).

SG58 H. Schopper and S. Galster, Nucl. Phys. 6, 125 (1958).

SOS61 R. E. Segel, J. W. Olness, and E. L. Sprenkel, Phys. Rev. 123, 1382 (1961).

T56 H. A. Tolhoek, Rev. Mod. Phys. 28, 277 (1956).

T63 S. B. Treiman, Structure of Weak Interactions, in Weak Interactions, C. Fronsdal, Ed. (W. A. Benjamin, New York, 1963).

T68 D. Tadić, Phys. Rev. 174, 1694 (1968).

TC52 H. A. Tolhoek and J. A. M. Cox, Physica 18, 356 (1952).

TS64 W. J. Tomlinson III and H. H. Stroke, Nuclear Phys. 60, 614 (1964).

W12 R. W. Wood, Phil. Mag. 23, 689 (1912).

W31 V. Weisskopf, Ann. der Physik 9, 23 (1931).

W57 C. S. Wu, et. al., Phys. Rev. 105, 1413 (1957).

W61 H. A. Weidenmüller, Rev. Mod. Phys. 33, 574 (1961).

W65 S. Wahlborn, Phys. Rev. 138, B530 (1965).

WSM69 W. L. Wiese, M. W. Smith, and B. M. Miles, Atomic Transition Probabilities, Vol.II, NSRDS-NBS 22 (1969).

Z27 M. W. Zemansky, Phys. Rev. 29, 513 (1927).

TECHNICAL INFORMATION DIVISION
LAWRENCE BERKELEY LABORATORY
UNIVERSITY OF CALIFORNIA
BERKELEY, CALIFORNIA 94720